UNIVERSITY OF COPENHAGEN
FACULTY OF SCIENCE

Master thesis

Elastic objects ejected from harmonic plate

With analytical and numerical solutions

Nikka Mosleh

Supervised by Joachim Mathiesen

Handed in: January 3, 2022

Abstract

The energy transfer from a plate in harmonic motion to an elastic object is investigated. When the object is ejected from the plate it will gain an amount of translational kinetic energy compared to the amount that a rigid object would have gained, and this is represented by the energy transfer factor. The main goal of this thesis is to find the maximum energy transfer factor with the corresponding optimal set of parameter values when assuming linear elasticity and one-dimensional deformations of the elastic objects. This is done both analytically and numerically. For a homogeneous object the energy transfer factor has a maximum of 253% and depends on a single parameter describing the plate frequency relative to the basic eigenfrequency of the material. If a point mass, i.e. a rigid material, is added, the energy transfer factor now also depends on a second parameter describing the mass of the rigid material relative to that of the elastic material. The maximum energy transfer factor for this system goes towards 313% when the mass ratio goes towards infinity and the frequency ratio goes towards zero. But it becomes larger than 300% when the mass ratio is larger than 10. For a general system consisting of two elastic materials the energy transfer factor depends on four independent parameters: the dimensionless frequency, the dimensionless Young's modulus, the dimensionless density and the dimensionless length. The maximum energy transfer factor for this system is for parameter values where this system is reduced to the second system consisting of a homogeneous elastic material with a point mass on top, where only the dimensionless frequency and dimensionless mass matter. The homogeneous system and point mass system with internal friction included, are also investigated. The damping of the elastic waves is described by the Kelvin-Voigt model, and from analytical considerations the characteristic time for the damping of the elastic waves together with the critical value of the damping parameter is found in terms of the physical parameters of the objects.

Contents

1 Introduction

The subject of energy transfer from one object to another in combination with the elastic properties of materials, and the storage of elastic energy and later release of it as kinetic energy are of great importance in many situations. The fact that elastic energy can be stored and later released is widely used in the anatomy of different life forms. It is for example used in insect jumping and flight and in mammal running [1]. The role of elasticity also plays an important role in the biology of humans, where the elastic properties of the tendon structures is very essential on the jump performance [2]. Humans are alomst the only primates that regularly throw objects with high speed and accuracy, and this throwing ability is mainly because of the energy storage and release at the shoulder [3]. But not only is elastic properties important in a biological sense, it is also very widely used and taken advantage of in many different sports. One example is badminton where it has been shown that the shaft's elasticity can be utilized to increase the velocity of the racket's head [4]. Another sport example is marathon running where it is favorable to reduce the energy cost of running. Nike has made different shoes, of which the Nike Vaporfly 4% is one of them, that tries to optimize the cost of running [5]. Nike's shoes at the time they were introduced were different from conventional running shoes in terms of the midsole material and thickness and by having an embedded carbon-fiber plate [5, 6]. A study was conducted to determine if and how much these shoes reduce the energy cost of running compared to conventional marathon racing shoes, and it was shown that Nike's shoes provided a 4% improvement in the metabolic cost of running and an estimation of 3.4% increase in the running speed [6]. In a follow-up article they conclude that the metabolic savings of this shoe appear to be due to energy storage in the midsole foam, the lever effects of the carbon-fiber plate on the ankle joint mechanics, and the stiffening effects of the metatarsophalangeal joint (the joint that connects the foot bones with the toe bones) [7].

The effect and importance of a material's elastic properties on the optimization of a system can be investigated in different ways and by examining different systems. One such example is the energy transfer from an engine to a projectile. At the University of Nice, a group of scientists have investigated the behaviour of elastic objects placed on a plate which moves harmonically in time. The goal is to look into how much translational kinetic energy the elastic objects have gained at the time they are ejected from the plate compared to a rigid object. In the article "Superpropulsion of Droplets and Soft Elastic Solids" by C. Raufaste et al [8] they consider a homogeneous elastic object on the harmonic plate in the linear elasticity regime. They solve this system numerically and compare with their experiments. The same considerations are done in the follow-up article "Contact Layer as a Propelling Advantage in Throwing" by F. Celestini et al [9] for an object consisting of a homogeneous elastic material with an approximately rigid material stuck to the top of it. In figure 1, which is taken from the article by F. Celestini et al [9], an illustration of the set up is shown at the inital time and the ejection time together with the maximum heights that three different objects reached after ejecting from the plate which had frequency 76 Hz.

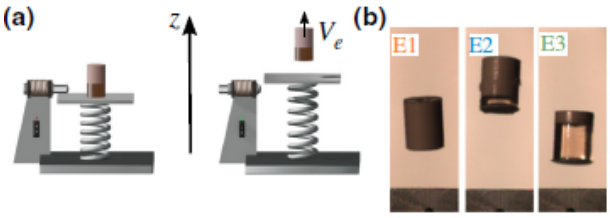

Figure 1: The figure is taken from the second article [9] and shows the experimental set up. (a) The position of the plate and elastic object is illustrated at the initial time and at the ejection time. (b) The maximum heights of three objects with different rigid-elastic ratios after ejection for the plate frequency 76 Hz (E1: rigid, E2: small elastic layer, E3: large elastic layer).

The main focus of the articles is that one can find elastic objects that are more optimal in the sense that

they have an energy transfer factor of more than one. They find that the elastic objects are transferred more translational kinetic energy from the plate than a purely rigid object.

These are the systems that I will be investigating in this thesis. I have previously worked on this subject in my bachelor project [10] where I only considered the analytical solution to the system consisting of the homogeneous elastic object on the plate. In this thesis this system is considered again but also with a numerical solution together with the analytical solution[1]. In addition, the homogeneous system with a point mass (rigid material) on top of it is also considered and so is the general system where the object consists of two elastic materials where each material is homogeneous. At last the homogeneous system and the point mass system are also considered when including internal friction of the material.

My contribution to the subject of this thesis are all the analytical solutions with the corresponding considerations which are derived using Laplace transformations. The main analytical equations found for the three systems are the displacement functions with an associated equation describing the poles, after which an equation for the ejection time can be derived and then the dimensionless ejection velocity, which is the square root of the energy transfer factor, can be found. For the homogeneous system and point mass system with internal friction included it has not been possible to find the corresponding functions and equations analytically. But the solution in Laplace space can be found and from this an expression for the poles. By considering these poles the critical value of the damping parameter and the characteristic time for the damping have then been found.
The numerical solutions used in this thesis are also new contributions to the subject. These are found by using finite difference methods based on second order approximations in space while fourth-order Runge-Kutta is used in time. For all systems considered the numerical solutions are found by discretizing the space, and the corresponding set of ordinary differential equations have been derived. Then from the ejection time condition, a function can be found where its root is the ejection time and is found by using the bisection method. Then the energy transfer can be found when approximating the integrals in the expression by using the trapez method.

To be able to begin analyzing the systems, a brief introduction is given to elastic properties, linear elasticity and the equation of motion of elastic materials (the wave equation), all in one dimension. The two methods (analytical and numerical) that are used to solve the wave equation with associated initial and boundary conditions are then described. A description is also given of the general system where the object consists of two elastic materials (since the two other systems are special cases of this system), after which the three systems are investigated. Generally for each system the solution to the wave equation is derived, an ejection time equation is found and the energy transfer factor is computed. The numerical scheme is also derived and the corresponding numerical ejection time function and the numerically computed energy transfer factor are also shown. Afterwards, the Kelvin-Voigt model for the damping of the elastic waves is introduced and used to describe the homogeneous system and point mass system with damping. The approach for these two systems are the exact same as for the systems without damping, but when damping is included it becomes harder to solve analytically. An attempt has been made though, and a critical value of the damping parameter is found analytically together with the characteristic time of the damping. At last, the different systems are discussed and compared.

[1]The only difference in the analytical solution in this thesis compared to my bachelor project is the definition of one of the dimensionless variables - this makes the intermediate equations a little different but the main results are the same

2 Equation of motion for elastic materials

When an elastic object is affected by an external force the whole object will not feel the effect of this immediately. For many materials the force will cause the object to deform, and the information of this force is propogated throughout the object by elastic waves [11, 12]. This is illustrated in figure 2. The figure shows an example of the deformation of an elastic object with cross section S when it is affected by a force F. A point P originally at position x is displaced with an amount u to the point P'. The same is seen for another point Q (originally an infinitesimal distance dx from the first point) which is displaced by, generally, another amount $u + du$. To describe the strength of the force that causes the deformation of the object, and the deformation of the object itself, stress σ and strain $\epsilon = \partial u/\partial x$ are introduced.

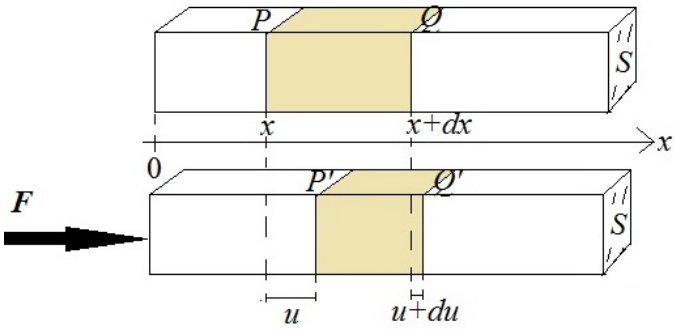

Figure 2: Illustration of the effect of an external force on an elastic object. The top figure shows some element of the object before it was affected by the force, and the bottom figure shows the element some time after where a stress wave is passing through and the element is displaced from its original position.

In figure 2 the force is applied perpendicular to the object's cross sectional area and the deformation of the object is a change in its length. The stress is then given as the force per area while the strain is given as the relative length change, which is positive for tensile strain and negative for compression. If the stress applied to the object and the resulting deformations are small, i.e. in the linear elasticity regime, the relationship between the stress and strain is given by Hooke's law [11, 12, 13]:

$$\sigma = E\,\epsilon \tag{1}$$

where E is the Young's modulus of the object. The larger Young's modulus a material has, the harder it is to stretch it since a larger stress is needed for a given strain [12].

Now consider figure 2. The resulting force on the element $P'Q'$ is the difference between the forces acting on each site, i.e. $\sigma\,S - (\sigma + d\sigma)\,S$, and from Newton's second law the equation of motion then gives:

$$\frac{\partial \sigma}{\partial x}\,dx\,S = \rho\,S\,dx\,\frac{\partial^2 u}{\partial t^2} \Leftrightarrow \rho\,\frac{\partial^2 u}{\partial t^2} = \frac{\partial \sigma}{\partial x} \Leftrightarrow \frac{\partial^2 u}{\partial t^2} = c^2\,\frac{\partial^2 u}{\partial x^2} \tag{2}$$

where $c^2 = E/\rho$ is the speed of the stress wave and ρ is the density of the object, so it is assumed that the material properties are the same throughout the entire object. The last step is found by using Hooke's law, and so it is also assumed that there are only deformations in the linear elastic regime. Furthermore it is assumed that the deformations of the object only occur in one dimension and that there are no transverse displacements of the elements of the object.

2.1 Solution method

Consider the wave equation for a function $f(\tau, z)$ in the form

$$\frac{\partial^2 f}{\partial \tau^2} = \frac{\partial^2 f}{\partial z^2} \tag{3}$$

and assume there are some associated initial and boundary conditions to describe the system.

The one-dimensional wave equation can for some systems be solved both analytically and numerically. For the first couple of systems considered in this thesis analytical solutions can be found, but for the last systems trying to solve it analytically becomes too complicated and we must settle with a numerical solution. The same solution methods for the analytical and numerical solutions are used for all systems throughout this thesis and they are descibed in the sections below.

2.1.1 Analytical method

To solve the partial differential equation analytically it is first Laplace transformed with respect to τ. Let the Laplace transform of the function $f(\tau, z)$ be $F(s, z)$, where s is generally complex. When the partial differential equation and its boundary conditions have been Laplace transformed, an ordinary differential equation with respect to z is obtained, which can then easily be solved. It is then used that in all cases this solution can be written as

$$F(s, z) = \frac{P(s, z)}{Q(s, z)} \tag{4}$$

where the order (in s) of the numerator P is less than that of the denominator Q, and they have no common roots. If the poles s_i are all simple poles, the residue theorem gives the inverse Laplace transform [14]:

$$f(\tau, z) = \sum_i \frac{P(s_i, z)}{Q'(s_i, z)} e^{s_i \tau} \quad , \quad Q(s_i, z) = 0\,,\ P(s_i) \neq 0 \tag{5}$$

where $Q'(s, z) = \frac{\partial Q}{\partial s}$. This is then the solution to the displacement in real space.

2.1.2 Numerical method

As will be seen, analytical solutions are nice and fun to calculate but not always easy to obtain and often one must settle with finding the solutions numerically. These can also be used to get an idea of whether or not the analytical solutions are correctly calculated by seeing if the two solutions are consistent.

The partial differential equation can be solved numerically by discretizing in the spatial direction z by using finite difference methods based on second order approximations. This way the partial differential equation is transformed into a set of ordinary differential equations, that can then be solved by integration in the temporal direction τ by using fourth order Runge-Kutta (RK4).

A spatial mesh is used such that the object considered consists of N points, each with spacing $\Delta z = 1/N$ between its neighbours. The function $f(\tau, z)$ is now discretized in space such that at some time, the displacement of some inner spatial point i is $f_i(\tau)$. The nearest neighbours of this point are then the points $i - 1$ and $i + 1$. A second order finite difference approximation to the second derivative in z can be found by taylor expanding the function f at the two points $i - 1$ and $i + 1$ around the point i to get [15]:

$$\begin{cases} f_{i-1} = f_i - \Delta z \left.\frac{\partial f}{\partial z}\right|_i + \frac{\Delta z^2}{2} \left.\frac{\partial^2 f}{\partial z^2}\right|_i - \frac{\Delta z^3}{6} \left.\frac{\partial^3 f}{\partial z^3}\right|_i + O(\Delta z^4) \\ f_{i+1} = f_i + \Delta z \left.\frac{\partial f}{\partial z}\right|_i + \frac{\Delta z^2}{2} \left.\frac{\partial^2 f}{\partial z^2}\right|_i + \frac{\Delta z^3}{6} \left.\frac{\partial^3 f}{\partial z^3}\right|_i + O(\Delta z^4) \end{cases} \Rightarrow \tag{6}$$

$$f_{i+1} + f_{i-1} = 2\, f_i + \Delta z^2 \left.\frac{\partial^2 f}{\partial z^2}\right|_i + O(\Delta z^4) \Leftrightarrow \left.\frac{\partial^2 f}{\partial z^2}\right|_i = \frac{f_{i+1} + f_{i-1} - 2\, f_i}{\Delta z^2} + O(\Delta z^2)$$

For the boundary points, the boundary conditions must be used to determine the second derivative in space. For the simple wave equation in equation 3 the second derivative in space is the same as the second derivative in time.

To evolve in time fourth order Runge-Kutta (RK4) is used - but in order for this to be possible the system must consist of first order differential equations. So the system of equations is transformed by calling the first derivative with respect to time g such that:

$$\frac{df_i}{d\tau} = g_i(\tau) \quad , \quad \frac{dg_i}{d\tau} = \left.\frac{\partial^2 f}{\partial z^2}\right|_i \tag{7}$$

The displacements f_i and the velocities g_i are put in a vector Y such that the first N elements are the displacements of the N points and the last N elements are the corresponding velocities. The derivative of this vector with respect to τ then consists of $2N$ ordinary first order differential equations.

3 Description of the system

The wave equation and the solution methods described in previous sections are used to investigate the motion of elastic objects placed on a harmonic plate. The main goal is to find the maximum translational kinetic energy transferred to the elastic objects from the plate compared to if the objects were rigid. This is quantified by the energy transfer factor ν^2, where ν is the ratio of the ejection velocities of the elastic object and that of a rigid object.

Consider a system where an elastic object of total length L and cross section S sits on a plate and a coordinate system is placed as shown in figure 3. Initially the object is at rest on the plate and at time $t = 0$ the plate starts its harmonic motion given by $A\,[1 - \cos(\omega\, t)]$, where A is the plate amplitude and ω its (angular) frequency. The bottom of the object (initially at $x = 0$) follows the motion of the plate, while the top of the object (initially at $x = L$) will be stress and strain free. When the plate starts moving, stress waves will propogate through the object with velocity determined by the material used. First consider the general case where it is assumed that the object consists of two elastic materials each with their own material properties (but constant throughout the material).

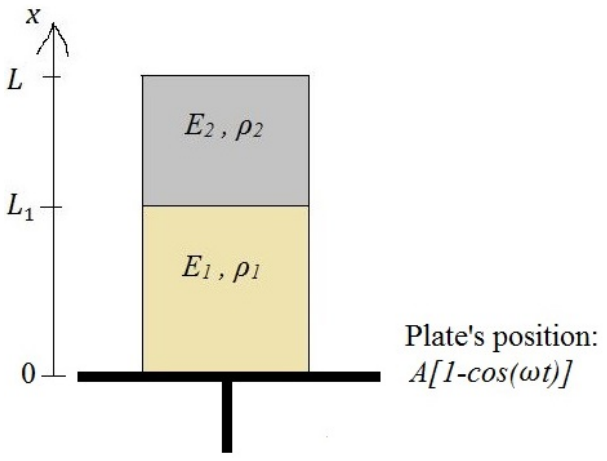

Figure 3: Initial position of an elastic object with total length L placed on a plate, which moves harmonically in time.

The first material ends at $x = L_1$ where the second material also starts. The density and Young's modulus of the first material are ρ_1 and E_1 and for the second material these are ρ_2 and E_2 respectively. The wave velocities in the two materials are then given by $c_1 = \sqrt{\frac{E_1}{\rho_1}}$ and $c_2 = \sqrt{\frac{E_2}{\rho_2}}$.

Notice that gravity is ignored and the only force acting on the object is the force that the plate exerts on it. Gravity is ignored to simplify the system, and also because it does not have a very significant effect on the object compared to the plate. In appendix A it is shown that the strain from gravity is small compared

to the strain from the stress wave for the system described in the article [9] where the second material is rigid. When the plate frequency becomes very small the two strains become comparable and the effect of gravity cannot be ignored when comparing with experimental results. But in the articles [8, 9] they have chosen moderate plate frequencies where the effect of gravity is not dominating. So in the sections where the experimental results are used gravity is negligible.

To analyze the system we will first consider the simplest case where the object is homogeneous, then the case where the second material is rigid, i.e. it can be considered as a point mass, and at last the actual system itself which in general is nonhomogeneous and consists of two elastic materials.

4 homogeneous system

First consider the case where the object only consists of the first elastic material such that the total length of the object is L_1. The system is illustrated in figure 4 where the relevant information is also shown. The displacement of each point of the object at all times obey the wave equation. The equation and the initial and boundary conditions that describe the motion of this object are

$$\begin{aligned} \frac{\partial^2 u}{\partial t^2} &= c_1^2 \frac{\partial^2 u}{\partial x^2} \\ u(0,x) = 0 \quad , \quad \left.\frac{\partial u}{\partial t}\right|_{t=0} &= 0 \qquad \forall \quad 0 < x < L_1 \\ u(t,0) = A\ [1 - \cos(\omega t)] \quad , \quad \left.\frac{\partial u}{\partial x}\right|_{x=L_1} &= 0 \qquad \forall \quad t > 0 \end{aligned} \tag{8}$$

where $u(t,x)$ is the displacement at time t of a point of the body that was initially at position x. The last boundary condition describes that the end of the object, which is not in contact with the plate, is stress free. When the object ejects from the plate the bottom of the object will also become a free end and so the solution for the problem in equation 8 is only valid as long as the object is in contact with the plate.
The problem above can be transformed into dimensionless form by introducing the following dimensionless variables and parameter:

$$\begin{aligned} z = \frac{x}{L_1} \quad , \quad \tau = \frac{c_1\, t}{L_1} \\ f = \frac{u}{A} \quad , \quad \beta = \frac{\omega\, L_1}{c_1} \end{aligned} \tag{9}$$

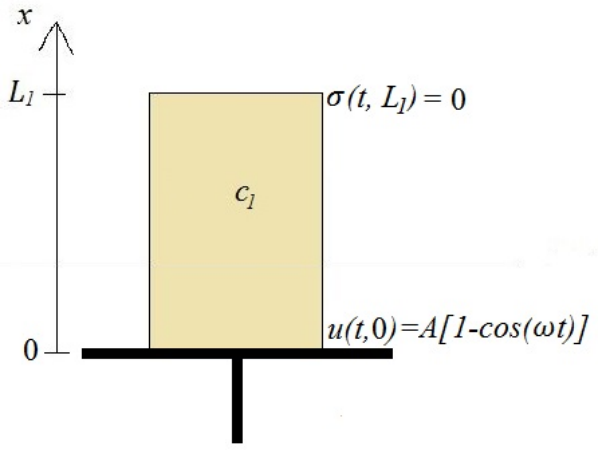

Figure 4: Initial position of a homogeneous elastic object with total length L_1 placed on a plate, which moves harmonically in time.

The dimensionless position z now lies between 0 and 1. The dimensionless time $\tau = \frac{t}{L/c}$ indicates the number of times a wave moves from one end to the other of the object. f is the dimensionless displacement, and the parameter $\beta = \frac{\omega}{c_1/L_1}$ describes the ratio between the plate frequency and the object's basic eigenfrequency. The partial differential equation and its initial and boundary conditions

then become:

$$\frac{\partial^2 f}{\partial \tau^2} = \frac{\partial^2 f}{\partial z^2} \tag{10}$$
$$f(0,z) = 0 \quad , \quad \left.\frac{\partial f}{\partial \tau}\right|_{\tau=0} = 0 \qquad \forall \quad 0 < z < 1$$
$$f(\tau,0) = 1 - \cos(\beta\,\tau) \quad , \quad \left.\frac{\partial f}{\partial z}\right|_{z=1} = 0 \qquad \forall \quad \tau > 0$$

In appendix B the solution methods have been described in detail and all intermediate calculations are shown.

4.1 Analytical solution

Everything calculated in this section has been done using the method explained in section 2.1.1. For detailed calculations of the results shown and explained, see appendix B.1. [2]
The partial differential equation can be solved analytically by Laplace transforming with respect to the time τ from which an ordinary differential equation is gained with respect to z. Then finding the inverse Laplace transform gives the following solution (see appendix B.1.1):

$$f(\tau,z) = 1 - \frac{\cos\left[(1-z)\beta\right]}{\cos(\beta)}\,\cos(\beta\,\tau) + 2\,\beta^2 \sum_{n=0}^{\infty} \frac{\sin(\lambda_n\,z)}{\lambda_n\,(\beta^2-\lambda_n^2)}\,\cos(\lambda_n\tau) \quad , \quad \beta \neq \lambda_n \tag{11}$$

where

$$\lambda_n = \frac{\pi}{2}\,(2n+1) \quad , \quad n = 0,1,2,... \tag{12}$$

are the poles of the solution in Laplace space. They describe the different wave modes that can propogate through the object. It is seen from the infinite sum that the first couple of waves will have the biggest effect on the displacement since the denominator goes as λ_n^3 and the nominator always lies between -1 and 1.

4.1.1 Ejection time and energy transfer factor

When the displacement of every point of the object is known at all times, an expression for the time at which the object ejects from the plate, $\tau = \tau_e$, can be found. Then a quantity describing how much translational kinetic energy the plate has transferred to the object can be found by calculating the energy transfer factor v^2. Its square root is defined as the dimensionless ejection velocity, $v = \frac{v_e}{A\,\omega}$, i.e. the ejection velocity of the elastic object v_e relative to that of a rigid object $A\,\omega$.
As mentioned, the object ejects when the bottom of it, $z = 0$, is also stress-free: $\left.\frac{\partial u}{\partial x}\right|_{x=0} = 0 \Rightarrow \left.\frac{\partial f}{\partial z}\right|_{z=0} = 0$, which gives an equation for the ejection time (see appendix B.1.2):

$$\tan(\beta)\,\cos(\beta\,\tau_e) + 2\,\beta \sum_{n=0}^{\infty} \frac{\cos(\lambda_n\tau_e)}{\beta^2-\lambda_n^2} = 0 \Rightarrow \sum_{n=0}^{\infty} \frac{\cos(\beta\,\tau_e) - \cos(\lambda_n\tau_e)}{\beta^2-\lambda_n^2} = 0 \tag{13}$$

[2] As mentioned, everything in this section about the analytical solution has been reported before in my bachelor project [10], and the only difference is in the definition of z, which makes the solution to the displacement f and the intermediate calculations shown in the appendix a little different.

Since β is proportional to the frequency of the plate, small β means that the plate oscillates slowly. So considering the first equation in equation 13 for $\beta \to 0$ and also assuming that τ_e is finite so that also $\beta\,\tau_e \to 0$ ane upper bound on the ejection time can be found to be $\tau_e^{max} = 4$. In this limit the actual time is $t_e = 2 \cdot \frac{2\,L}{c}$ where $\frac{2L}{c}$ is the period of a stress wave. The upper bound on the ejection time then means that in this limit two stress waves will have time to travel a wavelength each before the object is ejected.

Now that an equation determining the ejection time τ_e for a given plate frequency β is found, an expression for the energy transfer factor can be found. The energy transfer factor is given by the ratio between the ejection velocity of the elastic object and a rigid object. The object's ejection velocity is calculated as the average velocity at ejection time and is in general given by the total momentum divided by the total mass. For this object this is simply $v_e = 1/L \int_0^L \left.\frac{\partial u}{\partial t}\right|_{t=t_e} dx$. So the dimensionless ejection velocity or the (square root of) the energy transfer factor is given by (see appendix B.1.3):

$$\nu = \frac{1}{\beta} \int_0^1 \left.\frac{\partial f}{\partial \tau}\right|_{\tau=\tau_e} dz \Rightarrow \nu = \frac{\tan(\beta)}{\beta}\,\sin(\beta\,\tau_e) + 2\,\beta \sum_{n=0}^{\infty} \frac{\sin(\lambda_n\,\tau_e)}{\lambda_n\left(\beta^2 - \lambda_n^2\right)} \tag{14}$$

It is seen that for $\beta \to 0 \Rightarrow \nu \to 0$. The maximum energy transfer is given by $\frac{d\nu}{d\beta} = 0$ and this then gives an equation for the optimal parameter value β_{opt}:

$$0 = \sin(\beta_{opt}\,\tau_e)\left(\frac{1}{\cos^2(\beta_{opt})} - \frac{\tan(\beta_{opt})}{\beta_{opt}}\right) + \tau_e\,\tan(\beta_{opt})\,\cos(\beta_{opt}\,\tau_e) - 2\,\beta_{opt} \sum_{n=0}^{\infty} \frac{\left(\beta_{opt}^2 + \lambda_n^2\right)\,\sin(\lambda_n \tau_e)}{\lambda_n\,\left(\beta_{opt}^2 - \lambda_n^2\right)} \tag{15}$$

To solve equation 13 such that the energy transfer can be plotted as a function of parameter value, the Newton-Raphson method is used. When calculating the energy transfer there is no need for too many terms in the infinite sum since the numerator only contains cosines which lie between -1 and 1 and the denominator contains λ_n to third order so these terms will quickly become very small.

4.2 Numerical solution

Everything calculated in this section has been done using the method explained in section 2.1.2. For detailed calculations of the results shown and explained, see appendix B.2.
There are N points in the mesh with spacing $\Delta z = 1/N$ between neighbouring points. In figure 5 below the discretization in the z-direction is illustrated, and it also shows the relationship between the Y-vector and the mesh points. The first N elements of the vector are the displacements of the corresponding N mesh points, and the last N elements are the belonging velocities. Notice that the boundary $z = 0$ is not included since the displacement and velocity at this point is already known from the boundary condition.

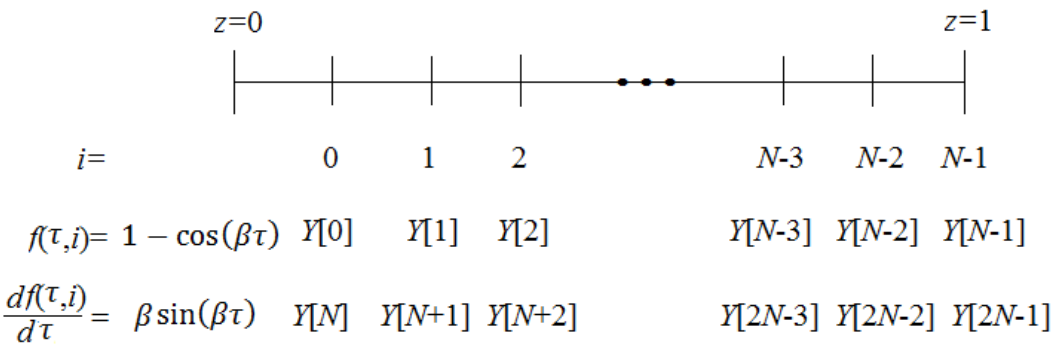

Figure 5: The figure shows that there are N points in the z direction and how the displacements and velocities of these points are related to the Y-vector.

The set of first order ordinary differential equations are then given by (see appendix B.2.1):

$$\begin{aligned}
&\frac{dY[i]}{d\tau} = Y[N+i] \quad \text{for} \quad i = 0, ..., N-1 \\
&\frac{dY[N+i]}{d\tau} = \frac{Y[i+1] - 2\,Y[i] + Y[i-1]}{\Delta z^2} \quad \text{for} \quad i = 1, ..., N-2 \\
&\frac{dY[N]}{d\tau} = \frac{Y[1] - 2\,Y[0] + 1 - \cos(\beta\,\tau)}{\Delta z^2} \\
&\frac{dY[2\,N-1]}{d\tau} = \frac{8\,Y[N-2] - Y[N-3] - 7\,Y[N-1]}{2\,\Delta z^2}
\end{aligned} \tag{16}$$

with initial conditions

$$Y[i] = 0 \quad \text{for} \quad i = 0, 1, ..., 2\,N-1 \tag{17}$$

The last differential equation is found by taylor expanding the displacements at the two points before the boundary $z = 1$ around this point and using the boundary condition.
The set of differential equations above is solved using RK4 as explained earlier (see appendix B.2.4 for the algorithm). But the time step $\Delta\tau$ used to integrate in time cannot be chosen independently from the spatial step Δz. First use non-dimensionless variables, such that the time step is Δt and the spatial step is Δx. When the wave moves from one point in the spatial mesh to another and the amplitude is to be calculated, also at discrete time steps, then this time step has to be less than the time it takes the wave to travel from the first point to the second [15]: $\Delta t < \frac{\Delta x}{c}$, giving that the stability condition is $\Delta\tau \leq \Delta z$ (this is always chosen to be an equality for the numerical solutions).

4.2.1 Ejection time and energy transfer factor

From the section above the displacements and velocities of all N spatial points can be found at all times - as long as the object is still in contact with the plate. To find the time at which the object ejects from the plate the finite difference method based on second order approximations is used again.

The ejection time is found by Taylor expanding the first two points next to the boundary $z = 0$ around this point and using the ejection condition $\left.\frac{\partial f}{\partial z}\right|_{z=0} = 0$. From this the ejection time function below is obtained:

$$E(\tau) = 2\,\beta^2\,\Delta z^2\,(\cos(\beta\,\tau_e) - 1) - 8\,Y[0] + Y[1] + 7\,(1 - \cos(\beta\,\tau)) \tag{18}$$

where the ejection time is given by the first $\tau > 0$ where $E(\tau) = 0$, which can be found by using the bisection method. In bisection E is calculated in each time step and if it changes sign between two subsequent time steps the object ejects at some point between the two time steps. The ejection time itself is then calculated by assuming a linear relationship between the two points (see appendix B.2.2 for a detailed explanation of how to find this τ).

The calculated ejection time is then used to calculate the energy transfer factor which is given by equation 14. The expression for the numerically calculated energy transfer factor is found by using the trapez method as a numerical approximation for the integral and is given by (see appendix B.2.3 for a detailed explanation):

$$\nu = \frac{\Delta z}{\beta}\left(\frac{1}{2}\left(Y[2N-1] + \beta\,\sin(\beta\,\tau)\right) + \sum_{i=0}^{N-2} Y[N+i]\right)\Bigg|_{\tau=\tau_e} \tag{19}$$

4.3 Results

In figure 6 below the ejection time and energy transfer factor have been plotted for different plate frequencies using both the analytical and numerical solutions.

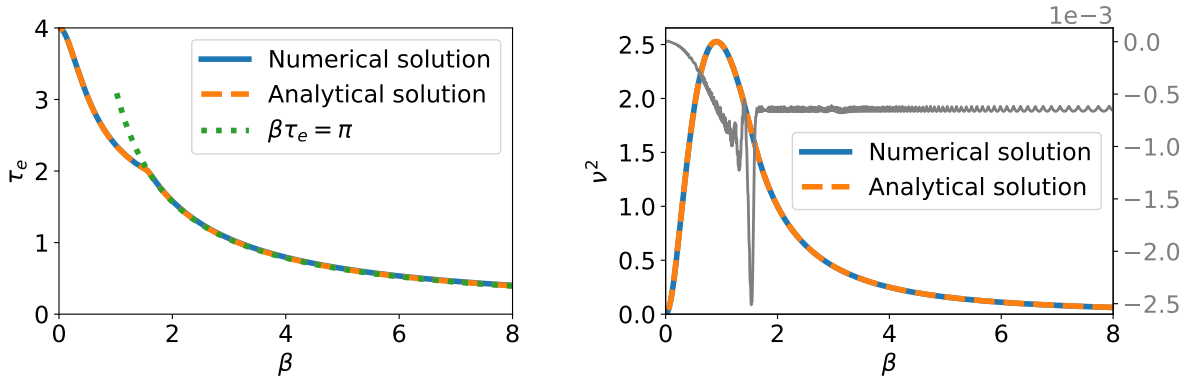

Figure 6: Ejection time τ_e (left) and energy transfer factor ν^2 (right) as a function of parameter value β. The solutions have been found both numerically (blue) and analytically (orange). The grey curve shows the difference between the numerical solution and the analytical solution and is shown on the right vertical axis. The dashed line shows where $\beta\,\tau_e = \pi$. To obtain these plots the mesh has $N = 100$ and the infinite sum has $n_{max} = 100$.

It is seen that the numerical and analytical solutions give approximately the same results. For these plots the number of points in the mesh is $N = 100$ and the number of terms in the infinite sum is $n_{max} = 100$. They grey curve shows the difference between the numerical solution and the analytical solution and it is seen that the difference between the two are of the order 10^{-3} (when considering the energy transfer factor). If both N and n_{max} were instead 50 (or possibly less) it would still be enough such that there is no visible difference, but when finding the maximum energy transfer with several significant digits these have to be increased. The maximum is found at the following parameter value and corresponding ejection time:

$$\beta_{opt} = 0.907 \quad : \quad \tau_e = 2.45 \quad , \quad \nu^2_{max} = 2.53 \tag{20}$$

The homogeneous object is transferred about 253% more translational kinetic energy than a rigid object would have been transferred from the plate. The most optimal ratio of the plate frequency and the basic eigenfrequency is 0.9, and here the object will eject before the plate reaches its maximum displacement from its initial position (corresponding to $\beta\,\tau = \pi$).

It is also seen that for $\beta > \pi/2$ (at this value of β the graph 'breaks') the solutions to the ejection time are given by $\beta\tau_e = \pi$. These solutions corresponds to the object ejecting when the position of the plate is at at $f(\tau_e, 0) = 1 - \cos(\beta\,\tau_e) = 2$, which is its maximum displacement from equilibrium and also where the plate velocity is zero. So it looks like the object will eject from the plate when the position of the plate reaches its maximum for larger plate frequencies. Also, as seen on figure 6 (left), the object will always eject before the plate reaches its maximum the first time since $\beta\,\tau_e \leq \pi\ \forall\ \beta$.

4.3.1 Article comparison

This system has already been solved by C. Raufaste et al [8], where they have introduced f_0/f as the dimensionless frequency - that is the ratio between (double) the eigenfrequency $f_0 = c_1/L_1$ of the elastic wave and the frequency of the plate f. As their dimensionless ejection time they have t_e/T which is the ratio between the actual ejection time and the period of the plate. The relationship between their dimensionless quantities and those used in this thesis are:

$$\frac{f_0}{f} = \frac{\pi}{\beta} \quad , \quad \frac{t_e}{T} = \frac{\beta\,\tau_e}{2\,\pi} \tag{21}$$

In figure 7 below this new dimensionless ejection time (left) and the energy transfer factor (defined the same way) (right) has been plotted as a function of the new dimensionless frequency.

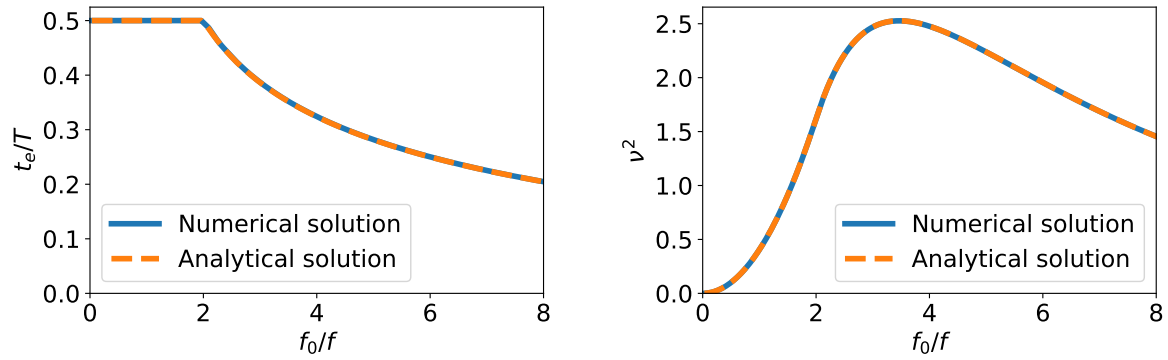

Figure 7: The same plots as they have in the article by C. Raufaste et al [8]. The solutions have been found both numerically (blue) and analytically (orange). To obtain these plots the mesh has $N = 100$ and the infinite sum has $n_{max} = 100$.

Comparing with appendix C where the results from the article are shown, it is seen that these are consistent with the results shown in figure 7. The numerical and analytical solutions used in this thesis give the same results as those in the article. The variable values at maximum are:

$$\frac{f_0}{f} = 3.46 \quad : \quad \frac{t_e}{T} = 0.354 \quad , \quad \nu^2 = 2.53 \tag{22}$$

The region on figure 7 (left) where $t_e/T = 0.5$ is the same region where $\beta\,\tau_e = \pi$. For $f_0/f > 2$ the t_e/T graph decreases and this corresponds to the region where $\beta < \pi/2$. This means that when the plate frequency becomes larger than the eigenfrequency (which is $\frac{1}{2}\,f_0$) the ejection time of the object will always be half the plate period. For smaller plate frequencies, the object will eject sooner.

4.3.2 The $\beta\,\tau_e = \pi$ solutions

It looks like $\beta\,\tau_e = \pi$ is a solution to the ejection time for $\beta > \pi/2$. To see if this is true, this is inserted into the ejection time equation (equation 13) where the left-hand side of the equation gives:

$$\sum_{n=0}^{\infty} \frac{1 + \cos(\lambda_n\,\tau_e)}{(\lambda_n\,\tau_e)^2 - \pi^2} \equiv j(\tau_e) \tag{23}$$

I could not show that this is equal to zero analytically, so the next best thing is to show it numerically. In figure 8 below this function of the ejection time has been plotted for different values of the number of terms n_{max} in the infinite sum.

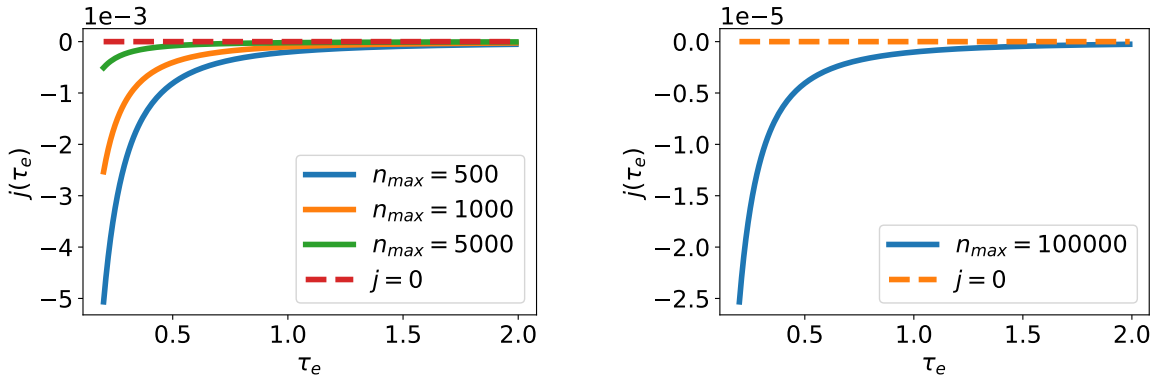

Figure 8: The figure shows the left-hand side of the ejection time equation, equation 13, when inserting $\beta\,\tau_e = \pi$ for $0.2 < \tau < 2$. The value of j has been plotted for different n_{max}.

It is seen that when increasing the number of terms in the sum the quicker the graphs goes to zero. But for all n_{max} the graph becomes very steep for smaller τ_e. This may be because the function $\beta = \pi/\tau_e$ has a very large slope for small τ_e, meaning that β changes quickly between two neighbouring values of τ_e.

For larger β when plotting the figures on figure 6 the analytical solutions will therefore require more terms in the infinite sum than would otherwise be needed for the rest of the β range. For the figures on figure 7 this then means that more terms for smaller values of f_0/f are needed. On the figures themselves it is not very clear that the solutions do not lie exactly on the graph of $\beta\,\tau_e = \pi$, but zooming in or looking more closely on the actual function values of the ejection times it can be seen that these graphs are not exactly the same. This is because of the behaviour of the ejection time equation as shown on figure 8. When more terms in the infinite sum in the analytical expression is needed, it will most likely also mean that more mesh points are needed in the numerical solution.

5 Point mass system

The simplest limit of the general system illustrated in figure 3 is illustrated in figure 4 and this system had a maximum energy transfer factor of about 250%. One can now try to find the largest value of the energy transfer factor for the next simplest limit which is illustrated in figure 9 below.

This time, let there be a second material but now assume that this second material is rigid, i.e. $E_2 \rightarrow \infty$. The object is illustrated in figure 9 with the relevant information also shown. All points in this second material will have the same displacement and so it can effectively be treated as a point mass on top of the first elastic material. This means that the only displacement $u(t,x)$ considered is that of the first material. This second system consisting of a homogeneous elastic material with a point mass on top still obeys the same initial conditions as the first system, and the boundary condition at $x = 0$ (the end of the object that is in contact with the plate) also still applies. But at the other boundary $x = L_1$, there is a material interface where the two materials meet, and this end is no longer free.

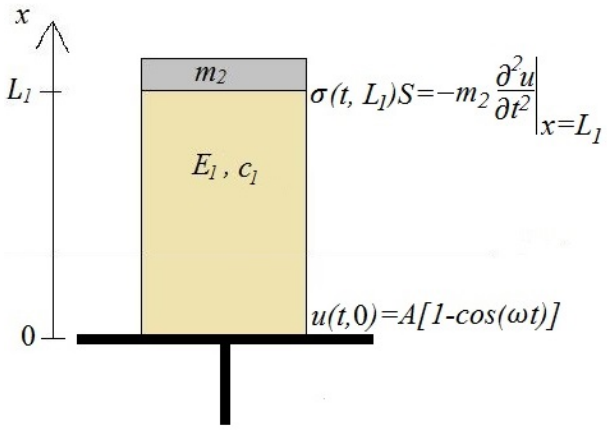

Figure 9: Illustration of an object consisting of a homogeneous elastic material with a point mass stuck to it on top placed on a harmonic plate with corresponding important physical parameters.

Since the point mass is stuck to the elastic material, its acceleration is the same as the acceleration of this end of the elastic material. So it experiences a force of $m_2 \left.\frac{\partial^2 u}{\partial t^2}\right|_{x=L_1}$. The end of the elastic material experiences a force of $\sigma(t, L_1)\, S$. From Newton's third law the two forces must be equal in magnitude but opposite in direction.

So the displacement of the elastic material obeys the following partial differential equation with its initial and boundary conditions:

$$\frac{\partial^2 u}{\partial t^2} = c_1^2 \frac{\partial^2 u}{\partial x^2} \tag{24}$$

$$u(0,x) = 0 \quad , \quad \left.\frac{\partial u}{\partial t}\right|_{t=0} = 0 \qquad \forall \quad 0 < x < L_1$$

$$u(t,0) = A\ [1 - \cos(\omega\, t)] \quad , \quad \left.\frac{\partial u}{\partial x}\right|_{x=L_1} = -\frac{m_2}{E_1\, S} \left.\frac{\partial^2 u}{\partial t^2}\right|_{x=L_1} \qquad \forall \quad t > 0$$

This can be transformed into dimensionless form again using the same dimensionless variables and parameter as for the first system:

$$\frac{\partial^2 f}{\partial \tau^2} = \frac{\partial^2 f}{\partial z^2} \tag{25}$$

$$f(0,z) = 0 \quad , \quad \left.\frac{\partial f}{\partial \tau}\right|_{\tau=0} = 0 \qquad \forall \quad 0 < z < 1$$

$$f(\tau,0) = 1 - \cos(\beta\, \tau) \quad , \quad \left.\frac{\partial f}{\partial z}\right|_{z=1} = -\mu \left.\frac{\partial^2 f}{\partial \tau^2}\right|_{z=1} \qquad \forall \quad \tau > 0$$

where $\mu = \frac{m_2}{m_1}$ is the mass ratios of the point mass and the elastic material. The second system is thus described by two parameters.
In appendix D the solution methods are described in detail and all intermediate calculations and further explanations are shown.

5.1 Analytical solution

Again, the solution method to finding the energy transfer is to first find the solution to the displacement function. From this an expression for the ejection time can be found (by using that the strain changes sign at ejection). And at last the velocity of the object (given as the derivative of the displacement) at ejection time can then be calculated and used to find the energy transfer factor. All the detailed calculations for the analytical solution are shown in appendix D.1.

The solution to the displacement is found to be (see appendix D.1.1):

$$f(\tau, z) = 1 - \frac{\cos\left[\beta(1-z)\right] - \mu\,\beta\sin\left[\beta(1-z)\right]}{\cos(\beta) - \mu\,\beta\sin(\beta)}\cos(\beta\,\tau) + 4\,\beta^2\sum_{n=0}^{\infty}\frac{\sin(\Lambda_n\,z)}{\Lambda_n^2 - \beta^2}\frac{\cos(\Lambda_n\,\tau)}{\sin(2\,\Lambda_n) + 2\,\Lambda_n} \tag{26}$$

where the $\Lambda_n \in \mathbb{R}$ are given by (the poles s_n of the solution in Laplace space are given by $\Lambda_n = is$)[3]

$$1 - \mu\,\Lambda_n\,\tan\left(\Lambda_n\right) = 0 \tag{27}$$

In appendix D.1.1 it is shown that there are only purely imaginary poles, i.e. the equation for the poles $1 - is\mu\tan\left(is\right) = 0$ has no solutions for $s \in \mathbb{R}$ or $s \in \mathbb{C}$.

The solutions to equation 27 lie on the intervals

$$n\pi < \Lambda_n < \frac{\pi}{2}(2n+1) = \lambda_n \quad , \quad n = 0, 1, 2, ... \tag{28}$$

As n increases the solutions move closer to the lower bound. For larger values of μ, the quicker $\Lambda_n \to n\,\pi$, and for smaller values of μ the solutions $\Lambda_n \to \lambda_n$ (which are the poles for the first system). It can also be shown that for $\mu \to 0$ (corresponding to the system with no point mass on top) the displacement function of this system becomes the same as the displacement for the first system.

These poles represent the different wave modes, and the first couple of n have the biggest influence, for example on the displacement f. For smaller values of μ the difference between this second system and the first system will therefore not be very large because the poles are approximately the same for the first couple of n. But for larger values of μ the poles quickly become different from those of the first system and so there is a bigger difference between the two systems. This means that the two objects, the point mass object and the homogeneous object, behave similarly for small μ while it is expected that there will be a larger and larger difference when μ is increased.

[3]It is important to note that it is assumed $\Lambda_n \neq 0$ and $\Lambda_n \neq \beta$ for all n. Zero is already a pole and for $\mu \to \infty$ it seems like it becomes a pole of second order, but it turns out that it then becomes a removable singularity. Then we have the same poles as before but now $\Lambda_n = n\pi$ for $n = 1, 2, ...$ This system is also the system where the second boundary condition is changed to $f(\tau, 1) = 0$, which has these poles (see appendix D.1.3 for the solution to this system).

5.1.1 Ejection time and energy transfer factor

The displacement function can now be used to find an expression for the ejection time. The ejection time condition, i.e. the stress free end condition, then gives the following ejection time equation for the second system (see appendix D.1.2)

$$\frac{\tan(\beta)+\mu\,\beta}{1-\mu\,\beta\,\tan(\beta)}\,\cos(\beta\,\tau_e)+4\,\beta\sum_{n=0}^{\infty}\frac{\Lambda_n}{\beta^2-\Lambda_n^2}\frac{\cos(\Lambda_n\,\tau_e)}{\sin(2\,\Lambda_n)+2\,\Lambda_n}=0 \tag{29}$$

For a set of parameter values, β and μ, the ejection time τ_e is thus found by solving the equation above together with the equation for the poles Λ_n (equation 27). When the ejection time is known, the energy transfer can be found. This is found as the total momentum divided by the total mass (equal to the average velocity of the object) divided by the maximum plate velocity. Since the second material is rigid, its velocity at every material point is the same, which means that its average velocity must be the velocity at $x = L_1$.
Calculating the ejection velocity this way, the following expression for the energy transfer is obtained (see appendix D.1.2):

$$\begin{aligned}
v &= \frac{1}{\beta\,(1+\mu)}\left[\mu\,\left.\frac{\partial f}{\partial\tau}\right|_{(\tau,z)=(\tau_e,1)}+\int_0^1\left.\frac{\partial f}{\partial\tau}\right|_{\tau=\tau_e}dz\right]\Rightarrow \\
v &= \frac{1}{1+\mu}\left[\frac{\sin(\beta)+\mu\,\beta\,\cos(\beta)}{\cos(\beta)-\mu\,\beta\sin(\beta)}\,\frac{\sin(\beta\,\tau_e)}{\beta}+4\,\beta\sum_{n=0}^{\infty}\frac{\sin(\Lambda_n\,\tau_e)}{\beta^2-\Lambda_n^2}\,\frac{1}{\sin(2\,\Lambda_n)+2\,\Lambda_n}\right]
\end{aligned} \tag{30}$$

Notice again, that the later terms in the infinite sum contribute less than the first terms since the denominator, goes as Λ_n^3 which increases with n while the nominator always lies between -1 and 1.

Equation 29 can be solved numerically the same way as for the first system, but for this system it is harder since an upper bound on the ejection time is unknown, and the initial guess is very important in order to get the correct ejection time (the first value of $\tau > 0$ which obeys equation 29).

5.2 Numerical solution

To solve the system numerically the system is again discretized into a set of $2N$ ordinary differential equation obtained from second order finite difference approximations. In appendix D.2 all intermediate calculations for the numerical method for this system are described in detail.

The mesh is again illustrated by figure 5, and the same stability condition is also used for this system. The set of differential equations are given by (see appendix D.2.1):

$$\begin{aligned}
&\frac{dY[i]}{d\tau}=Y[N+i]\quad\text{for}\quad i=0,...,N-1 \\
&\frac{dY[N+i]}{d\tau}=\frac{Y[i+1]-2\,Y[i]+Y[i-1]}{\Delta z^2}\quad\text{for}\quad i=1,...,N-2 \\
&\frac{dY[N]}{d\tau}=\frac{Y[1]-2\,Y[0]+1-\cos(\beta\,\tau)}{\Delta z^2} \\
&\frac{dY[2\,N-1]}{d\tau}=\frac{8\,Y[N-2]-Y[N-3]-7\,Y[N-1]}{2\,\Delta z\,(\Delta z+3\mu)}
\end{aligned} \tag{31}$$

where, just as before, the first N elements of the Y-vector are the displacements and the last N elements are the velocities. Again, the boundary point $z = 0$ is not included in the vector. This system of differential equations has the same initial conditions as the first system, and is also solved the excact same way. It is seen that the system of differential equations are the same as for the first system - the only difference is in the last equation describing the acceleration of the last point, where there is an extra term in the denominator containing the parameter μ.

The results of the solutions to the equations above are used to calculate the ejection time which is also found the same way as for the first system. This ejection time is then used to calculate the energy transfer factor which for this system is given by equations 30. The numerical expression for this is given by (see appendix D.2.2):

$$\nu = \left. \frac{\mu\, Y[2N-1] + \Delta z \left(\frac{1}{2} \left(Y[2N-1] + \beta \sin(\beta \tau) \right) + \sum_{i=0}^{N-2} Y[N+i] \right)}{\beta(1+\mu)} \right|_{\tau=\tau_e} \tag{32}$$

It is seen again that it looks like the energy transfer for the first system. The only difference is the extra term in the nominator describing the velocity of the pointmass, and the extra term in the denominator containing μ.
Solving the system described in equation 24 numerically using second order finite differences and fourth order Runge-Kutta is easily done when it has been done for the first system.

5.3 Results

For each value of μ plotting the ejection time and energy transfer as a function of β gives the same kind of plots as those for the first system in figure 6. Some of these are shown in figure 10 below for both the analytical (the dotted graphs) and numerical solutions (the solid graphs).

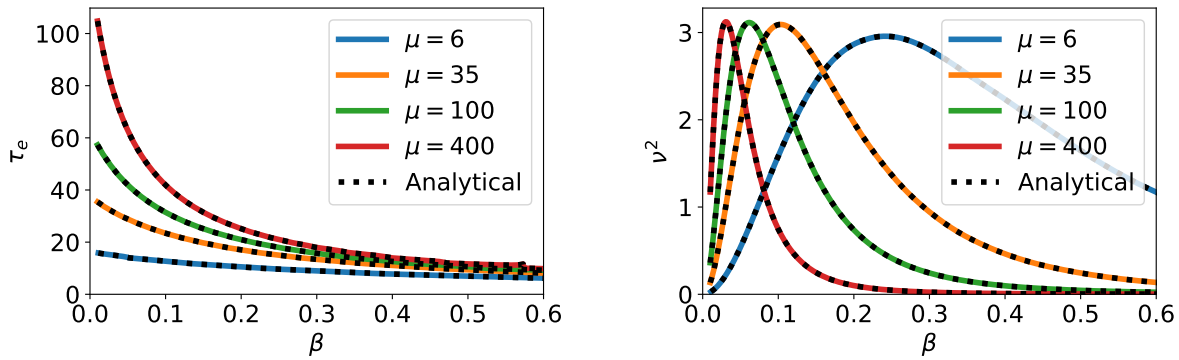

Figure 10: Plot of ejection time for some μ (left) and energy transfer factor (right) as a function of β. The solid curves show the numerical solution while the dotted curves show the corresponding analytical solutions. To obtain these plots the mesh has $N = 100$ and the infinite sum has $n_{max} = 100$.

It is seen that the larger μ becomes, the more narrow the ν^2 graph becomes and its maximum also increases, but slowly. Also notice that the value of β at maximum becomes smaller and smaller as μ

increases. A more clear behaviour can be seen by plotting the maximum of these plots for several μ as shown on figure 11 (top left).

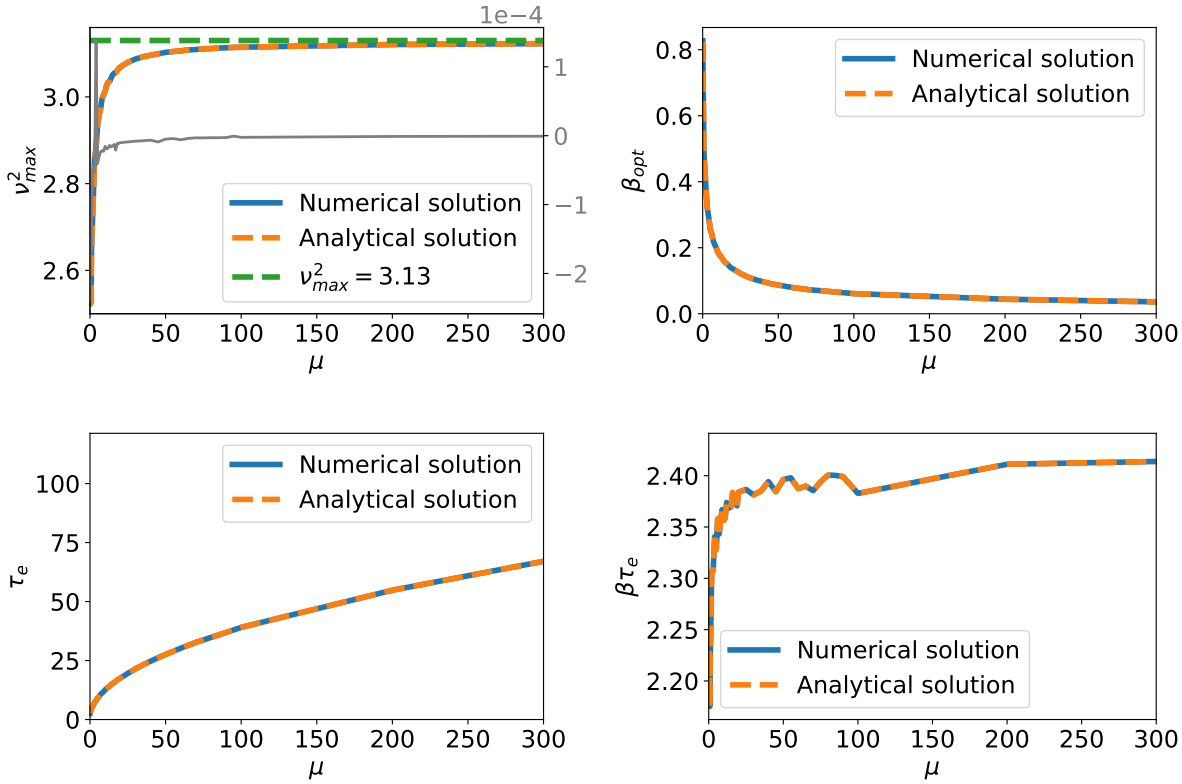

Figure 11: Maximum ν^2 where the difference between the numerical and analytical solution is also shown as the grey curve and on the right vertical axis (top left), the corresponding optimal value of β (top right), the corresponding ejection time (bottom left) and the product of the optimal β and the ejection time (bottom right) as a function of μ. To obtain these plots the mesh has $N = 100$ and the infinite sum has $n_{max} = 100$, and the spacing between neighbouring values of β has been set to 0.001.

Again it is seen that the two solution methods give approximately the same results. For the smallest couple of μ the difference between the numerical and analytical solution for the ν^2_{max} graph (represented by the grey curve) are of the order 10^{-4}, as they were for the first system. But as μ increases the difference becomes smaller, and for the last value of μ, the difference is of the order 10^{-7}.

The maximum energy transfer factor increases with μ and it looks like it has an asymptotic behaviour towards to 3.13 as μ goes to infinity. It is also seen on figure 11 (top right and bottom left) that as μ increases the maximum will have a smaller value of β_{opt} (which is always smaller than 1) and a larger value of τ_e. One could then think that the product of these $\beta\,\tau$ at ejection time for the maximum might also go towards some number. This is plotted in figure 11 (bottom right). If this product also goes towards some constant it means that as μ increases for all the plate frequencies where ν^2 has its maximum the object will eject at the same position of the plate's movement (since $\beta\,\tau$ indicates the plate's position - for example, $\beta\,\tau = \pi$ is the first time the plate reaches its maximum displacement from its original position). On figure 11 (bottom right) it is not as clear whether or not this product also has an asymptotic behaviour. On figure 10 (right) it is seen that for larger values of μ the spacing between neighbouring points of β needs to be smaller around the maximum if the correct maximum is to be found. So a reason that the

$\beta_{opt}\tau_e$ plot does not show a clear asymptotic behaviour could be that the found maximum is not close enough to the actual maximum because the loop over β has too large spacing between neighbouring values.

In figure 12 below the maxima of the type of graphs on figure 10 (right) are found for $\mu = 10^j$ with $j = 1, 1.2, 1.4, ..., 4$ where the spacing between neighbouring values of β is 10^{-4} for smaller values of μ, 10^{-5} for the middle values of μ and 10^{-6} for the larger values of μ. The figure below shows the same type of plots as in figure 11 above but on a logscale and on a wider range of μ.

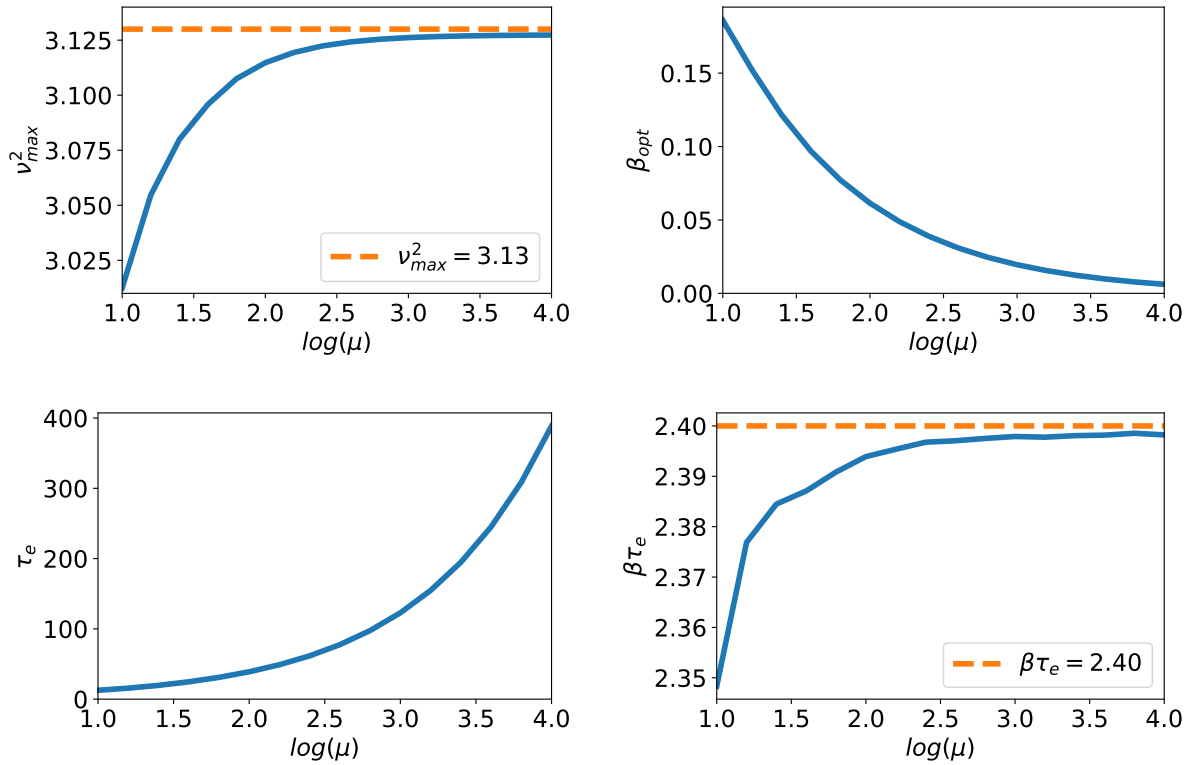

Figure 12: Maximum ν^2 (top left), the corresponding optimal value of β (top right), the corresponding ejection time (bottom left) and the product of the optimal β and the ejection time (bottom right) as a function of μ. To obtain these plots the numerical method has been used with $N = 100$. The spacing between neighbouring values of β range between 10^{-4} and 10^{-6}.

Trying to find more exact values of the maxima makes it clearer that the product $\beta\,\tau$ at ejection time for the maxima are the same for larger μ, it looks like there is an asymptote at the value 2.4. This position of the plate at ejection time for the maxima is smaller than its largest displacement from its initial position ($\beta\,\tau = \pi$), but is also larger than halfway through ($\beta\,\tau = \pi/2$).

The largest value of the energy transfer factor found for the parameter values investigated in these figures are:

$$\mu = 10^4 \quad ; \quad \beta_{opt} = 6.173 \cdot 10^{-3} \quad , \quad \tau_e = 388.5 \quad , \quad \nu^2_{max} = 3.127 \tag{33}$$

5.3.1 Article comparison

F. Celestini et al [9] have already worked with this system (see appendix C for the graphs of their article). In their article they consider the more general system as described in figure 3 that consists of two elastic materials. They then choose the second material such that the system can be considered the same as the theoretical system described in this section consisting of an elastic material and a point mass. So instead of the mass ratio of the two materials, they consider the length ratio $l = L_1/L$. Writing the two masses in μ in terms of their densities and lengths, the relationship between μ and l becomes:

$$\mu = \frac{\rho_2 S (L - L_1)}{\rho_1 S L_1} = \frac{1 - L_1/L}{\rho_1/\rho_2 L_1/L} = \frac{1 - l}{\rho l} \tag{34}$$

where $\rho = \rho_1/\rho_2$ is the ratio of the densities of the two materials. In their article they also have the dimensionless frequency in terms of the total length instead of just the length of the elastic material. Their dimensionless frequency in terms of the dimensionless variables used in this thesis is then

$$\frac{c_1}{L f} = \frac{c_1}{\omega L_1} \cdot 2\pi l = \frac{2\pi l}{\beta} \tag{35}$$

where they also use the plate frequency $f = \frac{\omega}{2\pi}$ instead of the angular frequency ω.
In figure 13 below the maximum energy transfer factor (left) and this new dimensionless frequency (right) have now been plotted as a function of l. These plots corresponds to those in the top part of figure 11.

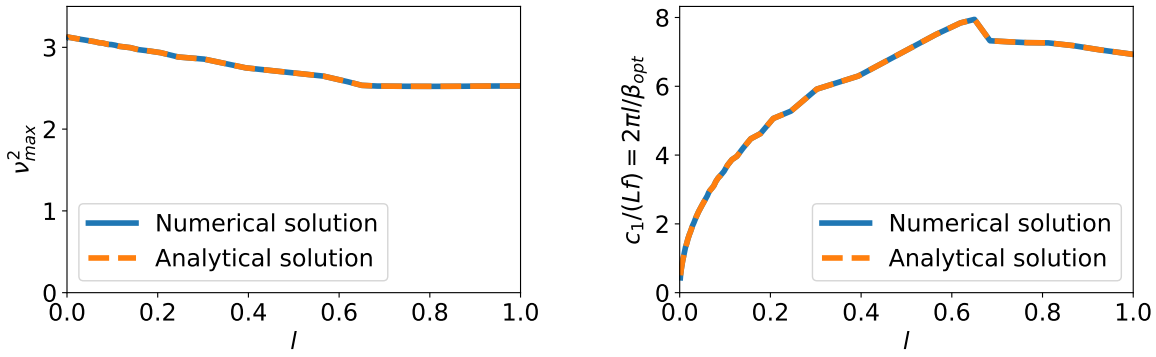

Figure 13: With the same data as in figure 11, the maximum value of v^2 (left) and the value of $\frac{c_1}{Lf} = \frac{2\pi l}{\beta_{opt}}$ (right) is plotted as a function of l. The mesh has $N = 100$ and the infinite sum has $n_{max} = 100$. The densities used are the same as those in the article: $\rho_1 = 1 \cdot 10^3$ kg/m^3 and $\rho_2 = 1.3 \cdot 10^3$ kg/m^3.

It is seen that the system with the largest energy transfer factor is the one where $l \to 0$ which corresponds to $\mu \to \infty$ and both dimensionless frequencies going to zero. It is also seen that for $l = 1$ which corresponds to the first system consisting only of a homogeneous elastic material, the maximum energy transfer factor is consistent with the value 2.5, which was also found for this system. The right plot is also consistent with the result for the first system, since the value of $\frac{c_1}{Lf}$ for $l = 1$ corresponds to the same $\beta_{opt} = 0.91$ found for this system.

In terms of the two new dimensionless variables, the values of these at the largest maximum energy transfer in equation 33 are:

$$l = 1.210 \cdot 10^{-4} \quad , \quad \frac{c_1}{L f} = 0.1323 \tag{36}$$

5.3.2 The $\beta\,\tau_e = \pi$ solutions

In figure 10 (left) it looks like all ejection time graphs for the different μ will follow each other for larger values of β. And for the first system the solutions to the ejection time were $\beta\,\tau_e = \pi$ for $\beta > \pi/2$, so one could think that this might also be the solution that all the graphs of figure 10 (left) are moving toward. Inserting $\beta\,\tau_e = \pi$ in the analytical ejection time equation, the left-hand-side becomes:

$$\frac{\tan(\beta) + \mu\,\beta}{1 - \mu\,\beta\,\tan(\beta)} - 4\,\beta \sum_{n=0}^{\infty} \frac{\Lambda_n}{\beta^2 - \Lambda_n^2} \frac{\cos(\Lambda_n\,\pi/\beta)}{\sin(2\,\Lambda_n) + 2\,\Lambda_n} \equiv j(\beta) \tag{37}$$

I could not show analytically that this is zero for larger values of β, but again this can be investigated numerically. Plotting this as a function of β for different values of μ the plot in figure 14 (top left) is obtained. In this plot the number of terms in the infinite sum has been set to $n_{max} = 50$.

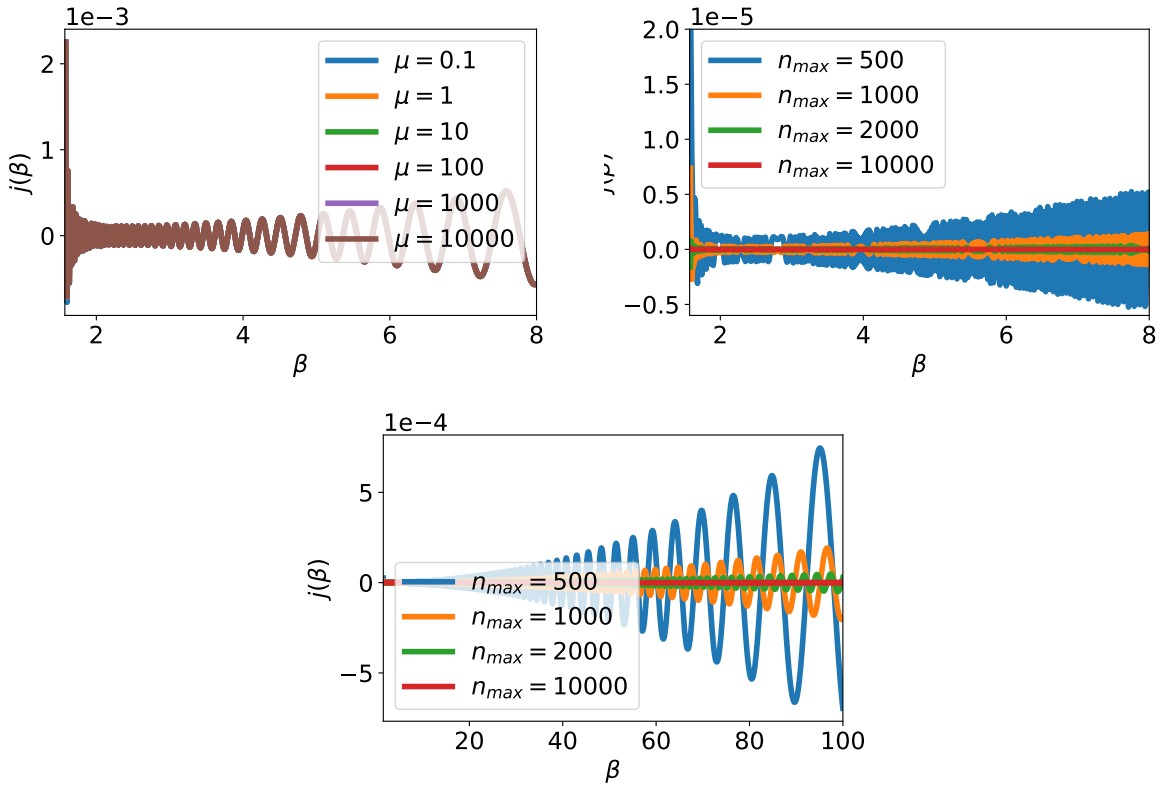

Figure 14: The plots show the graph of $j(\beta)$ for different values of μ with $n_{max} = 50$ (top left) and for different values of n_{max} for $\mu = 100$ (top right). The top right graph has also been shown on a larger range of β (bottom). All plots are shown for $\beta > \pi/2$.

In figure 14 (top left) all graphs lie on top of each other so there is no need to keep plotting for different values of μ when investigating the meaning of n_{max} (plotting for the same values of μ for all the different n_{max} the same behaviour is seen where all the graphs lie on top of each other). In figure 14 (top right) the same plot is shown but for for $\mu = 100$ and for larger values of the number of terms in the infinite sum. It is seen that when increasing the number of terms in the sum the closer to zero $j(\beta)$ will become. But for all n_{max} it also looks like the function makes larger and larger fluctuations away from zero for larger values of β as seen on figure 14 (bottom).

6 Nonhomogeneous system

From the most simple case of figure 3 where the object consists of a single homogeneous elastic material with a maximum energy transfer factor of 253% to the next most simple case where the object consists of an elastic homogeneous material with a point mass on top of it with a maximum energy transfer of 313%, now consider the third system where the object consists of two, generally different, elastic materials on top of each other. This system is illustrated again in figure 15, now where the relevant parameters and boundary conditions are also shown.

Since this nonhomogeneous object consists of two elastic materials, two displacement functions, $u_1(t,x)$ and $u_2(t,x)$, can be considered. u_1 and u_2 describe the displacement of the first material and second material respectively. So each material has its own wave equation for its displacement, but the displacements and stresses over material interfaces always have to be continuous since the two materials are attached. The system is thus described by the following two wave equations with associated initial and boundary conditions:

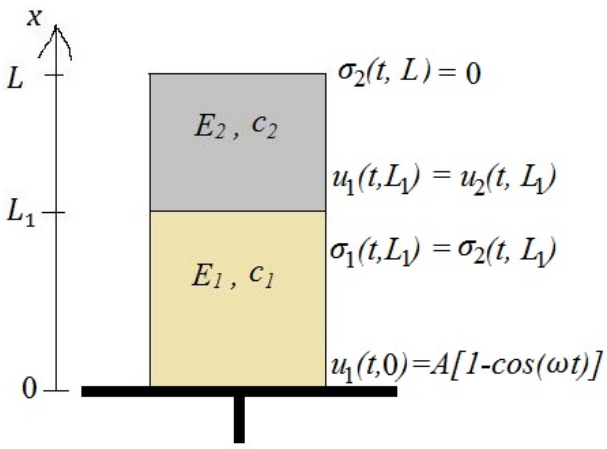

Figure 15: Initial position of a nonhomogeneous elastic object with total length L placed on a plate, which moves harmonically in time. The boundary conditions and relevant physical parameters are also shown.

$$\frac{\partial^2 u_1}{\partial t^2} = c_1^2 \frac{\partial^2 u_1}{\partial x^2} \qquad (38)$$
$$\frac{\partial^2 u_2}{\partial t^2} = c_2^2 \frac{\partial^2 u_2}{\partial x^2}$$
$$u_1(0,x) = 0 \quad , \quad \left.\frac{\partial u_1}{\partial t}\right|_{t=0} = 0 \quad , \quad u_2(0,x) = 0 \quad , \quad \left.\frac{\partial u_2}{\partial t}\right|_{t=0} = 0 \qquad \forall \quad 0 < x < L$$
$$u_1(t,0) = A\ [1 - \cos(\omega t)] \quad , \quad \left.\frac{\partial u_2}{\partial x}\right|_{x=L} = 0 \qquad \forall \quad t > 0$$
$$u_1(t,L_1) = u_2(t,L_1) \quad , \quad E_1 \left.\frac{\partial u_1}{\partial x}\right|_{x=L_1} = E_2 \left.\frac{\partial u_2}{\partial x}\right|_{x=L_1} \qquad \forall \quad t > 0$$

Just as for the two other systems this system can also be transformed into dimensionless form using dimensionless variables and parameters that look like those used for the other systems:

$$f_1 = \frac{u_1}{A} \quad , \quad f_2 = \frac{u_2}{A} \quad , \quad \hat{\tau} = \frac{c_1 t}{L} \quad , \quad \hat{z} = \frac{x}{L} \qquad (39)$$
$$\hat{\beta} = \frac{\omega L}{c_1} \quad , \quad l = \frac{L_1}{L} \quad , \quad e = \frac{E_1}{E_2} \quad , \quad c = \frac{c_1}{c_2} \quad , \quad \rho = \frac{e}{c^2} = \frac{\rho_1}{\rho_2}$$

Notice that the dimensionless displacements, time, position and frequency are defined the same way as for the two previous systems - the only difference is that they are now defined with respect to the total length L of the object (instead of only the length of the first material), but all wave velocities are still in terms of the first material's wave velocity c_1. Four new (but only three independent) parameters are

also introduced: the dimensionless length, the dimensionless Young's modulus, the dimensionless wave velocity and the dimensionless density. Also notice that these new parameters are the ratios of the first material's physical property and the second material's physical property - opposite to the way the mass ratio $\mu = m_2/m_1$ was defined earlier.
In dimensionless form the system then becomes:

$$\begin{aligned} \frac{\partial^2 f_1}{\partial \hat{\tau}^2} &= \frac{\partial^2 f_1}{\partial \hat{z}^2} \\ \frac{\partial^2 f_2}{\partial \hat{\tau}^2} &= \frac{1}{c^2}\frac{\partial^2 f_2}{\partial \hat{z}^2} \end{aligned} \tag{40}$$

$$f_1(0,\hat{z}) = 0 \quad , \quad \left.\frac{\partial f_1}{\partial \hat{\tau}}\right|_{\hat{\tau}=0} = 0 \quad , \quad f_2(0,\hat{z}) = 0 \quad , \quad \left.\frac{\partial f_2}{\partial \hat{\tau}}\right|_{\hat{\tau}=0} = 0 \qquad \forall \quad 0 < \hat{z} < 1$$

$$f_1(\hat{\tau},0) = 1 - \cos(\hat{\beta}\,\hat{\tau}) \quad , \quad \left.\frac{\partial f_2}{\partial \hat{z}}\right|_{\hat{z}=1} = 0 \qquad \forall \quad \hat{\tau} > 0$$

$$f_1(\hat{\tau},l) = f_2(\hat{\tau},l) \quad , \quad e\,\left.\frac{\partial f_1}{\partial \hat{z}}\right|_{\hat{z}=l} = \left.\frac{\partial f_2}{\partial \hat{z}}\right|_{\hat{z}=l} \qquad \forall \quad \hat{\tau} > 0$$

In appendix E the solution methods and all intermediate calculations are derived and shown in detail.

6.1 Analytical solution

The approach to obtaining an analytical solution is the same as for the two previous system, as explained in section 2.1.1. The intermediate steps are now a little harder and longer but it is not impossible to find an expression for the solution. Detailed calculations for the analytical solution are shown in appendix E.1.

The solution to the displacements of each material of the object are found to be (see appendix E.1.1):

$$\begin{aligned} f_1(\hat{\tau},\hat{z}) = 1 &- \frac{\cos\left[\hat{\beta}(\hat{z}-l)\right] + r\tan\left[\hat{\beta}c(1-l)\right]\,\sin\left[\hat{\beta}(\hat{z}-l)\right]}{\cos(\hat{\beta}l) - r\tan\left[\hat{\beta}c(1-l)\right]\,\sin(\hat{\beta}l)}\,\cos(\hat{\beta}\hat{\tau}) \\ &- 2\hat{\beta}^2\sum_n \frac{\sin\left[2c(1-l)\alpha_n\right]\,\sin(l\alpha_n)}{\alpha_n(\hat{\beta}^2-\alpha_n^2)}\,\frac{\cos\left[(\hat{z}-l)\alpha_n\right] + r\tan\left[c(1-l)\alpha_n\right]\,\sin\left[(\hat{z}-l)\alpha_n\right]}{l\sin\left[2c(1-l)\alpha_n\right] + c(1-l)\sin(2l\alpha_n)}\,\cos(\alpha_n\hat{\tau}) \end{aligned} \tag{41}$$

$$\begin{aligned} f_2(\hat{\tau},\hat{z}) = 1 &- \frac{\cos\left[\hat{\beta}c(1-\hat{z})\right]\,\cos(\hat{\beta}\hat{\tau})}{\cos(\hat{\beta}l)\,\cos\left[\hat{\beta}c(1-l)\right] - r\sin(\hat{\beta}l)\,\sin\left[\hat{\beta}c(1-l)\right]} \\ &- 4\hat{\beta}^2\sum_n \frac{\sin(l\alpha_n)}{\alpha_n(\hat{\beta}^2-\alpha_n^2)}\,\frac{\sin\left[c(1-l)\alpha_n\right]\,\cos\left[c(1-\hat{z})\alpha_n\right]\,\cos(\alpha_n\hat{\tau})}{l\sin\left[2c(1-l)\alpha_n\right] + c(1-l)\sin(2l\alpha_n)} \end{aligned}$$

where $r = c/e$, and the α_n which are generally complex (and are related to the poles $s_n = i\,\alpha_n$) are the solutions to the following equation:

$$1 - r\tan(l\alpha_n)\,\tan\left[c\alpha_n(1-l)\right] = 0 \tag{42}$$

Unlike the corresponding equation for the poles for the second system (equation 27) this equation has two trigonometric functions with different arguments. Because of this it is difficult to show whether or

not these $\alpha_n = \sqrt{-s_n^2}$ are either purely imaginary or real or actually complex (in one of the paragraphs in appendix E.1.1 it is shown that there are actually no real poles s_n). But assuming that it is possible to solve equation 42 for some set of parameter values, the two displacement functions are given by equation 41 and the ejection time and energy transfer factor are given by equation 44 and equation 45 written in the section below.

This system should still give the same results as those for the second system in the limit where the second material is a point mass. In the limit where the second material becomes rigid, i.e. $e \to 0$, this also corresponds to $c \to 0$. This is because densities of real materials do not lie on as large a range as the values of Young's modulus do. Considering equation 42 in this limit it is seen that this equation for the poles becomes equation 27 for the poles of the second system with $l\alpha_n = \Lambda_n$ (and these solutions are all real as shown in the paragraphs in appendix D.1.1).
Using that the relationship between the variables and parameters for the two systems are given by:

$$\hat{z} = z\,l \quad , \quad \hat{\tau} = \tau\,l \quad , \quad \hat{\beta} = \frac{\beta}{l} \quad , \quad \frac{1-l}{l\,\rho} = \mu \tag{43}$$

it can be shown that the displacement of the first material becomes the same solution for the displacement of the elastic material in the point mass system. And the displacement of the second material of this nonhomogeneous object can also be shown to be independent of z in this limit and equal to the value of f_1 at $z = l$. This is all shown in appendix E.1.1.

6.1.1 Ejection time and energy transfer factor

The object still ejects from the plate when the end $x = 0$ becomes a free end, and this condition for ejection gives the following ejection time equation (see appendix E.1.2)

$$\begin{aligned} 0 =& \frac{\tan(\hat{\beta}l) + r\tan\left[\hat{\beta}c(1-l)\right]}{1 - r\tan\left[\hat{\beta}c(1-l)\right]\tan(\hat{\beta}l)}\cos(\hat{\beta}\hat{\tau}_e) \\ &+ 2\hat{\beta}\sum_n \frac{\sin\left[2c(1-l)\alpha_n\right]\sin(l\alpha_n)}{\hat{\beta}^2 - \alpha_n^2}\frac{\sin(l\alpha_n) + r\tan\left[c(1-l)\alpha_n\right]\cos(l\alpha_n)}{l\sin\left[2c(1-l)\alpha_n\right] + c(1-l)\sin(2l\alpha_n)}\cos(\alpha_n\hat{\tau}_e) \end{aligned} \tag{44}$$

The energy transfer factor is again found as the total momentum at ejection time divided by the total mass (see appendix E.1.3)

$$\nu = \frac{1}{[l(\rho-1)+1]\,\hat{\beta}}\left[\rho\int_0^l \left.\frac{\partial f_1}{\partial\hat{\tau}}\right|_{\hat{\tau}=\hat{\tau}_e} d\hat{z} + \int_l^1 \left.\frac{\partial f_2}{\partial\hat{\tau}}\right|_{\hat{\tau}=\hat{\tau}_e} d\hat{z}\right] \Rightarrow \tag{45}$$

$$\begin{aligned} \nu = \frac{4\rho\hat{\beta}}{l(\rho-1)+1}\sum_n & \frac{\sin\left[c(1-l)\alpha_n\right]\sin(l\alpha_n)\cos(\alpha_n\hat{\tau}_e)}{(\hat{\beta}^2 - \alpha_n^2)\left(l\sin\left[2c(1-l)\alpha_n\right] + c(1-l)\sin(2l\alpha_n)\right)}\cdot \\ & \left(\frac{\tan(\alpha_n\hat{\tau}_e)}{\alpha_n} + \frac{\tan(\hat{\beta}\hat{\tau}_e)}{\hat{\beta}}\right)\left(\cos\left[c(1-l)\alpha_n\right]\sin(l\alpha_n) + r\sin\left[c(1-l)\alpha_n\right]\cos(l\alpha_n)\right) \end{aligned}$$

6.2 Numerical solution

As explained earlier, the analytical solution is not as easy to obtain systematically for all sets of parameter values as it was for the previous two systems. For the sets of parameter values corresponding to the first

or second system, it is easy to get the solutions because equation 42 for the poles becomes much simpler, but for this general system the pole equation consists of trigonometric functions with arguments that are different and depend on the set of parameter values chosen. So for this system the numerical solution is needed when the goal is to investigate the most optimal set of parameter values for the maximum energy transfer factor. The intermediate calculations for the numerical solution are shown in detail in appendix E.2.

The numerical approach is again the same as for the two previous systems. Now that the two displacement functions are each described by their own wave function the mesh is illustrated as shown on figure 16 below.

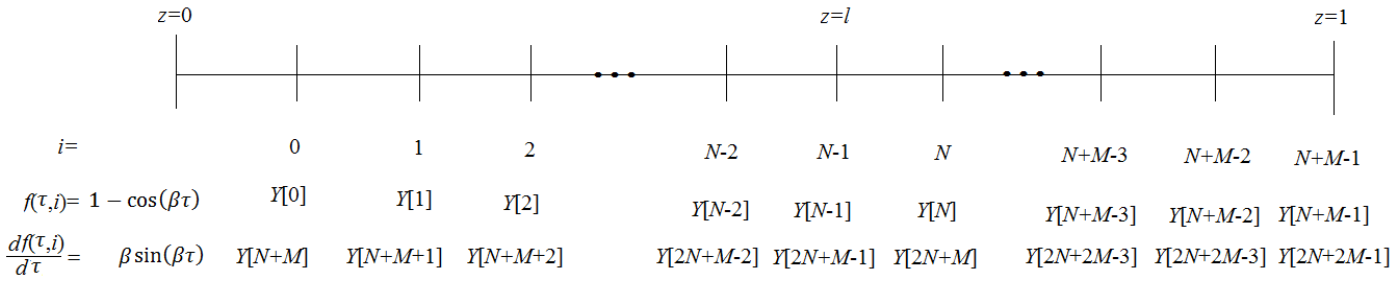

Figure 16: The figure shows how the object is discretized in space.

There are now N elements of the first material and M elements of the second. The first $N+M$ elements of the Y vector are the corresponding displacements of the mesh point, and the last $N+M$ elements are the corresponding velocities. So the Y vector now has $2(N+M)$ elements, and just as before, the boundary point at $z = 0$ is not included.
In the first material the spacing between neighbouring points is $\Delta z_1 = l/N$ while this is $\Delta z_2 = (1-l)/M$ for the second material. The set of differential equations for this system are then given by (see appendix E.2.1)

$$\frac{dY[i]}{d\hat{\tau}} = Y[N+M+i] \quad \text{for} \quad i = 1, ..., N-2 \tag{46}$$

$$\frac{dY[N+Mi]}{d\hat{\tau}} = \frac{Y[1] - 2\,Y[0] + 1 - \cos(\hat{\beta}\,\hat{\tau})}{\Delta z_1^2}$$

$$\frac{dY[N+M+i]}{d\hat{\tau}} = \frac{Y[i+1] - 2\,Y[i] + Y[i-1]}{\Delta z_1^2} \quad \text{for} \quad i = 1, ..., N-2$$

$$\frac{dY[2\,M+N-1]}{d\hat{\tau}} = \frac{e\,\Delta z_2\,(8\,Y[N-2] - Y[N-3]) + \Delta z_1\,(8Y[N] - Y[N+1]) - 7\,Y[N-1]\,(e\Delta z_2 + \Delta z_1)}{2\,\Delta z_1\,\Delta z_2\,\left(e\,\Delta z_1 + c^2\,\Delta z_2\right)}$$

$$\frac{dY[2\,N+M-1+i]}{d\hat{\tau}} = \frac{Y[N+i] - 2\,Y[N-1+i] + Y[N-2+i]}{c^2\,\Delta z_2^2} \quad \text{for} \quad i = 1, ..., M-1$$

$$\frac{dY[2\,N+2\,M-1]}{d\hat{\tau}} = \frac{8\,Y[N+M-2] - Y[N+M-3] - 7\,Y[N+M-1]}{2\,c^2\,\Delta z_2^2}$$

and the system is evolved in time by using RK4. Notice that for the mesh points that are only in one of the materials the equation for their acceleration looks exactly like if it was just a homogeneous system. For the mesh point at $z = l$, the equation for its acceleration is of the same form and consists of a combination

of the two materials parameters. The stability condition is still the same but now that there are two materials, the time step chosen must obey $\Delta\tau \leq \min(\Delta z_1, c\,\Delta z_2)$, where the factor of c comes from the dimensionless wave equation for the second material. As usual, the time step is chosen such that this is an equality.

Just as for the second system, the ejection time equation does not change, but the energy transfer does. Using the same method as for the other two systems, the two numerically calculated integrals that appear in the expression for the energy transfer in equation 45 are approximated using the trapez method to give (see appendix E.2.2):

$$\int_0^l \left.\frac{\partial f_1}{\partial \hat{\tau}}\right|_{\hat{\tau}=\hat{\tau}_e} d\hat{z} \approx \tag{47}$$
$$\Delta z_1 \left(\frac{1}{2}(\hat{\beta}\,\sin(\hat{\beta}\,\hat{\tau}) + Y[2\,N+M-1]) + \sum_{i=0}^{N-2} Y[N+M+i]\right)\Bigg|_{\hat{\tau}=\hat{\tau}_e}$$
$$\int_l^1 \left.\frac{\partial f_2}{\partial \hat{\tau}}\right|_{\hat{\tau}=\hat{\tau}_e} d\hat{z} \approx$$
$$\Delta z_2 \left(\frac{1}{2}(Y[2\,N+M-1] + Y[2\,N+2\,M-1]) + \sum_{i=0}^{M-2} Y[2\,N+M+i]\right)\Bigg|_{\hat{\tau}=\hat{\tau}_e}$$

6.3 Results

Now that the general system consisting of two elastic materials is considered, there are more than two parameters one can change to get different results (there are now four independent parameters). The usual plots for the ejection time and energy transfer can be found again for some sets of parameter values e, ρ, l. These are shown for two different systems in figure 17. The plots on the top of the figure are for an object where the first material (bottom material) is more elastic than the second material with $e = 0.01$, $\rho = 0.1$, and the plots on the bottom of the figure is the other way around with $e = 10$, $\rho = 1$.

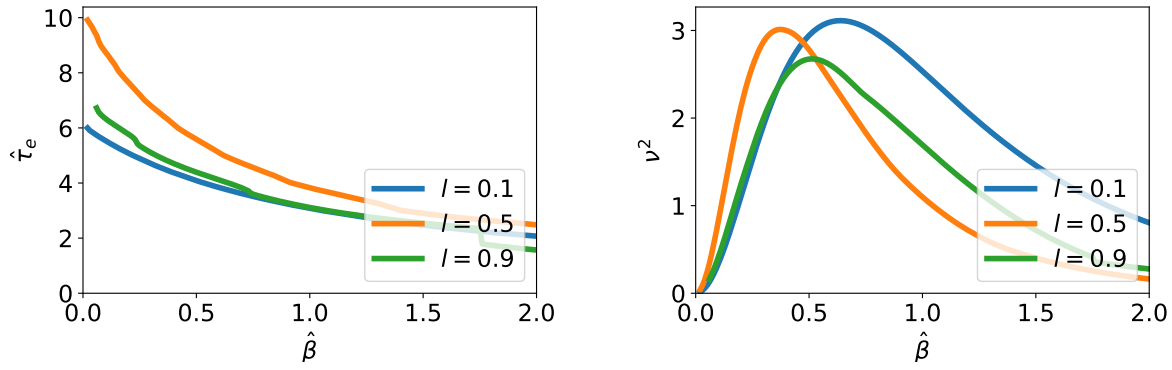

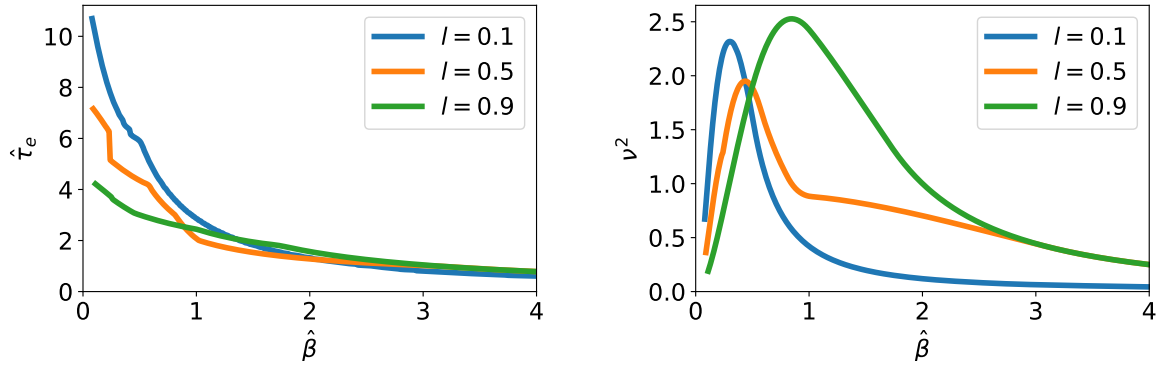

Figure 17: Ejection time (top and bottom left) and energy transfer factor (top and bottom right) as a function of β for different parameter values: $e = 0.01$, $\rho = 0.1$ (top) and $e = 10$, $\rho = 1$ (bottom). The mesh has $N = 100 = M$.

When e is small it corresponds to a system where the object consists of an elastic material with a rigid material on top, while for larger e it corresponds to a rigid material with an elastic material on top. It is seen that for the first plots, the maximum energy transfer is when the second material (rigid) is much longer than the first (elastic) material, while for the second plots the energy transfer factor is larger when the first material (rigid) is longer than the second material (elastic).

When finding the maximum v^2 for different sets of parameter values the results shown in table 3 in appendix E.3 are found. The tendency seen in figure 17 for the maximum is seen again for the other sets of parameter values. For $e < 1$ and $\rho < 1$ the maximum has its largest value for $l < 0.5$. This corresponds to the first material being more elastic and less dense than the second material and for the maximum v^2 to have its largest value the first material must also be shorter than the second material. If it is the other way around instead, where $e > 1$ and $\rho > 1$ the tendency is that the largest v^2_{max} is for $l > 0.5$.

In figure 18 below the tendency described above and some of the results from the table in the appendix are shown.

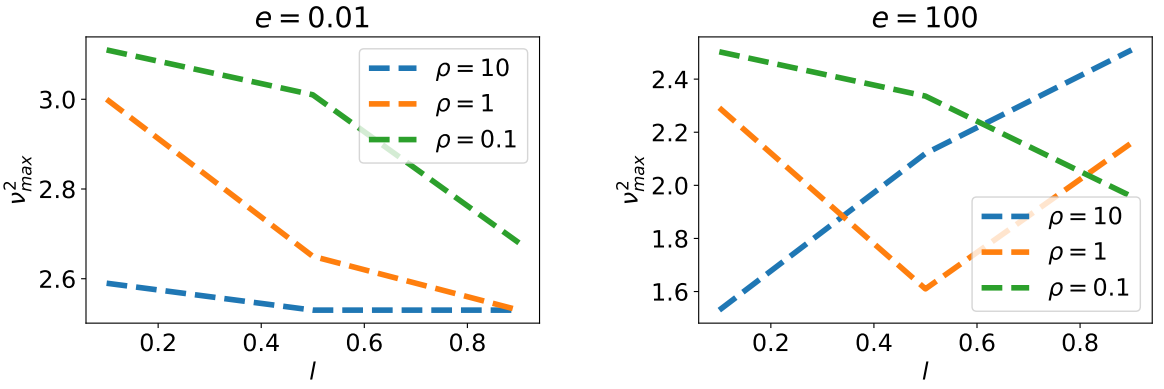

Figure 18: The figures show the maximum v^2 found from the type of graphs in figure 17 (right) as a function of l (only three values are used: 0.1, 0.5, 0.9) for different values of e and ρ. To obtain these plots the mesh has $N = 100 = M$.

When trying to find the largest value of v^2_{max} it is seen that this becomes larger for very small values of all the parameters e, ρ, l. In table 1 below some results are shown. These values were found when trying to find the largest v^2_{max}.

0.1	0.01	3.16	0.05	1900	0.22	10.87	2.99
	0.05	1.41	0.05	380	0.48	4.91	2.99
	0.1	1	0.05	190	0.68	3.47	2.98
0.01	0.01	1	0.05	1900	0.27	8.79	3.12
	0.05	0.45	0.05	380	0.61	3.92	3.12
	0.1	0.32	0.05	190	0.87	2.76	3.12
0.001	0.01	0.32	0.05	1900	0.2823	8.4948	3.1267
	0.05	0.14	0.05	380	0.63	3.81	3.12
	0.1	0.1	0.05	190	0.89	2.69	3.12
0.0001	0.01	0.1	0.05	1900	0.2831	8.4707	3.1268
	0.05	0.045	0.05	380	0.6326	3.7896	3.1241
	0.1	0.032	0.05	190	0.8937	2.6812	3.1208
			0.1	90	0.65	3.69	3.11
			0.3	23.3	0.42	5.68	3.08
			0.5	10	0.37	6.33	3.01
			0.7	4.29	0.39	5.95	2.90

Table 1: Ejection time and maximum energy transfer factor for different sets of parameter values. The values of c and μ for the three indenpendtly chosen parameter values are also shown. To obtain the data the mesh has $N = 100 = M$, and the spacing between neighbouring values of β is either 0.01 or 0.0001.

The length ratio $l = 0.05$ is chosen as the first length to investigate for all sets of e and ρ because it was clear that v_{max}^2 become larger when l was very small. But making l much smaller than this value would be very time consuming. Also when thinking about the system as a real system, it will be more diffucult to make an object where the first material is less than 5% shorter than the second material than just finding a material with a much smaller Young's modulus than the other. That is why e is chosen to be very much smaller than l.

From table 3 in appendix E.3 and also from table 1 above it is seen that one will always get $3 < v_{max}^2 < 3.13$ when $e < 0.1$ and $\mu > 10$. So the two parameters ρ and l can be combined into

a single parameter μ if one wants a maximum energy transfer factor to be more than 3. This can also be seen in figure 18 (left), where the orange and blue graphs have $\mu < 10$ for all the three points, while the green graph has $\mu \geq 10$ for the first two points.
Also notice that when $e < 0.1$, for example see the first rows in table 1 for $e = 10^{-2}, 10^{-3}, 10^{-4}$, it is as if this parameter does not really matter, but only the parameter μ does. So it looks like for $e < 0.1$ this nonhomogeneous system just becomes the point mass system with only the parameter μ distinguishing different objects.

The parameter values and ejection time for the largest value of the energy transfer factor found in this thesis are:

$$e = 10^{-4} \quad , \quad \rho = 0.01 \quad , \quad l = 0.05 \quad ; \quad \hat{\beta}_{opt}\, l = 0.01416 \quad , \quad \frac{\hat{\tau}_e}{l} = 169.4 \quad , \quad \nu^2_{max} = 3.1268 \tag{48}$$

This is the set of parameter values with the smallest values of e, ρ, l investigated, and as seen in the tables it looks like the the maximum energy transfer becomes larger for even smaller values of these. This corresponds to the second system, where the second material is rigid and $\mu \to \infty$. Also notice that the dimensionless plate frequency and ejection time has been rewritten in terms of the variables used for the two first systems so it is possible to compare the results.

6.3.1 Article comparison

As mentioned, F. Celestini et al [9] have already investigated this general system. To compare the numerical method used in this thesis to their numerical results the results are plotted as in their article (see appendix C for their graphs). Instead of changing the plate frequency as in figure 17, they choose two plate frequencies and plot their results as a function of the length ratio. They have these plots for an object where the first material is elastic and the second rigid. The density and Young's modulus for the elastic material are $\rho_1 = 1.0 \cdot 10^3$ kg/m^3, $E_1 = 1.2 \cdot 10^4$ Pa, and for the rigid material these are $\rho_2 = 1.3 \cdot 10^3$ kg/m^3, $E_2 = 3.6 \cdot 10^9$ Pa. The total length of the objects is $L = 15 \cdot 10^{-3}$ m. The two plate frequencies they use are 34 Hz and 76 Hz. In figure 19 below the results are shown. To solve the system numerically the rigid material (which can be thought of as a point mass) does not need to have many mesh points, so this material only has two mesh points (which is the minimum amount of points needed for this numerical method).

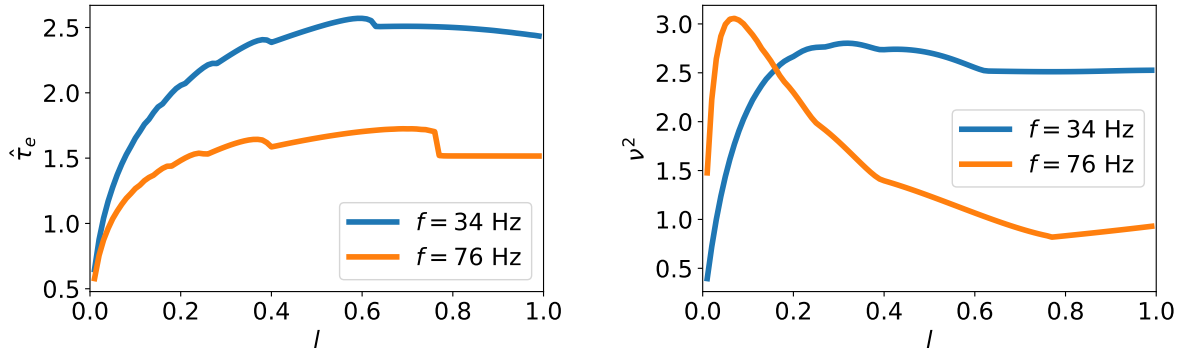

Figure 19: Ejection time and energy transfer factor for two plate frequencies. The rigid material has $M = 2$ mesh points, while the elastic material has $N = 100$ points.

7 Equation of motion for elastic materials with internal friction

For the systems above the elastic waves move throughout the material with a constant amplitude as if there is no type of resistance in the material. But for real materials there will be some kind of internal friction that will damp the elastic waves. This damping might not be large, but a more realistic model for the wave propogation would include the possibility of damping. One such model for viscoelastic materials is the Kelvin-Voigt model, where the damping property is described by the viscosity η and is represented by a dashpot. The elastic properties are described by the Young's modulus and is represented by a spring. In the Kelvin-Voigt model these are assumed to be in parallel (see figure 20).

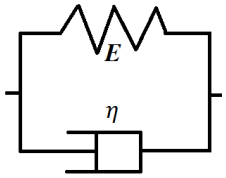

Figure 20: The Kelvin-Voigt model for viscoelastic solids.

Since the two components are in parallel, the strain $\epsilon(x,t)$ is the same, but the stresses might be different. For the elastic component the stress is still described by Hooke's law, $E\,\epsilon(x,t)$, while for the viscous component the stress is given by $\eta \frac{\partial \epsilon(x,t)}{\partial t}$. The total stress is then the sum of these stresses [16]:

$$\sigma(t,x) = E\,\epsilon(x,t) + \eta \frac{\partial \epsilon(x,t)}{\partial t} \tag{49}$$

In this model, a very slow compression ($\partial\epsilon/\partial t \approx 0$) will mean that the viscous term does not contribute much to the total stress. The Kelvin-Voigt model is the model for damping considered in this thesis because it is relatively simple since some analytical considerations can be made, while it is still easy to solve numerically using the same method as for the systems without damping. The model also gives a more realistic behaviour of the elastic materials considered in this thesis than if for example the two components were en series (Maxwell model). Asuming that a stress is applied, using this model would mean that the spring would compress immediately, while the dashpot would react after the spring. Instead, in the Kelvin-Voigt model the dashpot also reacts immediately [16].

Using the Kelvin-Voigt model, the equation of motion for an elastic object then gives the following

damped elastic wave equation:

$$\frac{\partial \sigma}{\partial x} = \rho \frac{\partial^2 u}{\partial t^2} \Leftrightarrow E \frac{\partial^2 u}{\partial x^2} + \eta \frac{\partial^3 u}{\partial t \, \partial x^2} = \rho \frac{\partial^2 u}{\partial t^2} \Leftrightarrow \frac{\partial^2 u}{\partial t^2} = \left(c^2 + \frac{\eta}{\rho} \frac{\partial}{\partial t} \right) \frac{\partial^2 u}{\partial x^2} \tag{50}$$

Consider the elastic objects on the harmonic plate again. The goal was to find the maximum energy transfer, and it is obvious that introducing damping will only lower this value. So it is no longer this maximum energy transfer that is interesting (since it will be largest for $\eta = 0$), but considering the figures from the two articles [8, 9] in appendix C it is seen that they have made some experiments and have data of v^2 for different plate frequencies or length ratios of the object. So using these data one could find the best fit value of η. This is the goal in the subsequent sections.

8 homogeneous object with damping

First consider the homogeneous elastic object on the harmonic plate again, but this time with damping of the elastic waves included. This is represented by the viscosity η of the material. Figure 4 describes the system again, but now there is an extra material parameter because of the viscosity. The displacement $u(t, x)$ of the object is now described by:

$$\begin{aligned} \frac{\partial^2 u}{\partial t^2} &= \frac{\partial^2}{\partial x^2} \left(c_1^2 \, u + \frac{\eta}{\rho_1} \frac{\partial u}{\partial t} \right) \\ u(0, x) = 0 \quad &, \quad \left. \frac{\partial u}{\partial t} \right|_{t=0} = 0 \\ u(t, 0) = A \left[1 - \cos(\omega \, t) \right] \quad &, \quad \sigma(t, L_1) = 0 \end{aligned} \tag{51}$$

It is seen that it is almost the same as equation 8 - only with a damping term included in the wave equation, and the boundary condition at $x = L_1$ now reads that the stress must be zero and not the strain (without damping the two are proportional and so the stress free condition reduces to a strain free condition).

Equation 51 can be written in a dimensionless form again using the same dimensionless variables and parameter as for the system without damping (equation 9), this gives the following dimensionless partial differential equation with corresponding initial and boundary conditions:

$$\begin{aligned} \frac{\partial^2 f}{\partial \tau^2} &= \frac{\partial^2}{\partial z^2} \left(f + R \frac{\partial f}{\partial \tau} \right) \\ f(0, z) = 0 \quad &, \quad \left. \frac{\partial f}{\partial \tau} \right|_{\tau=0} = 0 \\ f(\tau, 0) = 1 - \cos(\beta \, \tau) \quad &, \quad \left. \frac{\partial}{\partial z} \left(f + R \frac{\partial f}{\partial \tau} \right) \right|_{z=1} = 0 \end{aligned} \tag{52}$$

where the new parameter is given by $R = \frac{\eta}{\rho \, L_1 \, c_1} = \frac{\eta \, c_1}{E_1 \, L_1}$ and describes the viscous properties of the material compared to the elastic properties[4]. The function $\frac{\partial}{\partial z} \left(f + R \frac{\partial f}{\partial \tau} \right)$ is the dimensionless stress.

[4] η / E_1 has units of time so it is related to the characteristic time of the damping, and c_1 / L_1 is related to the characteristic time of the wave ($c_1 / (2 L_1)$ is the period of the wave).

8.1 Analytical method

Using the same analytical method as described in section 2.1.1, it is quickly seen that it is now much harder to obtain an analytical expression for the displacement $f(\tau, z)$, and in appendix F.1 the solution is only found in Laplace space. It becomes too complicated to find the inverse Laplace transform. But from the poles of the solution in Laplace space, one can find the critical value of R and the characteristic time for the damping. The interesting poles are given by:

$$s_n = \lambda_n \left(-\frac{R\,\lambda_n}{2} \pm \sqrt{\left(\frac{R\,\lambda_n}{2}\right)^2 - 1} \right) \quad , \quad \lambda_n = \frac{\pi}{2}(2\,n+1)\,,\; n = 0, 1, 2, \ldots \tag{53}$$

where $i\lambda_n$ are the poles for the homogeneous object with no damping (equation 12), and it is seen that for $R = 0$ the poles for the system with damping become the poles for the system without damping. Notice that when damping is included some of the poles are now complex in general compared to without damping where all the poles were only imaginary.

Let the argument of the square root be $D = (R\,\lambda_n/2)^2 - 1$. This term determines whether the poles are real or complex. If R is large enough such that for the first n the first term is larger than one, then D is positive for all n: if $R \geq \frac{4}{\pi} \Rightarrow D \geq 0$ and all $s_n \in \mathbb{R}$. If instead $\frac{4}{3\pi} \leq R < \frac{4}{\pi} \Rightarrow s_0 \in \mathbb{C}$ and all other $s_n \in \mathbb{R}$. If $\frac{4}{5\pi} \leq R < \frac{4}{3\pi} \Rightarrow s_0, s_1 \in \mathbb{C}$ and all other $s_n \in \mathbb{R}$ and so on. This means that for $R \geq \frac{4}{\pi}$ all the s_n poles are only real, but for any other $R < \frac{4}{\pi}$ there will be both real and complex poles.

Remembering that R is the ratio between the viscosity and the Young's modulus of the material, it looks like the s_n poles are only real when the viscosity is large and when the viscosity becomes smaller complex poles also appear. The smaller the viscosity, the smaller the real parts of the complex poles become, and at the same time more of the complex poles appear. Also noting that the inverse Laplace transform consists of terms with a factor $e^{s_n\,\tau}$, this means that real poles will have a damping effect, while imaginary poles will have an oscillation effect. So $R = \frac{4}{\pi}$ is the critically damped limit. For values below this R, the waves will be able to propogate and for values above this R they will not.

Not only does the analytical method give the critical value of the damping, it also gives a time scale of it from the first term in equation 53. This term is always real and negative so when inverse Laplace transforming this will give a factor of a decreasing exponential $e^{-R\lambda_n^2/2\,\tau}$ to each term. This is the effect of the viscosity - it will damp the wave amplitudes with a characteristic (dimensionless) time scale $\tau' = \frac{2}{R\,\lambda_n^2}$. Wave mode n has the characteristic time

$$\tau_n' = \frac{2}{R\,\lambda_n^2} = \frac{8}{\pi^2\,R}\,\frac{1}{(2n+1)^2} \quad , \quad n = 0, 1, 2, \ldots \tag{54}$$

From this it is seen that the higher modes die out quicker, and the most dominating mode is the first one which has the time scale $\tau_0' = 8/(\pi^2\,R)$. Since the relation to the real time t is $\tau = t\,c_1/L_1$, these τ' are also the number of times the wave moves from one end to the other of the object.

This then means that when the object is ejected into the air and if, for example by photo elastic effects (which F. Celestini et al [9] make use of in their experiments), it is made possible to see the waves, then the number of times the wave moves from one end to another can be counted and then an approximate scale of R can be found. For example if one counts that the number of times the wave moves from one

end to another is k at which point the wave amplitude has also dropped to some percentage $e^{-q} = e^{-k/\tau'}$ of its original size, then R is given by

$$k = q\,\tau_0' = \frac{8\,q}{\pi^2\,R} \Leftrightarrow R = \frac{8}{\pi^2}\,\frac{q}{k} \tag{55}$$

For example when looking at the movies F. Celestini et al [9] have as supplemental material it looks like the homogeneous object has $k \approx 20$ after which the wave has pretty much died out, i.e. the wave amplitude has dropped to $e^{-3} \approx 5\%$ of its original size, so for this material the scale of R would be around the value $R \approx 0.1$ with the corresponding viscosity $\eta \approx 6$ Pa·s when using that the article has that: $L = 15$ mm, $\rho_1 = 1000$ kg/m^3 and $E_1 = 12$ kPa. This value of viscosity lies in the range of viscosities they have found in the article [17]. In this article they have investigated the viscosity of different gelatins that are distinguished by concentration, hydration ratios on other parameters. They find that the viscosities lie in the range between 3 Pa·s and 44 Pa·s. The viscosities found in this article cannot be directly compared with the viscosities of the materials used in the two articles [8, 9] since all the paramters that the viscosity depends on is not known. But the article [17] gives an idea of the order of magnitude that the viscosity should have.

Analytically one could find the value of R such that the system is critically damped, and a time scale for the damping of the different wave modes. This is as far as we could get analytically, and to actually solve the system to get values of the energy transfer for different plate frequencies and damping parameters, we must resolve to the numerical solution.

8.2 Numerical method

The numerical solution is found the same way as for the system without damping, as described in section 2.1.2, and figure 5 is considered again as an illustration of the discretization in space. Discretizing the new partial differential equation (PDE) is done the same way as before - but now one has to keep in mind that there is an extra term in the PDE so every time the displacement has been Taylor expanded at some point and it has been used that the double derivative in time and space is the same one needs to add an extra term (coming from the damping term in the damped wave equation). This will affect the governing equations and the ejection time only. The expression for the energy transfer factor is the same.

Again, the procedure is to first find the set of ordinary differential equations for each point of the mesh, and then find the expression for the ejection time function. The equations for the velocities are the same, but the double derivative in time now also contains an extra term containing velocities with a factor R distinguishing this system from the system without damping:

$$\begin{aligned}
\frac{dY[i]}{d\tau} &= Y[N+i] \quad \text{for} \quad i = 0, 1, ..., N-1 \\
\frac{dY[N+i]}{d\tau} &= \frac{Y[i+1] + RY[N+1+i] - 2(Y[i] + RY[N+i]) + Y[i-1] + RY[N-1+i]}{\Delta z^2} \\
&\quad \text{for} \quad i = 0, 1, ..., N-2 \\
\frac{dY[2N-1]}{d\tau} &= \frac{8Y[N-2] - Y[N-3] + 7Y[N-1] + R(8Y[2N-2] - Y[2N-3] + 7Y[2N-1])}{2\Delta z^2}
\end{aligned} \tag{56}$$

The known displacement and velocity at the boundary $z = 0$ (or $i = -1$) has to be used when defining the acceleration at the neigbouring point $i = 0$.

For the boundary $z = 1$, the double derivative in space can be found by taylor expanding the function $f + R\frac{\partial f}{\partial \tau}$ at the points $i = N - 2$ and $i = N - 3$ around $i = N - 1$ (or $z = 1$) and inserting the stress-free boundary condition to get the acceleration at that point.

The numerical ejection time function is then given by

$$E(\tau) = 2\Delta z^2\beta^2\left(1 - \cos(\beta\tau)\right) + 8Y[0] - Y[1] - 7\left(1 - \cos(\beta\tau)\right) + R\left(8Y[N] - Y[N+1] - 7\beta\sin(\beta\tau)\right) \tag{57}$$

and the first time $\tau > 0$ where $E(\tau) = 0$ is found the same way as for all the other systems.

8.2.1 Stability condition

In order for the numerical method to be stable for this system the relationship between the spatial step Δz and the time step $\Delta\tau$ is

$$\Delta\tau \leq \Delta z\left(\sqrt{1 + \left(\frac{R}{\Delta z}\right)^2} - \frac{R}{\Delta z}\right) \tag{58}$$

and in all numerical calculations $\Delta\tau$ is chosen such that the above expression is an equality.

The absolute condition for stability above is derived in the article by Chengyu Sun et al [18]. In their article they derive this by considering finite difference approximations in both time and space. When using their expression for second order approximations in both the expression above is found. If it is true for second order approximations in τ it is also true when using fourth-order Runge-Kutta.

8.3 Results

Now that the set of differential equations, the numerical ejection time function and the stability condition are defined, one can proceed with finding the results the same way as for the first system without damping.

Solving equation 52 numerically for some values of R and plotting the ejection times and energy transfer factors as a function of β again will give the plots shown in figure 21 below.

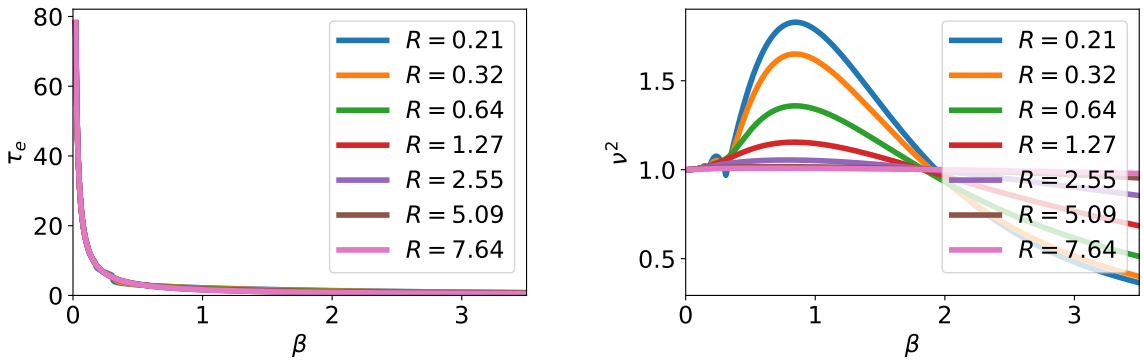

Figure 21: Ejection time (left) and energy transfer factor (right) as a function of β for different values of R, corresponding to $R = m \cdot 4/\pi$ where $m = \frac{1}{6}, \frac{1}{4}, \frac{1}{2}, 1, 2, 4, 6$. To obtain these plots the mesh has $N = 50$.

The value $R = 4/\pi = 1.27$ corresponds to the critically damped limit. It is seen that for all plate frequencies, the energy transfer around its maximum is lower than for $R = 0$, and the larger the value of R is, the smaller the energy transfer becomes. For $R > 4/\pi$, the energy transfer is very close to one for all plate frequencies, and for R smaller than this limit the energy transfer is closer to one (away from the maximum) the larger R is. This is due to the fact that when the system has a value of R larger than the critically damped limit then the waves cannot propagate, and the object then behaves as if it was just a rigid object.

On figure 21 it is also seen, for example on the blue graph, that for smaller values of β the value of ν^2 fluctuates around one. This also happens for the other graphs with smaller values of R. The larger R becomes the smaller the interval of β becomes where this fluctuation in ν^2 occurs.

When looking at the value of E (the numerically found ejection time function) for a value of β before and after the graph of ν^2 jumps, it is seen that the found ejection time makes a big jump compared to other neighbouring values of β (see appendix F.4). For smaller valus of R, corresponding to lower viscosities compared to Young's modulus, and relatively small values of β, corresponding to lower plate frequencies, this behaviour of the objects will begin. This jump in the ejection time, or the delay of it can be explained by realizing that for parameter values as just explained, the elastic properties of the object is stronger than the viscous properties. At first it will seem like the elastic wave can move through the object without damping, but just before it gets completely compressed so it can jump off the plate, the internal friction starts to have an effect and it damps the elastic wave so the object gets compressed slower than without friction, and so the ejection time gets delayed.

8.3.1 Fit of article data

The experimental data from the article by C. Raufaste et al [8] can be fitted to this model of damped elastic wave propogation. The data is fitted by finding the value of R such that the square of the residual r, which is the sum of the difference between the model $y_{model}(i)$ and the experiment $y_{exp}(i)$ of all data points i,

$$r^2 = \sum_i \left[y_{exp}(i) - y_{model}(i) \right]^2 \tag{59}$$

is as small as possible. When doing this for the data points of ν^2 of the soft balls from the graph shown in appendix C it is found that $R \approx 0.1$ with $r^2 \approx 2$, is the best fit to the experimental data. In figure 22 below the experimental data and the model with the best fitted value of R is shown.

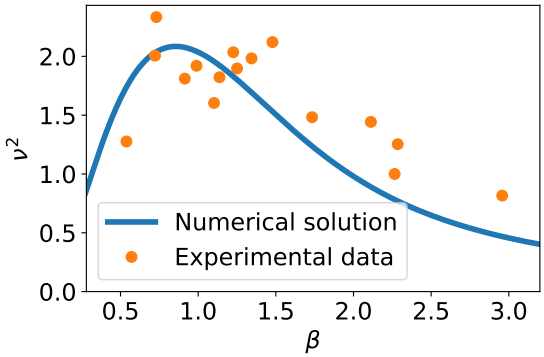

Figure 22: ν^2 as a function of parameter value β for the experimental data and the model for $R = 0.109$ with $r^2 = 1.778$. The mesh has $N = 50$.

As can be seen in figure 22 the experimental method used to obtain the data points are not very good since the points are so spread out and they do not clearly follow any of the curves regardless of which value of R is used. Based on these data it cannot be concluded whether or not viscosity has any significance. But the found value of $R \approx 0.1$ is the one that best fits the given data, and using this, one can then find the best fit for the viscosity.

In the article they write ranges of the values of the Young's modulus and eigenfrequency of the material:

$$2\,\text{kPa} \leq E_1 \leq 20\,\text{kPa} \quad , \quad 50\,\text{Hz} \leq f_0 = \frac{c_1}{L_1} \leq 200\,\text{Hz} \tag{60}$$

Using the definition of R, the viscosity is then given by $\eta = \frac{E_1 R}{f_0}$. So the experimentally determined viscosity of the material lies in the range

$$1\ \text{Pa} \cdot \text{s} \leq \eta \leq 44\ \text{Pa} \cdot \text{s} \tag{61}$$

This is a large range of possible values of the viscosity, but in their article they do not write the specific values of E and f_0 that the material has which they use to get the data points.

In their other article [9] they do write specific values. Assuming that the materials used are similar such that the value of $E_1 = 12$ kPa and $\rho_1 = 1000$ kg/m^3 are the same for these data points, and also using that for the soft balls their radius lies between 5 and 100 mm, so assume that $L_1 = 15$ mm, then the viscosity becomes

$$\eta = R\, L_1 \sqrt{E_1\, \rho_1} \Rightarrow \eta \approx 6\ \text{Pa} \cdot \text{s} \tag{62}$$

Also, in the first article it is not possible to count the number of times a wave moves from one end to the other in their videos. But in the other article the materials are photo elastic and therefore it is possible to do this counting. The found viscosity above when assuming the two materials in the two articles are the same, is very close to the one found when looking at the video and counting the number of times the wave moves back and forth until the wave has almost died out.

9 Point mass system with damping

Now consider the same system as described in the previous section but now the homogeneous object also has a point mass stuck to it at its end $x = L_1$, i.e. the second system with damping included. To describe the damping of the elastic waves the Kelvin-Voigt model is used again, and the only difference between the two systems with or without the point mass is, as it was without damping, that the last boundary condtion (at the end $x = L_1$) is no longer zero but one has to use Newton's third law. Figure 9 describes the system again, but now there is an extra material parameter because of the viscosity. This system is thus described by:

$$\begin{aligned} \frac{\partial^2 u}{\partial t^2} &= \frac{\partial^2}{\partial x^2}\left(c_1^2\, u + \frac{\eta}{\rho_1}\frac{\partial u}{\partial t}\right) \\ u(0,x) = 0 \quad &, \quad \left.\frac{\partial u}{\partial t}\right|_{t=0} = 0 \\ u(t,0) = A\,[1-\cos(\omega\, t)] \quad &, \quad \sigma(t,L_1) = -\frac{m_2}{S}\left.\frac{\partial^2 u}{\partial t^2}\right|_{x=L_1} \end{aligned} \tag{63}$$

Using the same dimensionless variables and parameter as in equation 9, this gives the following dimensionless partial differential equation with corresponding initial and boundary conditions:

$$\begin{aligned} \frac{\partial^2 f}{\partial \tau^2} &= \frac{\partial^2}{\partial z^2}\left(f + R\frac{\partial f}{\partial \tau}\right) \\ f(0,z) = 0 \quad &, \quad \left.\frac{\partial f}{\partial \tau}\right|_{\tau=0} = 0 \\ f(\tau,0) = 1-\cos(\beta\,\tau) \quad &, \quad \left.\frac{\partial}{\partial z}\left(f + R\frac{\partial f}{\partial \tau}\right)\right|_{z=1} = -\mu\left.\frac{\partial^2 f}{\partial \tau^2}\right|_{z=1} \end{aligned} \tag{64}$$

Notice that, again, the only difference between the two models with and without damping is the extra term in the partial differential equation together with the last boundary condition that describes the stress at the end $x = L_1$. Again the last boundary condition just changes such that the left-hand-side reads the new stress from the Kelvin-Voigt model.

9.1 Analytical method

Using the exact same analytical method as for all other four systems, it is again possible to get an expression for the poles of the displacement in Laplace space. Just as for the homogeneous system with damping, it is too complicated to then inverse Laplace transform this solution, but from the expression for the poles a critical value for the damping parameter and the characteristic time for the damping can be found again. In appendix G.1 all the intermediate calculations for the analytical solution are shown. The poles s of this system are given by:

$$\tan(\alpha) = \frac{1}{\mu\,\alpha} \quad , \quad \alpha^2 = \frac{-s^2}{1+R\,s} \tag{65}$$

Notice that the equation above is the exact same equation as equation 27 describing the poles of the system without damping, so the solutions of this equation lie on the same intervals as the Λ_n:

$$n\pi < \alpha_n < \lambda_n = \frac{\pi}{2}(2n+1) \quad , \quad n = 0, 1, 2, ... \tag{66}$$

Just as for the Λ_n (which were related to the poles for the point mass system without damping), these α_n lie closer to the lower bound for larger values of μ and closer to the upper bound for smaller μ. And for increasing n the solutions move closer to the lower bound. All these $\alpha_n \in \mathbb{R}$, and the poles s_n themselves are then given by

$$s_n = \alpha_n \left(-\frac{R\,\alpha_n}{2} \pm \sqrt{\left(\frac{R\,\alpha_n}{2}\right)^2 - 1} \right) \tag{67}$$

Notice that this is the exact same equation as for the homogeneous system with damping - just with α_n instead of λ_n. From this equation a critical value of $R = R_c$ can be found by considering the argument of the square root. If the argument is positive for the first mode, $n = 0$, there will only be real poles, while if it is negative for $n = 0$ there will also be complex poles. So, again, the critical value of the damping parameter is given by this argument being zero for the first wave mode:

$$R_c = \frac{2}{\alpha_0} \Rightarrow R_c > \frac{4}{\pi} \tag{68}$$

Since the lower bound of α_0 is zero the upper bound on the critical value of the damping parameter is infinity. Now the critical value of the damping parameter depends on μ (because α_0 depends on μ), and the larger μ is, the larger this critical value is. For $\mu \to \infty$, the critical value also goes to infinity. The lower bound of the critical value is the critical value for the homogeneous system with damping, corresponding to $\mu = 0$. So for very large values of μ, a large value of the viscosity is needed to overdamp the elastic waves.

From equation 67 it is also possible to get an expression for the characteristic time τ_n' of the damping of each wave mode. This is given by the first term:

$$\tau_n' = \frac{2}{R\,\alpha_n^2} \Rightarrow \frac{2}{\pi^2\,R}\,\frac{4}{(2n+1)^2} < \tau_n' < \frac{2}{\pi^2\,R}\,\frac{1}{n^2} \quad \Rightarrow \quad \tau_1' > \frac{8}{\pi^2\,R} \tag{69}$$

This characteristic time describes how many times the nth wave mode moves from one end to the other and it becomes smaller and smaller for larger wave modes. Thus, just as expected, the dominating wave is the mode $n = 0$. This wave has an upper bound on its characteristic time of infinity. The smaller the value of μ is, the closer the characteristic time is to the lower bound (which, again, is the exact same value as for the homogeneous system with damping), while for very large μ the first mode has $\alpha_0 \to 0$ so the characteristic time goes to infinity. This is consistent with the result just above where it is shown that the critical value of R also goes to infinity for $\mu \to \infty$. This means that, as the point mass becomes larger the wave can move infinitely many time from one end to the other before the wave dies out, i.e the internal friction will never be large enough to make the wave die out.

9.2 Numerical method

Just as before, it is too complicated to try to go further with an analytical solution, and obtaining the ejection times and energy transfer factors for different parameter values is only done by using the numerical method.

Just as for the two first systems described where the discretization gave the excact same governing equations except for the equation for the acceleration at the boundary $z = 1$ where the only difference was an extra term containing μ in the denominator, it is expected that this will again be the only difference between the homogeneous system with damping and the point mass system with damping. I.e. the set of ordinary differential equations should be the same as for the system without damping except for an extra term with the damping parameter R multiplied by the velocities of the same points of the mesh that has their displacements included when considering the system without damping.

Taylor expanding the exact same way again as was done to obtain the last differential equation in equation 56 and inserting the new boundary condition gives (see appendix G.2):

$$\frac{dY[2N-1]}{d\tau} = \frac{8Y[N-2] - Y[N-3] + 7Y[N-1] + R(8Y[2N-2] - Y[2N-3] + 7Y[2N-1])}{2\Delta z(\Delta z + 3\mu)} \tag{70}$$

This equation for the acceleration of the last point in the mesh together with the equation for the other points in equation 56 (except for the last equation which is replaced with the equation above) are the discretized equations for the system. The ejection time is then found the same way as for the homogeneous object with damping, and the energy transfer factor is found the same way as for the point mass system without damping.

9.3 Results

Solving the system numerically and making the same type of plots as usual, figure 23 below is obtained for $\mu = 0.5$ (top part of the figure) and $\mu = 10$ (bottom part of the figure). The system has only been solved for $\beta > 0.05$ and with large spacings between neighbouring values of β. This is because it takes a very long time to get the data points for smaller values of β, especially when R is also large. Larger values of μ also makes it take a long time.

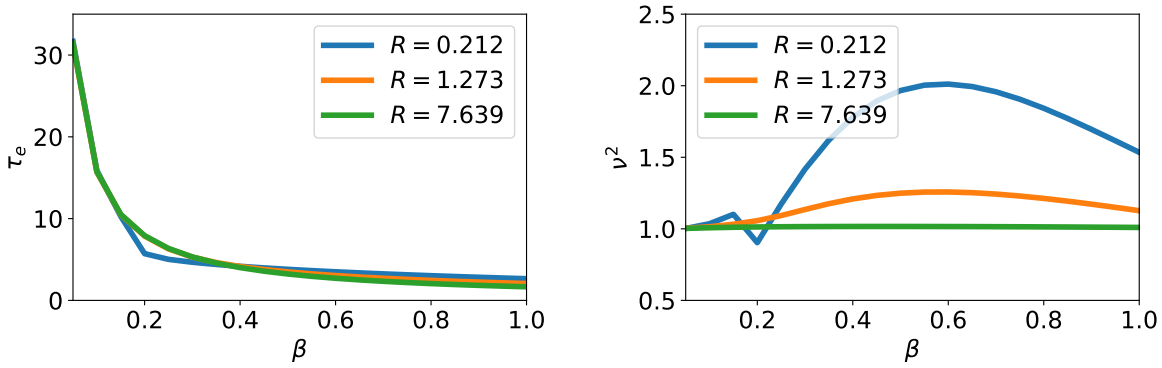

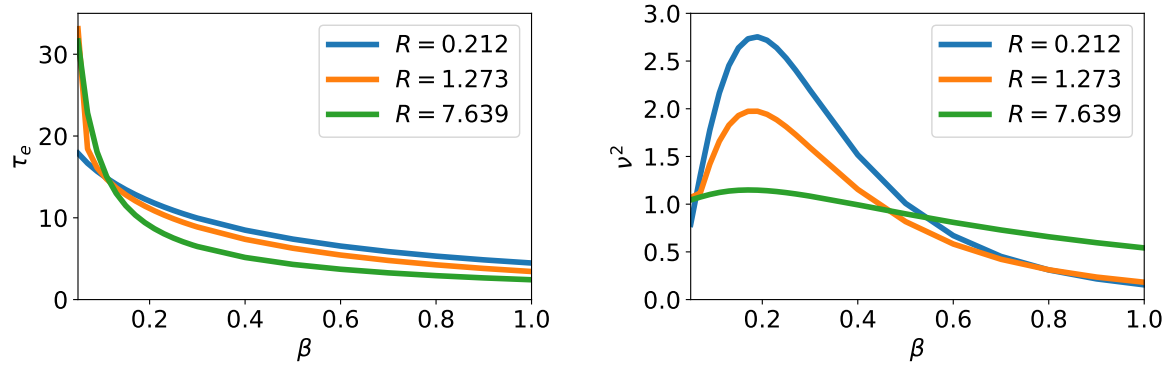

Figure 23: Ejection time (left) and energy transfer factor (right) for $\mu = 0.5$ (top) and $\mu = 10$ (bottom) as a function of β. The graphs are for $R = m \cdot 4/\pi$ with $m = \frac{1}{6}$, 1, 6.The mesh has $N = 100$.

The energy transfer factor graph for $\mu = 0.5$ looks like it is completely flat for $R = 6 \cdot \frac{4}{\pi} \approx 7.64$ at $\nu^2 = 1$ while the graph for $\mu = 10$ is not quite as flat for $R = 6 \cdot \frac{4}{\pi}$. This indicates that the critical value for the damping parameter R is larger for the larger value of μ. For $\mu = 10$ it looks like the critical value of the damping parameter lies between $\frac{4}{\pi} \approx 1.27$ and $6 \cdot \frac{4}{\pi}$. But the behaviour is still the same: the larger the value of R, the smaller the maximum becomes and the graph flattens out and will eventually for some value of R larger than the critical value just behave like a rigid object.

9.3.1 Fit of article data

Fitting the experimental data from the article by F. Celestini et al [9] is done the same way as for the damped homogeneous system. In this article they do experiments for two plate frequencies and vary the length ratio of the two materials. To find the best fit the goal is again to minimize the square of the residual r^2, but since there are two plots the sum of the two r^2 are minimized instead to get an overall best fit for η.

The value of η that fits both sets of experimental data the best is $\eta \approx 2$ with $r^2_{tot} \approx 1$. In figure 24 the model with the best fit for η has been plotted together with the experimental data.

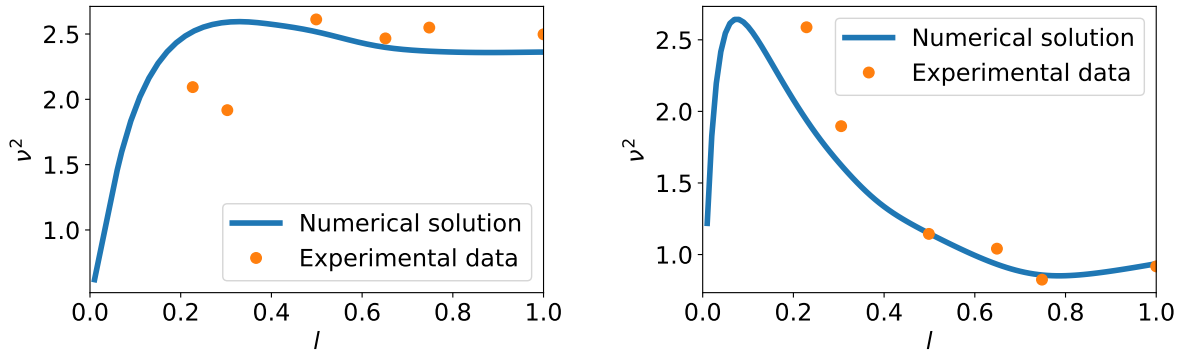

Figure 24: The energy transfer factor as a function of the length ratio for $\eta = 1.673$ that best fit both sets of data points with the total residual $r^2_{tot} = 1.189$. The left plot is for the plate frequency 34 Hz, while the right plot is for plate frequency 76 Hz. The mesh has $N = 100$.

Again it is seen that the fit shown in figure 24 is not a very good one since the data points are too spread out.

10 Discussion

The elastic wave equation for the displacement of three types of elastic objects considered in this thesis has been solved both analytically and numerically. When the solution to the displacement has been found, an expression for the time at which the object ejects from the plate can be found after which the energy transfer factor can be calculated. During the thesis process it quickly became very clear that the numerical method used, was a very time consuming one - especially when the point mass system had a large point mass or viscosity. The precision of the method was also affected by a larger point mass or viscosity. To make the numerical method faster one could define the time in another way: instead of using the absolute time (the real time) t, one could use a relative time $t_r = t - x/c$ where x/c is the local time, i.e. the time it takes the wave to move from 0 to x. With this substitution, the wave equation, which is a second order (in both time and space) partial differential equation, transforms to a first order partial differential equation, in both space and time. This is much faster to solve numerically for the same number of mesh point, since there will now only be N ordinary differential equations when the space is discretized, compared to the $2N$ ordinary differential equations if it was the normal wave equation. On the other hand, the analytical method was relatively easy, and making this substitution would not make it any easier. An analytical expression to the three functions: the solution to the displacement, an expression for the ejection time and energy transfer factor, have been found. What may make the analytical solution hard to obtain is the equation for the poles - especially for the nonhomogeneous system, where the equation for the poles becomes too complicated to solve for a general set of parameter values. But for the homogeneous system and the point mass system the poles are easily obtained or the equation for them can easily be solved numerically. The only difference between these two systems is the introduction of a second parameter μ describing the mass ratios of the two materials. Even though I could not show it analytically, for (dimensionless) plate frequencies $\beta > \pi/2$ it seems like the ejection time equations are independent of μ and have the solution $\beta\,\tau_e = \pi$ to the (dimensionless) ejection time τ_e, while for $\beta < \pi/2$ the ejection time equations for each system needs to be solved to find the ejection time.
$\beta\,\tau_e = \pi$ corresponds to the position of the plate being at its maximum from its initial position the first time. This means that for larger plate frequencies the object will always eject at this plate position, while it will eject earlier in the plate's position for smaller plate frequencies. These larger plate frequencies, i.e. $\beta > \pi/2 \Rightarrow \omega > \omega_0/2$ where $\omega_0 = 2\pi\, c_1/(2L_1)$ is the eigenfrequency of the elastic material, correspond to plate frequencies that are larger than half the eigenfrequency of the first wave mode. For these plate frequencies the ejection time will be $\tau_e < 2 \Rightarrow t_e\, c_1/(2\, L_1) < 1$, meaning that when ejected at the real time t_e the wave will have moved through less than one period. In other words; a stress wave can move from the bottom of the object to the top of it but it will not have had enough time to move the whole way back to the bottom again to push the object off the plate before the plate reaches its maximum displacement. At this point the plate also has zero velocity and after this point it will have negative velocities, so the object has to eject at this time the latest. So for $\beta > \pi/2$ the plate moves so fast that the elastic material does not have time to compress enough to eject by itself as it would for smaller plate frequencies where it ejects before the latest time it has to.

When considering the energy transfer factor it is seen that all three systems have energy transfer factors that are larger than one, meaning that they are transferred more translational kinetic energy from the plate

at ejection time than a rigid object. It is also seen that the system with the largest energy transfer is the point mass system with $v^2_{max} \to 3.13$ for $\mu \to \infty$ where the corresponding $\beta_{opt} \to 0$ and $\tau_e \to \infty$ while the position of the plate at ejection time for this optimum parameter value goes towards some constant, $\beta_{opt}\,\tau_e \to 2.4$.
Considering the nonhomogeneous system, it is found that to get such a large value of the energy transfer, it is not necessary that the second material is a point mass that has much larger mass than the elastic material. Instead what is necessary is that the Young's modulus of the first material is much smaller than that of the second, i.e. the relative Young's modulus e has to be small, the first material has to be very short compared to the second, i.e. the relative length l also has to be small, and the density of the first material relative to the second also has to be small, i.e. the relative density ρ has to be small. Furthermore it looks like the two last parameters can be combined into one: the mass of the second material relative to the first, μ, and this then has to be large. It is also found that for the energy transfer to be in the range $3 < v^2_{max} < 3.13$ these two parameters have to be: $e < 0.1$ and $\mu > 10$. It also looks like as long as $e < 0.1$ this parameter is no longer important and only μ matters in terms of getting a larger v^2_{max}.

In table 2, a summary of the results have been shown. The table shows the parameter and variable values for the largest value of the maximum energy transfer found. Especially for the two last systems one could find even larger values of μ or even smaller values of e, ρ, l to get a larger value for v^2_{max} but when investigating such parameter values it takes a lot more time to get results and the change in v^2_{max} is so small that it is no longer interesting to keep going.

System	e	ρ	l	μ	β_{opt}	τ_e	$\beta_{opt}\,\tau_e$	v^2_{max}
homogeneous	-	-	-	-	0.9070	2.451	2.223	2.528
Point mass	-	-	-	10^4	$6.173 \cdot 10^{-3}$	388.5	2.398	3.127
Nonhomogeneous	10^{-4}	0.01	0.05	$1.9 \cdot 10^3$	$14.16 \cdot 10^{-3}$	169.4	2.398	3.127

Table 2: Summary of the most optimal set of parameter values and corresponding variable values found when investigating the largest value of the maximum energy transfer factor for the three systems without damping.

Also notice that the point mass system has a value of $\beta_{opt}\,\tau_e$ closer to π than the homogeneous system. Since the point mass system is more optimal than the homogeneous system it is expected that this object ejects from the plate closer to the value $\beta\,\tau_e = \pi$ at its maximum since this is the point at which the plate stops transferring positive energy to the object. So the longer an object stays on the plate the more energy it will be able to be transferred. Comparing with a rigid object, which would eject at $\beta\,\tau_e = \pi/2$, it is seen that all the elastic objects always eject at a time after this and that they also have an energy transfer factor of more than one at maximum.

The homogeneous system and point mass system have also been considered where a model for damping of the elastic waves has been included. The model considered in this thesis is the simplest model for viscoelastic solids, the Kelvin-Voigt model where the damping is represented by the viscosity η of the material. For both system some analytical considerations could be made and this gave some interesting insight of the effect of the damping. It was found that the characteristic time of damping of the different wave modes is largest for the first wave mode. The characteristic time for this dominating wave mode

lies on the interval $\frac{8}{\pi^2 R} < \tau_0' < \infty$ where R is the new dimensionless parameter describing the damping properties relative to the elastic properties of the material. For the homogeneous system with damping the characteristic time is exactly equal to the lower bound of the interval, while for larger values of μ the characteristic time moves closer to the upper bound. The critical value of the damping parameter has also been found to lie on the interval $\frac{4}{\pi} < R_c < \infty$, where again for $\mu = 0$ the critical value is exactly equal to the lower bound and as μ increases, the critical value moves the closer to the upper bound. This means that when the point mass gets larger, the larger the viscosity has to be such that the system is overdamped, and thus it takes longer time for the wave to die out. This is because some of the elastic energy converts to kinetic energy in the point mass, and the larger the velocity of the point mass becomes, the more the elastic material can be compressed and thus decompressed afterwards.
For the homogeneous system and point mass system with damping, the numerical solutions were found to be consistent with the critical value of the damping parameter when plotting the energy transfer factor for different dimensionless plate frequencies β. For small values of μ the graphs for $R > 4/\pi$ were flattened out a lot more than the graphs for $R < 4/\pi$. For larger values of μ the critical value of R looked like it was larger than the critical value for the homogeneous system. For values larger than this critical value the objects just behave like a rigid object.

For both the homogeneous system and the point mass system the fit of the model to the experimentally determined ν^2 values were not very good because the data points were too spread out. So from these fits we cannot conclude that the Kelvin-Voigt model for the damping of the elastic waves can describe the data points. The experimental values of ν^2 are calculated by finding the maximum height h of the objects of the free flight after ejection, i.e. the ejection velocity is calculated as $v_e = \sqrt{2gh}$ where g is the gravitational acceleration. To get a better fit one could instead of fitting the model to the ν^2 data, fit it to the data for the ejection time which could be measured very precisely.

As mentioned in the article by F. Celestini et al [9], the results for these systems imply that running shoes can be designed to give the runners a technical advantage. For example, shoes can be optimized such that the energy cost of running decreases (which directly translates to faster running performance) by changing the shoe mass, its cushioning and the longitudinal bending stiffness [6]. The regulation for running shoes in competitions is being debated, and many people in the running community think that the Vapofly shoes blur the line between physiological and technological performance [5]. As could be implied by the results in this thesis, one of the parameters that can be used to optimize running performance is the thickness of the sole, and it has been proposed that this is to be regulated [5] such that the number of parameters that can be tuned for optimization is decreased. One can model a runner with the shoes as the point mass system described in this thesis such that the runner is represented by the point mass, the shoe by the elastic material and the force that the runner pushes their foot to the ground with is represented by the plate. The results of this thesis then insinuate that the change on the thickness of the sole can be substituted with a change in the elastic properties of the shoe in respect to optimization. This is seen by the importance of the parameter β where the length of the material and the elastic wave velocity are combined and this is one of the parameters that determine the maximum energy transfer factor. Thinking of the runner with running shoes as the nonhomogeneous system, the shoe must be much more elastic than the runner such that they can be thought of as a point mass. Furthermore the results tells us that the shoe must be much lighter than the runner and that the eigenfrequency of the elastic material of the shoe must be much larger than the eigenfrequency of the force that the runner pushes the shoe down with.
Modelling a runner this way is of course a great simplification, and in reality it is important to look at the runner as a whole person with muscles, tendons and so on. Making the shoes lighter actually does reduce

the energetic cost of running [19], and this is most likely due the reduced inertia for moving the leg [6]. Then it might seem like it is most optimal to run barefoot, but it is not - barefoot running requires larger muscular effort for cushioning the impact of the foot to the ground [20]. Experiments on treadmills with cushioned surfaces have demonstrated that running on these surfaces reduces the energy cost of running, and this is caused by two things: cushioning allows the runner to run with straighter legs which means that their muscles need to use less effort, and mechanical energy can be stored and then returned on treadmill surfaces [6, 21, 22]. To be realistic one also has to consider the shoes as viscoelastic because most modern running shoes have midsoles that consists of different foam materials, which cushion impact and store and return mechanical energy, and these are viscoelastic [6, 23]. The important factor when the foam is affected by a force, is not only how much the foam is compressed (and thus the amount of energy stored), i.e its compliance, but also how much of the stored energy that is returned (because of the viscous property of the material, some of the energy is dissipated as heat), i.e. its resilience. So the ideal running shoe would have a midsole foam that is very light and also very compliant and resilient [6, 7]. Another factor that can be used to reduce the energy cost of running is to make a shoe that strengthens how the human foot acts like a lever, meaning that the force generated by the calf is transferred to the ground such that the runner is pushed upward and forward [6, 7], and this is the role of the carbon-fiber plate which is used in Nike's Vaporfly shoes. This plate is incorporated into the midsole and as a result, it increases the longitudinal bending stiffness. The energy savings are because of the change in the leverage of the ankle joint and the foot-toe joint [6, 7, 24, 25].

11 Conclusion

The ejection of elastic objects placed on a harmonic plate has been investigated. The quantity of interest is mainly the energy transfer factor describing the amount of translational kinetic energy the elastic object has gained at ejection time compared to the amount that a rigid object would have been transferred. For a homogeneous elastic object the maximum energy transfer is found to be 253% and depends on a single parameter describing the plate frequency relative to the object's eigenfrequency. If a point mass, i.e. a rigid material, is added to the top of the elastic material the energy transfer factor now also depends on the mass of the rigid material relative to the mass of the elastic material. The maximum energy transfer factor becomes larger for this system, and for the mass ratio going to infinity it looks like the maximum energy transfer factor goes towards 313%. But as long as the rigid material has a mass of ten times that of the elastic material, the energy transfer factor becomes larger than 300%. If the second material is another elastic material instead of just a point mass, the energy transfer factor now depends on three other parameters instead of the mass ratio. These new parameters are the Young's modulus and density of the first material relative to that of the second material, and the length of the first material relative to the total length of the object. When investigating the maximum energy transfer again, it is found that the energy transfer factor becomes larger and larger and goes towards 313% when the relative Young's modulus, density and length all become small. The relative density and length can be combined into the same relative mass as was used for the point mass system, and when the Young's modulus of the second material becomes much larger than that of the first material it is only the mass ratio that has an effect on the maximum energy transfer factor. This means that in this case this nonhomogeneous third system reduces to the second system (point mass system). For the nonhomogeneous system, as long as the Young's modulus and mass of the second material is ten times larger than that of the first material, then the maximum energy transfer factor will be more than 300%.

The homogeneous system and point mass system have also been considered when including internal friction in terms of the Kelvin-Voigt model. For both systems it was possible to find analytical expressions for the critical value of the damping and its characteristic time. It has been found that for the homogeneous system with damping, there are specific values for the critical damping parameter and the characteristic time of the damping. For the point mass system with damping, there is only a lower bound on these given by those exact values for the homogeneous system. The upper bounds are infinity, and this means that the greater the point mass is, the larger the viscosity has to be to overdamp the elastic waves. When using the Kelvin-Voigt model and comparing with the data points from the two articles [8, 9] one can find the best fit for the viscosity of the two materials used in the articles. From these fits it cannot be concluded that the experimental homogeneous and point mass system can be described by the Kelvin-Voigt model because of the large spread of the data points.

But in respect to the maximum energy transfer factor, including damping will not optimize this. The larger the damping parameter is, the more the objects will just behave as rigid objects and the energy transfer factor will go towards one for alle plate frequencies.
So in terms of energy transfer, a homogeneous elatic object is more optimal than a purely rigid object, and an object consisting of a homogeneous elastic material with a rigid material on top is even more optimal. The homogeneous object is transferred 2.53 times more translational kinetic energy than a purely rigid object while an object represented by the point mass system is transferred 3.13 times more translational kinetic energy.

Putting the results of this thesis in perspective, it is implied that, for example, running shoes can be optimized in the sense that the runners need to use less energy to run faster. Thinking of this situation as the point mass system described in this thesis (a very gross simplification), the results imply that for maximum energy transfer the important parameters are: the elastic properties of the shoe sole and the thickness of it and the mass of the shoe compared to the mass of the runner. The results of this thesis tells us that optimization of running performance can be accomplished by making the shoes very light and by changing the sole thickness or changing the elastic properties of the material that the shoe is made of. This is consistent with research on the subject of optimizing running shoes to reduce the energy cost of running [6, 7], but the real reason is explained by physiological and biomechanical mechanisms of running that needs to be taken into account to understand the system better.

References

[1] R. McN. Alexander, H. C. Bennet-Clark, *Storage of elastic strain energy in muscle and other tissues*, Nature, January 1977.
Link: https://www.nature.com/articles/265114a0

[2] Keitaro Kubo, Yasuo Kawakami, Tetsuo Fukunaga, *Influence of elastic properties of tendon structures on jump performance in humans*, Journal of Applied Physiology, December 1999.
Link: https://journals.physiology.org/doi/full/10.1152/jappl.1999.87.6.2090

[3] Neil T. Roach, Madhusudhan Venkadesan, Michael J. Rainbow, Daniel E. Lieberman, *Elastic energy storage in the shoulder and the evolution of high-speed throwing in Homo*, Nature, June 2013.
Link: https://www.nature.com/articles/nature12267

[4] M. Phomsoupha, G. Laffaye, C. Cohen, C. Clanet, *How to use the elasticity of a badminton racket to increase its speed by 80%?*, Computer Methods in Biomechanics and Biomedical Engineering, October 2015.
Link: https://www.tandfonline.com/doi/full/10.1080/10255842.2015.1069607?needAccess=true

[5] Geoffrey T Burns, Nicholas Tam, *Is it the shoes? A simple proposal for regulating footwear in road running*, British Journal of Sports Medicine, 2020.
Link: https://bjsm.bmj.com/content/54/8/439

[6] Wouter Hoogkamer, Shalaya Kipp, Jesse H Frank, Emily M Farina, Geng Luo, Rodger Kram, *A Comparison of the Energetic Cost of Running in Marathon Racing Shoes*, Sports Medicine, 2018.
Link: https://link.springer.com/article/10.1007%2Fs40279-017-0811-2

[7] Wouter Hoogkamer, Shalaya Kipp, Rodger Kram, *The Biomechanics of Competitive Male Runners in Three Marathon Racing Shoes: A Randomized Crossover Study*, Sports Medicine, 2019.
Link: https://link.springer.com/article/10.1007%2Fs40279-018-1024-z

[8] Christophe Raufaste, Gabriela Ramos Chagas, Thierry Darmanin, Cyrille Claudet, Frédéric Guittard, Franck Celestini, *Superpropulsion of Droplets and Soft Elastic Solids*, Physical Review Letters, September 2017.
Link: https://journals.aps.org/prl/abstract/10.1103/PhysRevLett.119.108001

[9] Franck Celestini, Joachim Mathiesen, Médéric Argentina, Christophe Raufaste, *Contact Layer as a Propelling Advantage in Throwing*, Physical Review Letters, October 2020.
Link: https://journals.aps.org/prapplied/abstract/10.1103/PhysRevApplied.14.044026

[10] Nikka Mosleh, *Energy transfer from oscillator to elastic object*, June 2019.

[11] Alan Giambattista, Betty McCarthy Richardson, Robert C. Richardson, *College physics, with an integrated approach to forces and kinematics*, Boston, McGraw-Hill, 2010.

[12] Hugh D. Young, Roger A. Freedman, *University Physics With Modern Physics*, Pearson, 14th edition, 2016.

[13] B. Lautrup, *Physics of Continuous Matter*, CRC Press, NW, 2nd edition, 2011.

[14] K. F. Riley, M. P. Hobson, *Essential Mathematical Methods*, Cambridge University Press, 2011.

[15] Michael T. Heath, *Scientific computing: an introductory survey*, McGraw-Hill, 2nd edition, 2002.

[16] Kelly, PA., *Mechanics Lecture Notes: An introduction to Solid Mechanics - chapter 10*, [Online; accessed 05-dec-2021]
Link: https://pkel015.connect.amazon.auckland.ac.nz/SolidMechanicsBooks/Part_I/index.html

[17] Ching-Wen Liu, Li-Ching Chang, Kai-Jen Lin, Tsan-Jung Yu, Ching-Chung Tsai, Hao-Kuang Wang, Tong-Rong Tsai, *Preparation and Characterization of Gelatin-Based Mucoadhesive Nanocomposites as Intravesical Gene Delivery Scaffolds*, BioMed Research International, December 2014.
Link: https://www.hindawi.com/journals/bmri/2014/473823/

[18] Chengyu Sun, Yunfei Xiao, Xingyao Yin, Hongchao Peng, *Stability condition of finite difference solution for viscoelastic wave equations*, Earthquake Science, October 2009.
Link: https://www.equsci.org.cn/article/app/id/b447ec09-80b8-4b6f-98b8-bc50d2311852/relative?pageType=en

[19] Jason R. Franz, Corbyn M. Wierzbinski, Rodger Kram, *Metabolic Cost of Running Barefoot versus Shod*, Medicine & Science in Sports & Exercise, August 2012.
Link: https://journals.lww.com/acsm-msse/Fulltext/2012/08000/Metabolic_Cost_of_Running_Barefoot_versus_

[20] David Kryztopher Tung, Jason R. Franz, Rodger Kram, *A Test of the Metabolic Cost of Cushioning Hypothesis during Unshod and Shod Running*, Medicine & Science in Sports & Exercise, February 2014.
Link: https://journals.lww.com/acsm-msse/Fulltext/2014/02000/A_Test_of_the_Metabolic_Cost_of_Cushioning

[21] Amy E. Kerdok, Andrew A. Biewener, Thomas A. McMahon, Peter G. Weyand, Hugh M. Herr, *Energetics and mechanics of human running on surfaces of different stiffnesses*, Journal of Applied Physiology, February 2002.
Link: https://journals.physiology.org/doi/full/10.1152/japplphysiol.01164.2000

[22] James A. H. Smith, Alexander D. McKerrow, Tertius A. Kohn, *Metabolic cost of running is greater on a treadmill with a stiffer running platform*, Journal of Sports Sciences, August 2016.
Link: https://pubmed.ncbi.nlm.nih.gov/27575734/

[23] M. R. Shorten, *The energetics of running and running shoes*, Journal of Biomechanics, 1993.
Link: https://pubmed.ncbi.nlm.nih.gov/8505351/

[24] Jean-Pierre R. Roy, Darren J. Stefanyshyn, *Shoe Midsole Longitudinal Bending Stiffness and Running Economy, Joint Energy, and EMG*, Medicine & Science in Sports & Exercise, March 2006.
Link: https://journals.lww.com/acsm-msse/Fulltext/2006/03000/Shoe_Midsole_Longitudinal_Bending_Stiffness

[25] Keonyoung Oh, Sukyung Park, *The bending stiffness of shoes is beneficial to running energetics if it does not disturb the natural MTP joint flexion*, Journal of Biomechanics, February 2017.
Link: https://www.sciencedirect.com/science/article/abs/pii/S0021929017300155?via%3Dihub

[26] Murray R. Spiegel *Schaum's outlines: Mathematical Handbook*, McGraw-Hill, 1996.

A Strain from gravity compared to stress wave for point mass system

Assume now that gravity is present such that the second material also provides a strain to the first material. This strain is given by

$$\frac{F_g}{S} = \sigma = E_1 \epsilon_g \Leftrightarrow \epsilon_g = \frac{\rho_2 (L - L_1) g}{E_1} \tag{71}$$

using $\rho_2 = 1300$ kg/m^3, $E_1 = 1.2 \cdot 10^4$ Pa, $L = 1.5 \cdot 10^{-2}$ m and $g = 9.82$ m/s^2. If $l = 0.1$ the strain becomes $\epsilon_g = 0.01436 = 1\%$.
Now the strain at the end of the elastic object is given by

$$\epsilon_e = \left.\frac{\partial u_p}{\partial x}\right|_{x=L_1} = \frac{A}{L_1} \left.\frac{\partial f_p}{\partial z}\right|_{z=1} = -\frac{A}{L_1}\mu \left.\frac{\partial^2 f_p}{\partial \tau^2}\right|_{z=1} \tag{72}$$

where $\left.\frac{\partial^2 f_p}{\partial \tau^2}\right|_{z=1}$ can be found numerically. The plate amplitude is $A = 1 \cdot 10^{-3}$ m.
When plotting the strain as a function of time until the object ejects for two plate frequencies we get the graphs in figure 25 below.

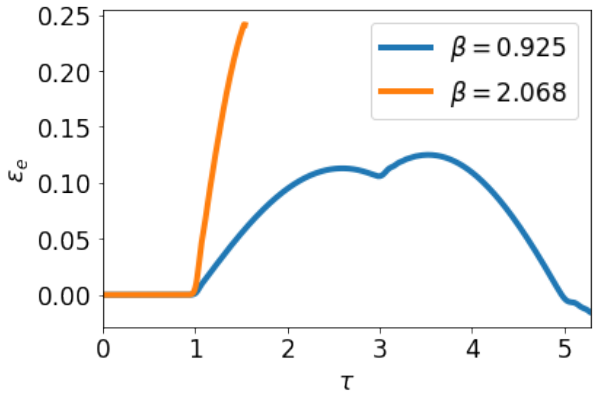

Figure 25: The figure shows plots of the strain on top of the elastic material as a function of time for two plate frequencies (correspoinding to real frequencies 34 Hz and 76 Hz). The number of points in the mesh has ben set to 100.

The maximum strains are $\epsilon_e = 0.125 = 13\%$ and $\epsilon_e = 0.241 = 24\%$ for the frequencies 34 Hz and 76 Hz respectively. Lowering the frequency even more also lowers the maximum strain. This means that for smaller plate frequencies the strain caused by gravity is not negigible compared to the elastic strain when doing experiments.

B Intermediate calculations for homogeneous system

Equation 10 describes the partial differential equation with corresponding initial and boundary condition that the displacement of the homogeneous elastic object must obey.

B.1 Analytical method

Everything in this section has already been reported once before in my bachelor project [10] though with $z \to z - 1$.

B.1.1 Solution to displacement

Solution in Laplace space To solve the partial differential equation we can use the method of Laplace transformation in τ to get an ordinary differential equation in z, which is easy to solve in Laplace space. Then we can inverse Laplace transform to get the solution in real space. In equation 73 below the definition of the Laplace transformation of a function $f(\tau, z)$ with respect to τ has been written. The Laplace transform of the different types of functions involved in the partial differential equation and its boundary condition has also been written [14]

$$\begin{gathered} \mathscr{L}\left[f(\tau,z)\right] = F(s,z) = \int_0^\infty e^{-s\,\tau}\, f(\tau,z)\, d\tau \\ \mathscr{L}\left[\frac{\partial^2 f}{\partial \tau^2}\right] = s^2\, F(s,z) - s\, f(0,z) - \left.\frac{\partial f}{\partial \tau}\right|_{\tau=0} \quad , \quad \mathscr{L}\left[\frac{\partial^2 f}{\partial z^2}\right] = \frac{d^2 F}{dz^2} \\ \mathscr{L}\left[1 - \cos(\beta\,\tau)\right] = \frac{1}{s} - \frac{s}{s^2+\beta^2} = \frac{\beta^2}{s\,(s^2+\beta^2)} \end{gathered} \tag{73}$$

where $s \in \mathbb{C}$ in general.
In Laplace space, equation 10 then becomes

$$\begin{gathered} \frac{d^2 F}{dz^2} + (-s^2)\, F^2 = 0 \\ F(s,0) = \frac{\beta^2}{s\,(s^2+\beta^2)} \quad , \quad \left.\frac{dF}{dz}\right|_{z=1} = 0 \end{gathered} \tag{74}$$

The general solution to this is

$$F(s,z) = k_1\, \sin\left(\sqrt{-s^2}\, z\right) + k_2\, \cos\left(\sqrt{-s^2}\, z\right) \Rightarrow \frac{dF}{dz} = \sqrt{-s^2}\left[k_1\, \cos\left(\sqrt{-s^2}\, z\right) - k_2\, \sin\left(\sqrt{-s^2}\, z\right)\right] \tag{75}$$

The first boundary condition gives

$$F(s,0) = k_2 = \frac{\beta^2}{s\,(s^2+\beta^2)} \tag{76}$$

and the second boundary condition gives

$$\left.\frac{dF}{dz}\right|_{z=1} = \sqrt{-s^2}\left[k_1\,\cos\left(\sqrt{-s^2}\right) - k_2\,\sin\left(\sqrt{-s^2}\right)\right] = 0 \Leftrightarrow k_1 = k_2\frac{\sin\left(\sqrt{-s^2}\right)}{\cos\left(\sqrt{-s^2}\right)} \tag{77}$$

Inserting into the general solution then gives the particular solution:

$$F(s,z) = \frac{k_2}{\cos\left(\sqrt{-s^2}\right)}\left[\sin\left(\sqrt{-s^2}\right)\,\sin\left(\sqrt{-s^2}\,z\right) + \cos\left(\sqrt{-s^2}\right)\,\cos\left(\sqrt{-s^2}\,z\right)\right] \Leftrightarrow \tag{78}$$

$$F(s,z) = \frac{\beta^2}{s\,(s^2+\beta)^2}\frac{\cos\left[\sqrt{-s^2}\,(1-z)\right]}{\cos\left(\sqrt{-s^2}\right)} \equiv \frac{P(s,z)}{Q(s,z)}$$

Poles Using the residue theorem the solution can be found in real space. Since $F(s,z)$ can be written as $F = P/Q$ where the nominator P has no common roots with the denominator Q and both can be written as polynomials but the order of the nominator is less than that of the denominator, the inverse Laplace transformation is simply given by

$$f(\tau,z) = \sum_{s_i}\frac{P(s_i,z)}{Q'(s_i,z)}\,e^{s_i\,\tau} \quad , \quad Q(s_i) = 0\,,\; P(s_i) \neq 0 \tag{79}$$

where all the poles s_i are simple.
The poles are given by:

$$Q = 0 \Rightarrow\; s_0 = 0 \quad , \quad s_\pm = \pm i\,\beta \quad , \quad \sqrt{-s^2} = \lambda_n = \frac{\pi}{2}\,(2n+1) \Leftrightarrow s_n = \pm i\,\lambda_n\,,\; n = 0, 1, \ldots \tag{80}$$

Solution in real space The value of derivative of Q and the value of P at the poles are:

$$Q'(s) = (s^2+\beta^2)\,\cos\left(\sqrt{s^2}\right) + 2\,s^2\,\cos\left(\sqrt{s^2}\right) + \frac{s^2}{\sqrt{-s^2}}\,\sin\left(\sqrt{-s^2}\right)\,(s^2+\beta^2) \tag{81}$$

$$Q'(s_0) = \beta^2 \quad , \quad Q'(s_\pm) = -2\,\beta\,\cos(\beta) \quad , \quad Q'(s_n) = -\lambda_n\,(\beta^2-\lambda_n^2)\,\sin(\lambda_n)$$

$$P(s_0) = \beta^2 \quad , \quad P(s_\pm) = \beta^2\,\cos\left[\beta\,(1-z)\right] \quad , \quad P(s_n) = \beta^2\,\cos\left[\lambda_n\,(1-z)\right]$$

So the solution to the displacement in real space is:

$$f(\tau,z) = 1 - \frac{1}{2}\,\frac{\cos\left[\beta\,(1-z)\right]}{\cos(\beta)}\,\left(e^{i\,\beta\,\tau} + e^{-i\,\beta\,\tau}\right) + \sum_{n=0}^{\infty}\frac{(-1)^{n+1}\,\beta^2\,\cos\left[\lambda_n\,(1-z)\right]}{\lambda_n\,(\beta^2-\lambda_n^2)}\,\left(e^{i\,\lambda_n\,\tau} + e^{-i\,\lambda_n\,\tau}\right) \tag{82}$$

$$\Leftrightarrow f(\tau,z) = 1 - \frac{\cos\left[\beta\,(1-z)\right]}{\cos(\beta)}\,\cos(\beta\,\tau) + 2\,\beta^2\sum_{n=0}^{\infty}\frac{\sin(\lambda_n\,z)}{\lambda_n\,(\beta^2-\lambda_n^2)}\,\cos(\lambda_n\tau) \quad , \quad \beta \neq \lambda_n$$

where it has been used that $\sin(\lambda_n)\,\cos\left[\lambda_n\,(1-z)\right] = \sin(\lambda_n)\,\left[\cos(\lambda_n)\,\cos(-\lambda_n\,z) + \sin(\lambda_n)\,\sin(-\lambda_n\,z)\right] = -\sin(\lambda_n\,z)$.

B.1.2 Ejection time

The ejection time equation is given by:

$$\frac{\partial f}{\partial z} = -\beta \frac{\sin\left[\beta\,(1-z)\right]}{\cos(\beta)}\,\cos(\beta\,\tau) + 2\,\beta^2 \sum_{n=0}^{\infty} \frac{\cos(\lambda_n\,z)}{\beta^2-\lambda_n^2}\,\cos(\lambda_n \tau) \tag{83}$$

$$\Rightarrow \left.\frac{\partial f}{\partial z}\right|_{z=0} = 0 \Leftrightarrow \tan(\beta)\,\cos(\beta\,\tau_e) + 2\,\beta \sum_{n=0}^{\infty} \frac{\cos(\lambda_n \tau_e)}{\beta^2-\lambda_n^2} = 0$$

Comparing with the partial fraction expansion for $\tan(\beta)$ [26]:

$$\tan(\beta) = -2\,\beta \sum_{n=0}^{\infty} \frac{1}{\beta^2-\lambda_n^2} \tag{84}$$

it is seen that we can get the following expression for the ejection time equation if this is inserted:

$$\sum_{n=0}^{\infty} \frac{\cos(\beta\,\tau_e) - \cos(\lambda_n \tau_e)}{\beta^2-\lambda_n^2} = 0 \tag{85}$$

Ejection time for small β An upper bound can be found for the ejection time if the first expression for the ejection time is considered for $\beta \to 0$ and also $\beta\,\tau_e \to 0$. In this limit the ejection time equaion becomes

$$1 - 2 \sum_{n=0}^{\infty} \frac{\cos(\lambda_n\,\tau_e)}{\lambda_n^2} = 0 \quad , \quad T_n = \frac{2\,\pi}{\lambda_n} = \frac{4}{2\,n+1} \tag{86}$$

It is seen that the left-hand side of the equation consists of a sum of periodic functions with periods T_n. The largest of periods is $T_0 = 4$. Also notice that for $\tau_e = 0$ the expression for the ejection time becomes [26]

$$b(0) = 1 - 2 \sum_{n=0}^{\infty} \frac{1}{\lambda_n^2} = 1 - \frac{8}{\pi^2} \sum_{n=0}^{\infty} \frac{1}{(2\,n+1)^2} = 1 - \frac{8}{\pi^2} \cdot \frac{\pi^2}{8} = 0 \tag{87}$$

The resulting period of a sum of periodic functions is the largest period. This means that $\tau_e = 4$ is the next time the expression will become zero - for small parameter values the ejection time will be close to 4. The parameter is the dimensionless frequency so small β means that the plate moves slowly, and that is why $\tau_e = 4$ is an upper bound on the ejection time. If the plate moves faster, the object would jump off sooner.

B.1.3 Energy transfer factor

The average ejection velocity is $v_e = 1/L \int_0^L \frac{\partial u}{\partial t}\Big|_{t=t_e} dx$, and a rigid object would eject with velocity $A\,\omega$, so the energy transfer factor is given by

$$\nu = \frac{v_e}{A\,\omega} = \frac{1}{A\,\omega\,L_1}\int_0^1 A\,\frac{\partial f}{\partial \tau}\Big|_{\tau=\tau_e}\frac{c_1}{L_1}L_1\,dz = \frac{1}{\beta}\int_0^1 \frac{\partial f}{\partial \tau}\Big|_{\tau=\tau_e} dz \Leftrightarrow \tag{88}$$

$$\nu = \frac{1}{\beta}\int_0^1 \left[\beta\,\frac{\cos\left[\beta\,(1-z)\right]}{\cos(\beta)}\,\sin(\beta\,\tau_e) - 2\,\beta^2\sum_{n=0}^{\infty}\frac{\sin(\lambda_n\,z)}{\beta^2-\lambda_n^2}\,\sin(\lambda_n\tau_e)\right] dz \Leftrightarrow$$

$$\nu = \frac{\tan(\beta)}{\beta}\,\sin(\beta\,\tau_e) + 2\,\beta\sum_{n=0}^{\infty}\frac{\sin(\lambda_n\,\tau_e)}{\lambda_n\left(\beta^2-\lambda_n^2\right)}$$

For $\beta \to 0 \Rightarrow \nu \to 0$.
The maximum energy transfer is given by $\frac{d\nu}{d\beta} = 0$, and this derivative is

$$d\nu = \frac{\partial \nu}{\partial \beta}\,d\beta + \frac{\partial \nu}{\partial \tau_e}\,d\tau_e \Leftrightarrow \frac{d\nu}{d\beta} = \frac{\partial \nu}{\partial \beta} + \frac{\partial \nu}{\partial \tau_e}\,\frac{d\tau_e}{d\beta} \tag{89}$$

The partial derivative with respect to β is:

$$\frac{\partial \nu}{\partial \beta} = -\frac{1}{\beta^2}\,\tan(\beta)\,\sin(\beta\,\tau_e) + \frac{\sin(\beta\,\tau_e)}{\beta\,\cos^2(\beta)} + \frac{\tau_e}{\beta}\,\tan(\beta)\,\cos(\beta\,\tau_e) \tag{90}$$

$$+ 2\sum_{n=0}^{\infty}\frac{\sin(\lambda_n\,\tau_e)}{\lambda_n}\left(\frac{1}{\beta^2-\lambda_n^2} - \frac{2\,\beta^2}{\left(\beta^2-\lambda_n^2\right)^2}\right) \Leftrightarrow$$

$$\frac{\partial \nu}{\partial \beta} = \frac{\sin(\beta\,\tau_e)}{\beta}\left(\frac{1}{\cos^2(\beta)} - \frac{\tan(\beta)}{\beta}\right) + \frac{\tau_e}{\beta}\,\tan(\beta)\,\cos(\beta\,\tau_e) - 2\sum_{n=0}^{\infty}\frac{\left(\beta^2+\lambda_n^2\right)\,\sin(\lambda_n\tau_e)}{\lambda_n\,\left(\beta^2-\lambda_n^2\right)}$$

The partial derivative with respect to τ_e is:

$$\frac{\partial \nu}{\partial \tau_e} = \tan(\beta)\,\cos(\beta\,\tau_e) + 2\,\beta\sum_{n=0}^{\infty}\frac{\cos(\lambda_n\,\tau_e)}{\beta^2-\lambda_n^2} = 0 \tag{91}$$

It is seen that this is the same as the the ejection time equation. Since this partial derivative is then zero, the total derivative of the energy transfer factor with respect to β is the same as the partial derivative. The equation determining the optimal parameter value β_{opt} is then given by

$$0 = \sin(\beta_{opt}\,\tau_e)\left(\frac{1}{\cos^2(\beta_{opt})} - \frac{\tan(\beta_{opt})}{\beta_{opt}}\right) + \tau_e\,\tan(\beta_{opt})\,\cos(\beta_{opt}\,\tau_e) - 2\,\beta_{opt}\sum_{n=0}^{\infty}\frac{\left(\beta_{opt}^2+\lambda_n^2\right)\,\sin(\lambda_n\tau_e)}{\lambda_n\,\left(\beta_{opt}^2-\lambda_n^2\right)} \tag{92}$$

and is coupled to the ejection time equation.

B.2 Numerical method

To solve the system numerically, second order finite difference approximations are made in the z-direction and fourth order Runge-Kutta is used in the τ-direction.

B.2.1 Discretization of the PDE

Using finite difference approximations in space z, we define a mesh of N points with spacing $\Delta z = 1/N$ between neigbouring points (see figure 26 below).

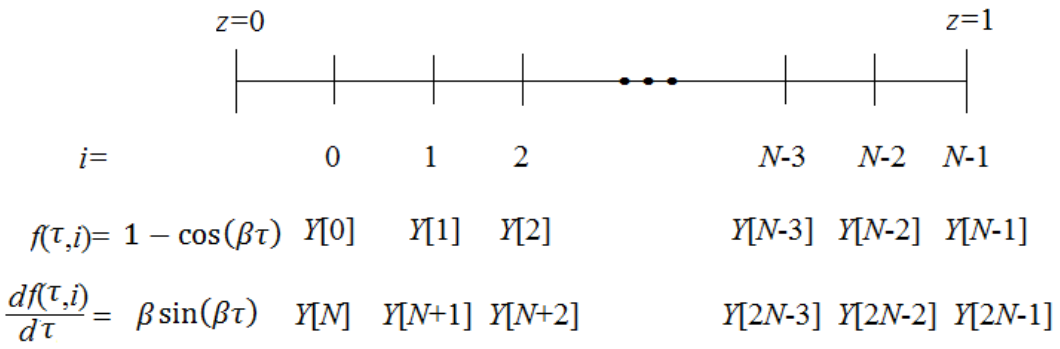

Figure 26: The figure shows that there are N points in the z direction and how the displacements and velocities of these points are related to the Y-vector.

Now the function $f(\tau, z)$ is discretized to $f(\tau, i)$ where i indicates which spatial point we are looking at. Using the central difference approximation for the second order derivative in z, we get

$$\left.\frac{\partial^2 f(\tau,z)}{\partial z^2}\right|_i \approx \frac{f(\tau,i+1) - 2\,f(\tau,i) + f(\tau,i-1)}{\Delta z^2} \tag{93}$$

and since the displacements obey the wave equation, the double derivative in z is the same as the acceleration at the same point. The set of second order differential equations can be transformed into a set of first order differential equations. This is done by defining a vector Y where the first $i = 0, ..., N-1$ entries are the function values $f(\tau, i)$ and the next $i = N, ..., 2N-1$ are the first order derivatives of this function with respect to τ. Then the derivative of this, $Y' \equiv F$ consists of first order derivatives of f and second order derivatives of f with respect to τ. Then the governing equations describing the displacements are given by

$$\begin{aligned} F[i] &= \frac{dY[i]}{d\tau} = Y[N+i] \quad \text{for} \quad i = 0, ..., N-1 \\ F[N+i] &= \frac{d^2Y[i]}{d\tau^2} = \frac{Y[i+1] - 2\,Y[i] + Y[i-1]}{\Delta z^2} \quad \text{for} \quad i = 1, ..., N-2 \\ F[N] &= \frac{d^2Y[0]}{d\tau^2} = \frac{Y[1] - 2\,Y[0] + 1 - \cos(\beta\,\tau)}{\Delta z^2} \end{aligned} \tag{94}$$

For the second boundary condition we find the second order approximation by writing the taylor expansion to third order around $i = N-1$ for the points $i = N-2$ and $i = N-3$ and insert the boundary condition

for the system to get

$$\begin{cases} Y[N-2] = Y[N-1] - \Delta z \left.\frac{\partial f}{\partial z}\right|_{z=1} + \frac{\Delta z^2}{2} \left.\frac{\partial^2 f}{\partial z^2}\right|_{z=1} - \frac{\Delta z^3}{6} \left.\frac{\partial^3 f}{\partial z^3}\right|_{z=1} \\ Y[N-3] = Y[N-1] - 2\,\Delta z \left.\frac{\partial f}{\partial z}\right|_{z=1} + \frac{4\,\Delta z^2}{2} \left.\frac{\partial^2 f}{\partial z^2}\right|_{z=1} - \frac{8\,\Delta z^3}{6} \left.\frac{\partial^3 f}{\partial z^3}\right|_{z=1} \end{cases} \Leftrightarrow \tag{95}$$

$$8\,Y[N-2] - Y[N-3] = 7\,Y[N-1] - 6\,\Delta z \left.\frac{\partial f}{\partial z}\right|_{z=1} + 2\,\Delta z^2 \left.\frac{\partial^2 f}{\partial z^2}\right|_{z=1} \Rightarrow$$

$$\left.\frac{\partial^2 f}{\partial z^2}\right|_{z=1} = F[2\,N-1] = \frac{8\,Y[N-2] - Y[N-3] - 7\,Y[N-1]}{2\,\Delta z^2} \Rightarrow$$

B.2.2 Ejection time

The ejection time is given by $\left.\frac{\partial f}{\partial z}\right|_{z=0} = 0$. To find the second order approximation we do the same as before, writing the Taylor series of the function at $i = 0$ and $i = 1$ around $z = 0$ to third order (where $f(0) = 1 - \cos(\beta\,\tau)$).

$$\begin{cases} Y[0] \approx f(0) + \Delta z \left.\frac{\partial f}{\partial z}\right|_{z=0} + \frac{\Delta z^2}{2} \left.\frac{\partial^2 f}{\partial z^2}\right|_{z=0} + \frac{\Delta z^3}{6} \left.\frac{\partial^3 f}{\partial z^3}\right|_{z=0} \\ Y[1] \approx f(0) + 2\,\Delta z \left.\frac{\partial f}{\partial z}\right|_{z=0} + \frac{(2\,\Delta z)^2}{2} \left.\frac{\partial^2 f}{\partial z^2}\right|_{z=0} + \frac{(2\,\Delta z)^3}{6} \left.\frac{\partial^3 f}{\partial z^3}\right|_{z=0} \end{cases} \Leftrightarrow \tag{96}$$

$$8\,Y[0] - Y[1] = 7\,f(0) + 6\,\Delta z \left.\frac{\partial f}{\partial z}\right|_{z=0} + 2\,\Delta z^2 \left.\frac{\partial f}{\partial^2 z^2}\right|_{z=0} \Rightarrow$$

$$\left.\frac{\partial^2 f}{\partial z^2}\right|_{(z,\tau)=(0,\tau_e)} = \frac{[8\,Y[0] - Y[1] - 7\,f(0)]_{\tau=\tau_e}}{2\,\Delta z^2}$$

But this is also equal to $\left.\frac{\partial^2 f}{\partial \tau^2}\right|_{(z,\tau)=(0,\tau_e)} = \beta^2\,\cos(\beta\,\tau_e)$, so the ejection time equation becomes

$$\begin{gathered} \beta^2\,\cos(\beta\,\tau_e) - \frac{[8\,Y[0] - Y[1] - 7\,f(0)]_{\tau=\tau_e}}{2\,\Delta z^2} = 0 \Leftrightarrow \\ 2\,\beta^2\,\Delta z^2\,\cos(\beta\,\tau_e) - [8\,Y[0] - Y[1] - 7\,f(0)]_{\tau=\tau_e} = 0 \end{gathered} \tag{97}$$

Now define this as a function of τ, $E(\tau)$. We know that we have $E(0) = 0$, so to make sure this is true we subtract this value to get

$$E(\tau) = 2\,\beta^2\,\Delta z^2\,(\cos(\beta\,\tau_e) - 1) - 8\,Y[0] + Y[1] + 7\,(1 - \cos(\beta\,\tau)) \tag{98}$$

To find the ejection time, we can evolve in time by using Runge-Kutta and for each step calculate E, such that at time $\tau = \tau_2$ we have $E = E_2$ and at the time just before $\tau = \tau_1$ we have $E = E_1$. Then if the product $E_1\,E_2 < 0$ we know that somewhere between the two points, $E = 0$.

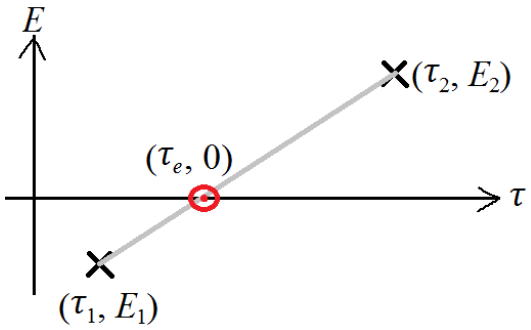

Figure 27: The figure illustrates the bisection method to find the root of a function.

We can approximate this root by using the straight line between the two points given by (see figure 27 above)

$$E - E_1 = \frac{E_1 - E_2}{\tau_1 - \tau_2}(\tau - \tau_1) \tag{99}$$

and so the ejection time $\tau = \tau_e$ at which $E = 0$ is given by

$$\tau_e = \tau_1 - \frac{\tau_1 - \tau_2}{E_1 - E_2} E_1 \tag{100}$$

The Y-vector at ejection time can be approximated the same way:

$$Y|_{\tau_e} = Y_2 + \frac{Y_2 - Y_1}{t_2 - t_1}(\tau_e - t_2) \tag{101}$$

B.2.3 Energy transfer

The energy tranfer factor is given by the first part of equation 14:

$$\nu = \frac{1}{\beta}\int_0^1 \left.\frac{\partial f}{\partial \tau}\right|_{\tau=\tau_e} dz \tag{102}$$

The integral is the same as a sum over the areas of all the trapez' (see figure 28 below) made by the velocities $Y[N+i]$ for $i = 0, \ldots, N-1$ and the known velocity at the boundary.

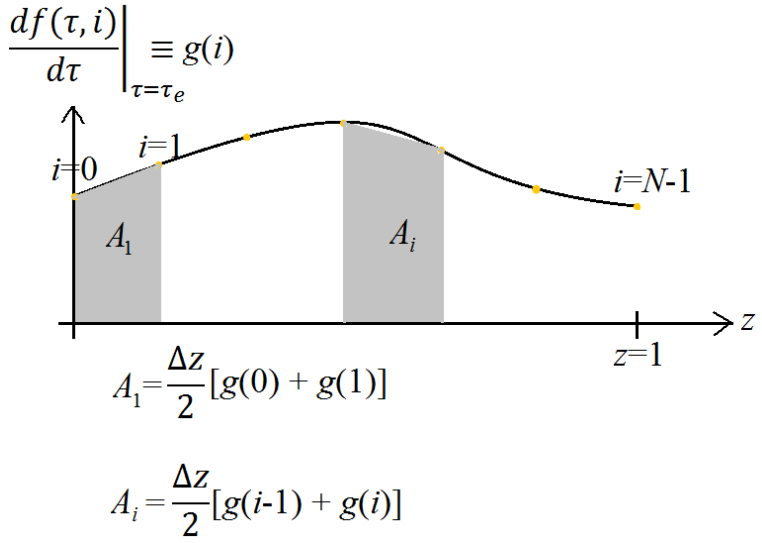

Figure 28: Illustration of the trapez method to approximate integrals.

So the integral is just given by the sum of all the velocities. This gives the following expression for the energy transfer:

$$\nu = \frac{\Delta z}{\beta}\left(\frac{1}{2}\left(Y[2N-1] + \beta\,\sin(\beta\,\tau_e)\right) + \sum_{i=0}^{N-2} Y[N+i]\right) \tag{103}$$

B.2.4 Integration in τ-direction

Now that we have transformed the original second order partial differential equation into first order ordinary differential equations we can solve these numerically using fourth order Runge-Kutta. This method gives the $Y(t+\Delta t)$ vector at a later time $t+dt$ when we know the value at an earlier time t when we have $F(Y,t) = Y'(t)$. The algorithm is [15]:

$$\begin{aligned} Y(t+\Delta t) &= Y(t) + \frac{\Delta t}{6}\,(k_1 + 2\,k_2 + 2\,k_3 + k_4) \\ k_1 &= F(Y,t) \quad , \quad k_2 = F\left(Y + \frac{k_1\,\Delta t}{2}, t + \frac{\Delta t}{2}\right) \\ k_3 &= F\left(Y + \frac{k_2\,\Delta t}{2}, t + \frac{\Delta t}{2}\right) \quad , \quad k_4 = F(Y + k_3\,\Delta t, t + \Delta t) \end{aligned} \tag{104}$$

this method is used to evolve in time until the object ejects from the plate.

Stability condition In order for the numerical method to be stable for this system we must have

$$\Delta\tau \leq \Delta z \tag{105}$$

and in all numerical calculations we have chosen $\Delta\tau$ such that the above expression is an equality.

The explanation for this is that when the wave moves from one point in the spatial mesh to another

and we want to calculate its amplitude also at discrete time steps, then this time step has to be less than the time it will take the wave to travel from the first point in the mesh to the second. This means that in real space we must have $\Delta t < \frac{\Delta x}{c}$ [15].

C Graphs from articles

The results from the article by C. Raufaste et al [8] are shown on the figure below. The red graphs show their numerical solution to the system.

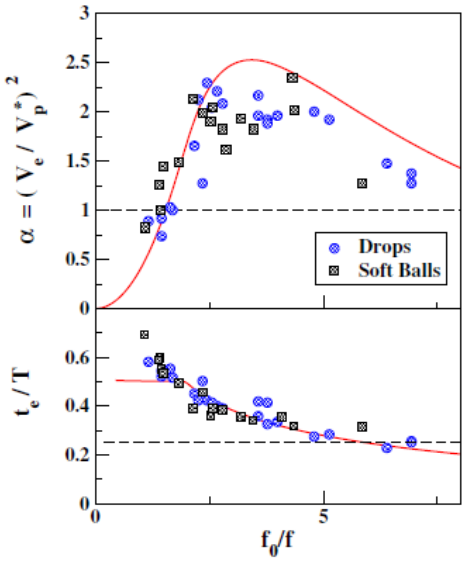

FIG. 3. The figure summarizes measurements performed with both droplets (circles) and hydrogel balls (squares). Top: Energy transfer factor α plotted as a function of the frequency ratio f_0/f. The dashed line represents $\alpha = 1$, the value expected for a rigid projectile, while the model based on the projectile deformation dynamics is represented by the solid line. Bottom: Same data and analysis for t_e/T as a function of f_0/f. The dashed line represents $t_e/T = 0.25$, the value expected for a rigid projectile.

The results from the article by F. Celestini et al [9] are shown on the figure below. The solid lines in figure (a) and (b) are the numerical results for the two plate frequencies. The solid curve on figure (e) shows the maximum for each l (the same type of plot as on figure 11 where the maximum energy transfer is plotted for each μ).

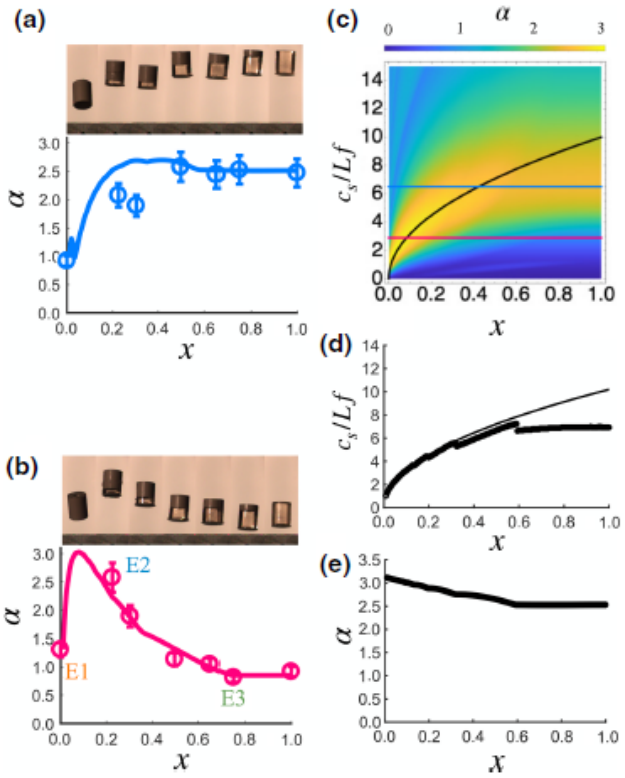

FIG. 3. Ejection of projectiles with a rigid top layer. We show the energy transfer factor α as a function of the soft ratio x for the engine frequencies 34 and 76 Hz in (a) and (b), respectively. Images of the maximal heights are displayed for each case. The experimental measurements are shown with symbols, while the numerical predictions are represented by solid curves. E1, E2, and E3 refer to Fig. 1. (c) Color plot of α as a function of c_s/Lf and x (color scale displayed on the right), deduced from the numerical model. The particular values of c_s/Lf , 2.9 from (a) and 6.5 from (b), are represented by horizontal lines (using the color scheme of the two cases). The dark solid curves shown in (c) and (d) correspond to the model $c_s/Lf = 10.2\sqrt{x}$. (d) The ratio c_s/Lf as a function of x for the maximal α value found along a vertical line in the α diagram (c). (e) Maximal α value as a function of x.

D Intermediate calculations for point mass system

Equation 25 describes the partial differential equation with corresponding initial and boundary conditions that the displacement of the elastic material must obey.

D.1 Analytical method

The first time I considered this system was also in my bachelor project [10] - but then I had the wrong boundary condition: I had a factor of $+\mu$ in the last boundary condition instead of a factor of $-\mu$. So everything in this section is the same as in my bachelor project with both $z \to z-1$ and $\mu \to -\mu$. Back then I also forgot to include the real solutions to the equation for the poles that will appear with this wrong sign in the boundary condition. Including these poles will make it much clearer that this boundary condition does not correctly describe the system that we want to describe. So this time I have also shown that there are only imaginary solutions to the equation for the poles.

D.1.1 Solution to displacement

Solution in Laplace space The solution to equation 25 can be found the same was as for the first system. In Laplace space this gives the following ordinary differential equation with corresponding boundary conditions:

$$\frac{d^2F}{dz^2} + (-s^2)\,F^2 = 0 \tag{106}$$
$$F(s,0) = \frac{\beta^2}{s\,(s^2+\beta^2)} \quad , \quad \left.\frac{dF}{dz}\right|_{z=1} = -\mu\, s^2\, F(s,1)$$

The general solution is again

$$F(s,z) = k_1\,\sin\left(\sqrt{-s^2}\,z\right) + k_2\,\cos\left(\sqrt{-s^2}\,z\right) \Rightarrow \frac{dF}{dz} = \sqrt{-s^2}\left[k_1\,\cos\left(\sqrt{-s^2}\,z\right) - k_2\,\sin\left(\sqrt{-s^2}\,z\right)\right] \tag{107}$$

Using the first boundary condition gives:

$$k_2 = \frac{\beta^2}{s\,(s^2+\beta^2)} \tag{108}$$

The second boundary condition gives:

$$\sqrt{-s^2}\left[k_1\,\cos\left(\sqrt{-s^2}\right) - k_2\,\sin\left(\sqrt{-s^2}\right)\right] = -\mu\, s^2\left[k_1\,\sin\left(\sqrt{-s^2}\right) + \cos\left(\sqrt{-s^2}\right)\right] \Leftrightarrow \tag{109}$$
$$k_1\left[\cos\left(\sqrt{-s^2}\right) - \mu\sqrt{-s^2}\,\sin\left(\sqrt{-s^2}\right)\right] = k_2\left[\sin\left(\sqrt{-s^2}\right) + \mu\sqrt{-s^2}\,\cos\left(\sqrt{-s^2}\right)\right] \Leftrightarrow$$
$$k_1 = k_2\,\frac{\sin\left(\sqrt{-s^2}\right) + \mu\sqrt{-s^2}\,\cos\left(\sqrt{-s^2}\right)}{\cos\left(\sqrt{-s^2}\right) - \mu\sqrt{-s^2}\,\sin\left(\sqrt{-s^2}\right)}$$

Such that the solution to the displacement in Laplace space is:

$$F = k_2 \frac{\sin\left(\sqrt{-s^2}\,z\right)\left[\sin\left(\sqrt{-s^2}\right)+\mu\sqrt{-s^2}\cos\left(\sqrt{-s^2}\right)\right]+\cos\left(\sqrt{-s^2}\,z\right)\left[\cos\left(\sqrt{-s^2}\right)-\mu\sqrt{-s^2}\sin\left(\sqrt{-s^2}\right)\right]}{\cos\left(\sqrt{-s^2}\right)-\mu\sqrt{-s^2}\sin\left(\sqrt{-s^2}\right)} \tag{110}$$

$$\Leftrightarrow F(s,z) = \frac{\beta^2}{s\,(s^2+\beta)^2}\frac{\cos\left[\sqrt{-s^2}\,(1-z)\right]-\mu\sqrt{-s^2}\sin\left[\sqrt{-s^2}\,(1-z)\right]}{\cos\left(\sqrt{-s^2}\right)-\mu\sqrt{-s^2}\sin\left(\sqrt{-s^2}\right)} = \frac{P(s,z)}{Q(s,z)}$$

Poles Using the residue theorem the solution can be found in real space. Since $F(s,z)$ can be written as $F = P/Q$ where the nominator P has no common roots with the denominator Q and both can be written as polynomials but the order of the nominator is less than that of the denominator, the inverse Laplace transformation is simply given by

$$f(\tau,z) = \sum_{s_i}\frac{P(s_i,z)}{Q'(s_i,z)}\,e^{s_i\,\tau} \quad , \quad Q(s_i)=0\,,\; P(s_i)\neq 0 \tag{111}$$

where all the poles s_i are simple.
Some of the poles are quickly found to be: $s_0 = 0$ and $s_\pm = \pm i\,\beta$. The other poles are given by:

$$\cos\left(\sqrt{-s^2}\right)-\mu\sqrt{-s^2}\sin\left(\sqrt{-s^2}\right)=0 \Leftrightarrow \mu\sqrt{-s^2}\tan\left(\sqrt{-s^2}\right)-1=0 \Leftrightarrow \tag{112}$$

$$\tan(\Lambda) = \frac{1}{\mu\,\Lambda} \quad , \quad \Lambda = \sqrt{-s^2} > 0$$

From the equation above it is seen that s can only be imaginary and so Λ is real, see the paragraphs below for clarification.
Below in figure 29 (left) the functions have been plotted for some μ.

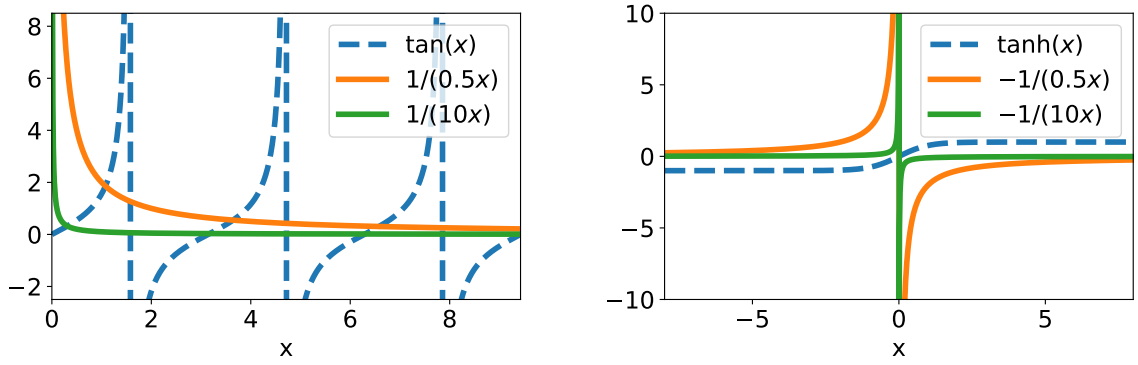

Figure 29: Plots of the two types of functions in equation 27 with two different values of μ for imaginary solutions to the pole equation $\sqrt{-s^2} = \Lambda$ (left) and assuming that there are real solutions $\sqrt{-s^2} = i\,R$ (right).

It is seen that for the first solution (for alle values of μ) $0 < \Lambda_0 < \frac{\pi}{2}$, for the second solution $\pi < \Lambda_1 < \frac{3\pi}{2}$ and so for the nth solution

$$n\pi < \Lambda_n < \frac{\pi}{2}(2n+1) = \lambda_n \quad , \quad n = 0,1,2,\ldots \tag{113}$$

The solutions move closer and closer to the lower bound of Λ_n the larger n gets. It's also seen that for larger μ the quicker $\Lambda_n \to n\,\pi$, while for smaller μ, $\Lambda_n \to \lambda_n$ (which were the poles for the first system). For $\mu \to \infty$ it seems like $s = 0$ becomes a pole of second order in the denominator - but then when considering P it is also seen that it is now a removable singularity (divide by $\sin(\sqrt{-s^2})$ to remove the singularity gained from $\mu \to \infty$). Then we have the same poles as before but now $\Lambda_n = n\pi$ for $n = 1, 2, \ldots$. This system is also the system with the second boundary condition changed to $f(\tau, 1) = 0$, which has these poles.

No real poles Assume that there are real solutions, $\sqrt{-s^2} = iR$ such that the equation becomes $\tanh(R) = -1/(\mu\,R)$. But the hyperbolic tangent function is negative for negative arguments and positive for positive arguments and crosses the origin and lies between -1 and 1. This function will never intersect with the other function which lies in the second and fourth quadrant. The larger μ is the closer the function will come to the origin but it will never touch it. See figure 29 (right).

No complex poles Assume that there are also some complex poles $s = a+ib$ (and that both the imaginary and real part are nonzero) such that the poles equation, $-\mu\,i\,s\tan(i\,s) + 1 = 0$ becomes:

$$\tanh(a+ib) = \frac{\tanh(a) + i\,\tan(b)}{1 + i\,\tanh(a)\,\tan(b)} = \frac{-1}{\mu(a+ib)} \Leftrightarrow \tag{114}$$

$$\mu\,a\,\tanh(a) - \mu\,b\,\tan(b) + i\,\left[\mu\,b\,\tanh(a) + \mu\,a\,\tan(b)\right] = -1 - i\,\tanh(a)\,\tan(b) \Leftrightarrow$$

$$\begin{cases} a\,\tanh(a) - b\,\tan(b) = \frac{-1}{\mu} \\ b\,\tanh(a) + a\,\tan(b) = \frac{-\tanh(a)\,\tan(b)}{\mu} \end{cases} \Leftrightarrow \begin{cases} a\tanh(a) - b\,\tan(b) = \frac{-1}{\mu} \\ \frac{b}{\tan(b)} + \frac{a}{\tanh(a)} = \frac{-1}{\mu} \end{cases} \Leftrightarrow$$

$$a\tanh(a) - b\,\tan(b) = \frac{b}{\tan(b)} + \frac{a}{\tanh(a)} \Leftrightarrow$$

$$a\,\left[\tanh(a) - \frac{1}{\tanh(a)}\right] - b\,\left[\tan(b) + \frac{1}{\tan(b)}\right] = 0 \Leftrightarrow$$

$$a\,\frac{-1}{\sinh(a)\,\cosh(a)} - b\,\frac{1}{\sin(b)\,\cos(b)} = 0 \Leftrightarrow$$

$$\frac{2\,a}{\sinh(2\,a)} + \frac{2\,b}{\sin(2\,b)} = 0$$

But the function $x/\sinh(x)$ always lies between 0 and 1 and the function $x/\sin(x)$ is always greater than 1 or at least less than -1 which means that the sum of the two will never be 0 and so there are no complex poles (see the figure below).

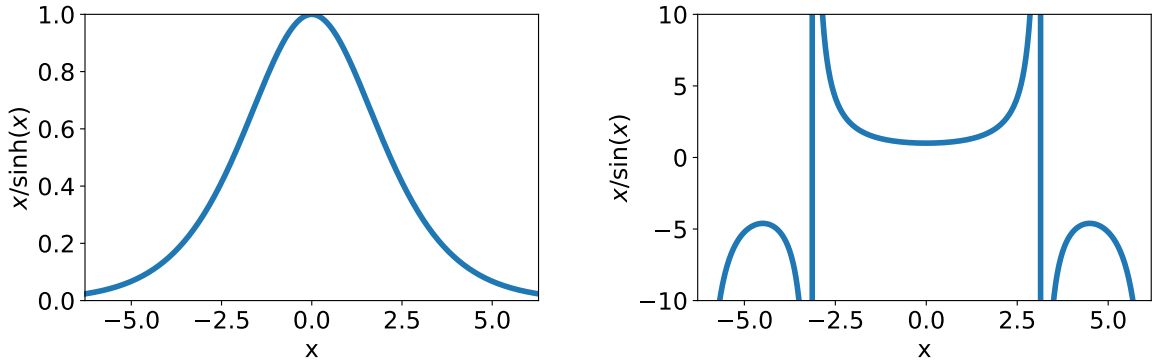

Figure 30: Graphs of the functions $x/\sinh(x)$ (left) and $x/\sin(x)$ (right).

Solution in real space To find the solution in real space $f(\tau, z)$ the derivative of Q is also needed:

$$\begin{aligned} Q'(s) = (s^2+\beta^2)\,&\left[\cos\left(\sqrt{-s^2}\right) - \mu\sqrt{-s^2}\,\sin\left(\sqrt{-s^2}\right)\right] \\ &+ 2\,s^2\,\left[\cos\left(\sqrt{-s^2}\right) - \mu\sqrt{-s^2}\,\sin\left(\sqrt{-s^2}\right)\right] \\ &- s\,(s^2+\beta^2)\,\left[\sin\left(\sqrt{-s^2}\right) + \mu\,\sin\left(\sqrt{-s^2}\right) + \mu\sqrt{-s^2}\,\cos\left(\sqrt{-s^2}\right)\right]\,\frac{-s}{\sqrt{-s^2}} \end{aligned} \tag{115}$$

The values of the derivative at the poles are

$$\begin{aligned} &Q'(s_0) = \beta^2 \quad , \quad Q'(s_\pm) = -2\beta^2\,[\cos(\beta) - \mu\,\beta\,\sin(\beta)] \\ &Q'(s_n) = \pm i\,\Lambda_n\,(\beta^2 - \Lambda_n^2)\,[\sin(\Lambda_n) + \mu\,\sin(\Lambda_n) + \mu\,\Lambda_n\,\cos(\Lambda_n)]\,\frac{\mp i\,\Lambda_n}{\Lambda_n} \Leftrightarrow \\ &Q'(s_n) = \Lambda_n\,(\Lambda_n^2 - \beta^2)\,[\sin(\Lambda_n) + \mu\,\sin(\Lambda_n) + \mu\,\Lambda_n\,\cos(\Lambda_n)] \Leftrightarrow \\ &Q'(s_n) = \Lambda_n\,(\Lambda_n^2 - \beta^2)\left[\sin(\Lambda_n) + \frac{\cos(\Lambda_n)}{\Lambda_n} + \frac{\cos^2(\Lambda_n)}{\sin(\Lambda_n)}\right] \Leftrightarrow \\ &Q'(s_n) = \Lambda_n\,(\Lambda_n^2 - \beta^2)\left[\frac{\cos(\Lambda_n)}{\Lambda_n} + \frac{1}{\sin(\Lambda_n)}\right] \Leftrightarrow \\ &Q'(s_n) = (\Lambda_n^2 - \beta^2)\frac{\cos(\Lambda_n)\,\sin(\Lambda_n) + \Lambda_n}{\sin(\Lambda_n)} \\ &Q'(s_n) = (\Lambda_n^2 - \beta^2)\frac{\sin(2\Lambda_n) + 2\Lambda_n}{2\,\sin(\Lambda_n)} \end{aligned} \tag{116}$$

Where it has been used that $\mu = \frac{\cos(\Lambda_n)}{\Lambda_n\,\sin(\Lambda_n)}$. The value of P at the poles are

$$\begin{aligned} &P(s_0) = \beta^2 \quad , \quad P(\pm i\beta) = \beta^2\,[\cos\,[\beta\,(1-z)] - \mu\,\beta\,\sin\,[\beta\,(1-z)]] \\ &P(s_n) = \beta^2\,[\cos\,[\Lambda_n\,(1-z)] - \mu\,\Lambda_n\,\sin\,[\Lambda_n\,(1-z)]] \Leftrightarrow \\ &P(s_n) = \frac{\beta^2}{\sin(\Lambda_n)}\,[\sin(\Lambda_n)\,\cos\,[\Lambda_n\,(1-z)] - \cos(\Lambda_n)\,\sin\,[\Lambda_n\,(1-z)]] \\ &P(s_n) = \beta^2\,\frac{\sin(\Lambda_n\,z)}{\sin(\Lambda_n)} \end{aligned} \tag{117}$$

The inverse Laplace transform, and the solution to the displacement, is then given by

$$f(\tau, z) = 1 - \frac{\cos\left[\beta\left(1-z\right)\right] - \mu\,\beta\sin\left[\beta\left(1-z\right)\right]}{\cos(\beta) - \mu\,\beta\sin(\beta)}\,\cos(\beta\,\tau) + 4\,\beta^2\sum_{n=0}^{\infty}\frac{\sin(\Lambda_n\,z)}{\Lambda_n^2-\beta^2}\frac{\cos(\Lambda_n\,\tau)}{\sin(2\,\Lambda_n)+2\,\Lambda_n} \tag{118}$$

D.1.2 Ejection time and energy transfer

The ejection time is given by

$$\left.\frac{\partial f}{\partial z}\right|_{z=0} = 0 \Leftrightarrow \tag{119}$$

$$\left[-\beta\,\frac{\sin\left[\beta\left(1-z\right)\right] + \mu\,\beta\,\cos\left[\beta\left(1-z\right)\right]}{\cos(\beta) - \mu\,\beta\sin(\beta)}\,\cos(\beta\,\tau) - 4\,\beta^2\sum_{n=0}^{\infty}\frac{\cos(\Lambda_n\,z)}{\beta^2-\Lambda_n^2}\frac{\Lambda_n\,\cos(\Lambda_n\,\tau)}{\sin(2\,\Lambda_n)+2\,\Lambda_n}\right]_{z=0} = 0 \Leftrightarrow$$

$$\frac{\sin(\beta) + \mu\,\beta\,\cos(\beta)}{\cos(\beta) - \mu\,\beta\sin(\beta)}\,\cos(\beta\,\tau_e) + 4\,\beta\sum_{n=0}^{\infty}\frac{\Lambda_n}{\beta^2-\Lambda_n^2}\frac{\cos(\Lambda_n\,\tau_e)}{\sin(2\,\Lambda_n)+2\,\Lambda_n} = 0 \Leftrightarrow$$

$$\frac{\tan(\beta) + \mu\,\beta}{1 - \mu\,\beta\,\tan(\beta)}\,\cos(\beta\,\tau_e) + 4\,\beta\sum_{n=0}^{\infty}\frac{\Lambda_n}{\beta^2-\Lambda_n^2}\frac{\cos(\Lambda_n\,\tau_e)}{\sin(2\,\Lambda_n)+2\,\Lambda_n} = 0$$

The ejection velocity of the object is given by its total momentum divided by its total mass and dividing by the maximum plate velocity gives the energy transfer factor. The point mass is attached to the end of the elastic material so it follows this points motion - this means that the velocity of the point mass is the velocity of the elastic material at $x = L_1$. The center of mass ejection velocity is then given by

$$v = \frac{1}{m_1+m_2}\left[m_2\,\left.\frac{\partial u}{\partial t}\right|_{(t,x)=(t_e,L_1)} + m_1\,\frac{1}{L_1}\int_0^{L_1}\left.\frac{\partial u}{\partial t}\right|_{t=t_e} dz\right] \Leftrightarrow \tag{120}$$

$$v = \frac{A\,c}{L_1}\,\frac{m_1}{m_1+m_2}\left[\mu\,\left.\frac{\partial f}{\partial \tau}\right|_{(\tau,z)=(\tau_e,1)} + \int_0^1\left.\frac{\partial f}{\partial \tau}\right|_{\tau=\tau_e} dz\right] \Leftrightarrow$$

and the energy transfer factor is then given by

$$\nu = \frac{v}{A\,\omega} = \frac{1}{\beta\left(1+\mu\right)}\left[\mu\,\left.\frac{\partial f}{\partial \tau}\right|_{(\tau,z)=(\tau_e,1)} + \int_0^1\left.\frac{\partial f}{\partial \tau}\right|_{\tau=\tau_e} dz\right] \tag{121}$$

The partial derivative with respect to τ at $\tau = \tau_e$ is:

$$\left.\frac{\partial f}{\partial \tau}\right|_{\tau=\tau_e} = \frac{\cos\left[\beta\left(1-z\right)\right] - \mu\,\beta\sin\left[\beta\left(1-z\right)\right]}{\cos(\beta) - \mu\,\beta\sin(\beta)}\,\beta\,\sin(\beta\,\tau_e) + 4\,\beta^2\sum_{n=0}^{\infty}\frac{\sin(\Lambda_n\,z)}{\beta^2-\Lambda_n^2}\frac{\Lambda_n\,\sin(\Lambda_n\,\tau_e)}{\sin(2\,\Lambda_n)+2\,\Lambda_n} \tag{122}$$

This derivative's value at $z = 1$, and the integral of the derivative are:

$$\left.\frac{\partial f}{\partial \tau}\right|_{(\tau,z)=(\tau_e,1)} = \frac{\beta\ \sin(\beta\,\tau_e)}{\cos(\beta) - \mu\,\beta\sin(\beta)} + 4\,\beta^2 \sum_{n=0}^{\infty} \frac{\sin(\Lambda_n)}{\beta^2 - \Lambda_n^2} \frac{\Lambda_n\ \sin(\Lambda_n\,\tau_e)}{\sin(2\,\Lambda_n) + 2\,\Lambda_n} \tag{123}$$

$$\int_0^1 \left.\frac{\partial f}{\partial \tau}\right|_{\tau=\tau_e} dz =$$

$$\left[\frac{-\sin\left[\beta\,(1-z)\right] - \mu\,\beta\,\cos\left[\beta\,(1-z)\right]}{\cos(\beta) - \mu\,\beta\sin(\beta)}\ \sin(\beta\,\tau_e) + 4\,\beta^2 \sum_{n=0}^{\infty} \frac{-\cos(\Lambda_n\,z)}{\beta^2 - \Lambda_n^2} \frac{\sin(\Lambda_n\,\tau_e)}{\sin(2\,\Lambda_n) + 2\,\Lambda_n}\right]_0^1 \Leftrightarrow$$

$$\int_0^1 \left.\frac{\partial f}{\partial \tau}\right|_{\tau=\tau_e} dz = \frac{\sin(\beta) + \mu\,\beta\ \cos(\beta) - \mu\,\beta}{\cos(\beta) - \mu\,\beta\sin(\beta)}\ \sin(\beta\,\tau_e) + 4\,\beta^2 \sum_{n=0}^{\infty} \frac{1 - \cos(\Lambda_n)}{\beta^2 - \Lambda_n^2} \frac{\sin(\Lambda_n\,\tau_e)}{\sin(2\,\Lambda_n) + 2\,\Lambda_n}$$

so the energy transfer factor is

$$\nu = \frac{1}{1+\mu}\left[\frac{\sin(\beta) + \mu\,\beta\ \cos(\beta)}{\cos(\beta) - \mu\,\beta\sin(\beta)}\ \frac{\sin(\beta\,\tau_e)}{\beta} + 4\,\beta \sum_{n=0}^{\infty} \frac{\sin(\Lambda_n\,\tau_e)}{\beta^2 - \Lambda_n^2} \frac{1}{\sin(2\,\Lambda_n) + 2\,\Lambda_n}\right] \tag{124}$$

Ejection time and energy transfer in the limit $\mu \to \infty$: In the limit $\mu \to \infty$, the poles $\Lambda_n \to n\,\pi$ where $n = 1, 2, 3, \ldots$ and the ejection time equation becomes

$$-\cot(\beta)\ \cos(\beta\,\tau_e) + 2\,\beta \sum_{n=1}^{\infty} \frac{\cos(n\,\pi\,\tau_e)}{\beta^2 - (n\,\pi)^2} = 0 \tag{125}$$

Inserting the partial fraction expansion of $\cot(\beta) = \frac{1}{\beta} + 2\,\beta\ \sum_{n=1}^{\infty} \frac{1}{\beta^2 - (n\,\pi)^2}$ the ejection time equation now becomes

$$2\,\beta \sum_{n=1}^{\infty} \frac{\cos(n\,\pi\,\tau_e) - \cos(\beta\,\tau_e)}{\beta^2 - (n\,\pi)^2} - \frac{\cos(\beta\,\tau_e)}{\beta} = 0 \tag{126}$$

The energy transfer in the same limit becomes

$$\nu_p = \frac{1}{\mu}\left[-\cot(\beta)\ \frac{\sin(\beta\,\tau_e)}{\beta} + 2\,\beta \sum_{n=1}^{\infty} \frac{\sin(n\,\pi\,\tau_e)}{\left(\beta^2 - (n\,\pi)^2\right)\ n\,\pi}\right] \Rightarrow \tag{127}$$

$$\nu_p = \frac{1}{\mu}\left[2\,\beta \sum_{n=1}^{\infty} \frac{1}{\beta^2 - (n\,\pi)^2}\left(\frac{\sin(n\,\pi\,\tau_e)}{n\,\pi} - \frac{\sin(\beta\,\tau_e)}{\beta}\right) - \frac{\sin(\beta\,\tau_e)}{\beta^2}\right]$$

D.1.3 Displacement solution in the limit $\mu \to \infty$

For $\mu \to \infty$ everything up until the solution of the Laplaces transform is fine. The Laplace transform was

$$F(s,z) = \frac{\beta^2\left[\cos\left(\sqrt{-s^2}\,z\right) + \mu\,\sqrt{-s^2}\ \sin\left(\sqrt{-s^2}\,z\right)\right]}{s\,(s^2+\beta^2)\ \left[\mu\,\sqrt{-s^2}\ \sin\left(\sqrt{-s^2}\right) + \cos\left(\sqrt{-s^2}\right)\right]} \tag{128}$$

which for $\mu \to \infty$ becomes:

$$F(s,z) = \frac{\beta^2 \, \sin\left(\sqrt{-s^2}\, z\right)/s}{\left(s^2+\beta^2\right) \, \sin\left(\sqrt{-s^2}\right)} = \frac{P(s,z)}{Q(s,z)} \tag{129}$$

where it is seen that the previous $s = 0$ singularity is now removable. The poles are now

$$s_\pm = \pm i\,\beta \quad , \quad \Lambda_n = \sqrt{-s^2} = n\,\pi \Rightarrow s_n = \pm i\,n\,\pi \;,\; n = 0, 1, 2, ... \tag{130}$$

The derivaive of Q is now

$$Q'(s,z) = 2\,s \, \sin\left(\sqrt{-s^2}\right) + \left(s^2+\beta^2\right) \, \frac{-s}{\sqrt{-s^2}} \, \cos\left(\sqrt{-s^2}\right) \tag{131}$$

and the P/Q' fractions at the poles become:

$$\left.\frac{P}{Q'}\right|_{s=\pm i\,\beta} = -\frac{\sin(\beta\,z)}{2\,\sin(\beta)} \quad , \quad \left.\frac{P}{Q'}\right|_{s=\pm i\,n\,\pi} = \frac{\beta^2 \, \sin(n\,\pi\,z)}{\left(\beta^2 - n^2\,\pi^2\right) \, n\,\pi \, \cos(n\,\pi)} \;,\; n \neq 0 \tag{132}$$

$$\left.\frac{P}{Q'}\right|_{s=0} = z$$

(the last fraction has been found by expanding the second fraction near $n = 0$ to first order).
So the solution to $f(\tau, z)$ becomes:

$$f(\tau,z) = z - \frac{\sin(\beta\,z)}{2\,\sin(\beta)} \cdot 2\,\cos(\beta\,\tau) + \sum_{n=1}^{\infty} \frac{\beta^2 \, \sin(n\,\pi\,z)}{\left(\beta^2 - n^2\,\pi^2\right) \, n\,\pi \, \cos(n\,\pi)} \cdot 2\,\cos(n\,\pi\,\tau) \Leftrightarrow \tag{133}$$

$$f(\tau,z) = z - \frac{\sin(\beta\,z)}{\sin(\beta)} \, \cos(\beta\,\tau) + 2\,\beta^2 \sum_{n=1}^{\infty} \frac{\sin\left[n\,\pi\,(1-z)\right] \, \cos(n\,\pi\,\tau)}{\left(n^2\,\pi^2 - \beta^2\right) \, n\,\pi}$$

(it has been used that $1/\cos(n\,\pi) = (-1)^n = \cos(n\,\pi)$ and that $\sin\left[n\,\pi\,(1-z)\right] = -\sin(n\,\pi\,z)\,\cos(n\,\pi)$).

Checking initial- and boundary conditions The solution has to obey the conditions:

$$f(0,z) = 0 \quad , \quad \left.\frac{\partial f}{\partial \tau}\right|_{\tau=0} = 0 \qquad \forall \quad 0 < z < 1 \tag{134}$$

$$f(\tau,1) = 1 - \cos(\beta\,\tau) \quad , \quad \left.\frac{\partial f}{\partial z}\right|_{z=0} = -\mu \, \left.\frac{\partial^2 f}{\partial \tau^2}\right|_{z=0} \qquad \forall \quad \tau > 0$$

It is easily seen that the found solution gives $f(\tau, 1) = 1 - \cos(\beta\,\tau)$.

The partial derivative with respect to τ is

$$\frac{\partial f}{\partial \tau} = \frac{\sin(\beta\,z)}{\sin(\beta)} \, \beta \, \sin(\beta\,\tau) + 2\,\beta^2 \sum_{n=1}^{\infty} \frac{\sin\left[n\,\pi\,(1-z)\right] \, \sin(n\,\pi\,\tau)}{n^2\,\pi^2 - \beta^2} \tag{135}$$

which gives $\left.\frac{\partial f}{\partial \tau}\right|_{\tau=0} = 0$.

The value of f at $\tau = 0$ is given by:

$$f(0,z) = z - \frac{\sin(\beta\, z)}{\sin(\beta)} + 2\,\beta^2 \sum_{n=1}^{\infty} \frac{\sin\left[n\,\pi\ (1-z)\right]}{\left(n^2\,\pi^2 - \beta^2\right)\ n\,\pi} \tag{136}$$

to see that this gives 0, part of the right hand side is written as a Fourier series (which will only consist of odd terms):

$$\frac{\sin(\beta\, z)}{\sin(\beta)} - z = \sum_{n=1}^{\infty} A_n\ \sin(n\,\pi\, z) \tag{137}$$

with the functions being orthogonal $\int_0^1 dz\ \sin(n\,\pi\, z)\ \sin(m\,\pi\, z) = \frac{1}{2}\,\delta_{nm}$ and the coefficients given by (the integral has been solved using an integral calculator):

$$A_n = \frac{\int_0^1 dz\ \left(\frac{\sin(\beta\, z)}{\sin(\beta)} - z\right)}{\int_0^1 dz\ \sin^2(n\,\pi\, z)} = -\frac{2\,\beta^2\ \cos(n\,\pi)}{n\,\pi\ \left(n^2\,\pi^2 - \beta^2\right)} \tag{138}$$

such that

$$\frac{\sin(\beta\, z)}{\sin(\beta)} - z = \sum_{n=1}^{\infty} -\frac{2\,\beta^2\ \cos(n\,\pi)}{n\,\pi\ \left(n^2\,\pi^2 - \beta^2\right)}\ \sin(n\,\pi\, z) = 2\,\beta^2 \sum_{n=1}^{\infty} \frac{\sin\left[n\,\pi\ (1-z)\right]}{\left(n^2\,\pi^2 - \beta^2\right)\ n\,\pi} \tag{139}$$

which gives that $f(0,z) = 0$.

Since $\mu \to \infty$ and $\left.\frac{\partial^2 f}{\partial \tau^2}\right|_{z=0} = 0$ this means that $\left.\frac{\partial f}{\partial z}\right|_{z=0}$ has to be finite. The partial derivative with respect to z is

$$\frac{\partial f}{\partial z} = 1 - \frac{\cos(\beta\, z)}{\sin(\beta)}\,\beta\ \cos(\beta\,\tau) - 2\,\beta^2 \sum_{n=1}^{\infty} \frac{\cos\left[n\,\pi\ (1-z)\right]\ \cos(n\,\pi\,\tau)}{n^2\,\pi^2 - \beta^2} \tag{140}$$

so at $z = 0$, it is:

$$\left.\frac{\partial f}{\partial z}\right|_{z=0} = 1 - \frac{\beta}{\sin(\beta)}\ \cos(\beta\,\tau) - 2\,\beta^2 \sum_{n=1}^{\infty} \frac{\cos(n\,\pi)\ \cos(n\,\pi\,\tau)}{n^2\,\pi^2 - \beta^2} \tag{141}$$

This expression will be convergent since a sum similar to the above sum can be written as the function

$$\cot(\beta) = \frac{1}{\beta} + 2\,\beta \sum_{n=1}^{\infty} \frac{1}{\beta^2 - n^2\,\pi^2} \Leftrightarrow 2\,\beta \sum_{n=1}^{\infty} \frac{1}{\beta^2 - n^2\,\pi^2} = \frac{1}{\beta} - \cot(\beta) \tag{142}$$

and since the remaining factors in the sum are cosine terms (which oscillate between -1 and 1) the actual sum in $\left.\frac{\partial f}{\partial z}\right|_{z=0}$ will also be convergent.

D.2 Numerical method

The ejection time for this system is found the excact same way as for the first system, and the stability condition is the same so again we have $\Delta t = \Delta z$.

D.2.1 Discretization of the PDE

The system is discretized the same way as for the first system, and figure 26 can be considered again. The velocities and acceleration for all the points except for the boundary $z = 1$ are again given by:

$$\begin{aligned} F[i] &= \frac{dY[i]}{d\tau} = Y[N+i] \quad \text{for} \quad i = 0, ..., N-1 \\ F[N+i] &= \frac{d^2Y[i]}{d\tau^2} = \frac{Y[i+1] - 2\,Y[i] + Y[i-1]}{\Delta z^2} \quad \text{for} \quad i = 1, ..., N-2 \\ F[N] &= \frac{d^2Y[0]}{d\tau^2} = \frac{Y[1] - 2\,Y[0] + 1 - \cos(\beta\,\tau)}{\Delta z^2} \end{aligned} \tag{143}$$

For the second boundary condition we find the second order approximation by writing the taylor expansion to third order around $i = N - 1$ for the points $i = N - 2$ and $i = N - 3$ like the first part of equation 95 before the boundary condition of the first system was inserted. If we instead insert the boundary condition for this system we get:

$$\begin{aligned} &\left.\frac{\partial^2 f}{\partial z^2}\right|_{z=1} + \frac{3\,\mu}{\Delta z}\left.\frac{\partial^2 f}{\partial \tau^2}\right|_{z=1} = \frac{8\,Y[N-2] - Y[N-3] - 7\,Y[N-1]}{2\,\Delta z^2} \Rightarrow \\ &\left.\frac{\partial^2 f}{\partial \tau^2}\right|_{z=1} = F[2\,N-1] = \frac{8\,Y[N-2] - Y[N-3] - 7\,Y[N-1]}{2\,\Delta z\,(\Delta z + 3\mu)} \end{aligned} \tag{144}$$

D.2.2 Energy transfer

The energy tranfer factor is given by the top of equation 30:

$$\nu = \frac{1}{\beta(1+\mu)}\left[\mu\left.\frac{\partial f}{\partial \tau}\right|_{(\tau,z)=(\tau_e,1)} + \int_0^1 \left.\frac{\partial f}{\partial \tau}\right|_{\tau=\tau_e} dz\right] \tag{145}$$

The integral part is the same as before, so numerically the energy transfer for this system is given by:

$$\nu = \frac{\mu\,Y[2N-1] + \Delta z\,\left(\frac{1}{2}\left(Y[2N-1] + \beta\,\sin(\beta\,\tau_e)\right) + \sum_{i=0}^{N-2} Y[N+i]\right)}{\beta(1+\mu)} \tag{146}$$

D.3 Energy of the pointmass-system

The kinetic energy of the system is given by

$$\begin{aligned} K &= \frac{m_2}{2}\left(\left.\frac{\partial u_p}{\partial t}\right|_{x=L_1}\right)^2 + \frac{m_1}{2\,L_1}\int_0^{L_1}\left(\frac{\partial u_p}{\partial t}\right)^2 dx \Rightarrow \\ \kappa &\equiv \frac{K}{m_1\,A^2\,(c_1/L_1)^2} = \frac{\mu}{2}\left(\left.\frac{\partial f_p}{\partial \tau}\right|_{z=1}\right)^2 + \frac{1}{2}\int_0^1\left(\frac{\partial f_p}{\partial \tau}\right)^2 dz \end{aligned} \tag{147}$$

where κ is the dimensionless kinetic energy. The potential energy of the system is given by

$$P = \frac{1}{2} S \int_0^{L_1} \sigma_1 \, \epsilon_1 \, dx = \frac{S}{2} E_1 \int_0^{L_1} \left(\frac{\partial u_p}{\partial x} \right)^2 dx \Rightarrow \tag{148}$$

$$\Pi \equiv \frac{P}{S \, E_1 \, A^2 / L_1} = \frac{P}{m_1 \, A^2 \, (c_1 / L_1)^2} = \frac{1}{2} \int_0^1 \left(\frac{\partial f_p}{\partial z} \right)^2$$

where Π is the dimensionless potential energy. The total energy is then

$$\xi = \kappa + \Pi = \frac{\mu}{2} \left(\left. \frac{\partial f_p}{\partial \tau} \right|_{z=1} \right)^2 + \frac{1}{2} \int_0^1 \left[\left(\frac{\partial f_p}{\partial \tau} \right)^2 + \left(\frac{\partial f_p}{\partial z} \right)^2 \right] dz \tag{149}$$

The velocities are solved for numerically and the strains can be found by using the central difference approximation

$$\left. \frac{\partial f_p}{\partial z} \right|_i = \frac{Y[i+1] - Y[i-1]}{2 \, \Delta z} \tag{150}$$

for the boundary point $z = 0$ taylor expanding the displacement at $i = 0$ and $i = 1$ around $z = 0$ gives the following approximation to the strain (where $f(0) = 1 - \cos(\beta \, \tau)$):

$$\begin{cases} Y[0] = f(0) + \Delta z \left. \frac{\partial f}{\partial z} \right|_{z=0} + \frac{\Delta z^2}{2} \left. \frac{\partial^2 f}{\partial z^2} \right|_{z=0} + \frac{\Delta z^3}{6} \left. \frac{\partial^3 f}{\partial z^3} \right|_{z=0} \\ Y[1] = f(0) + 2 \, \Delta z \left. \frac{\partial f}{\partial z} \right|_{z=0} + \frac{4 \, \Delta z^2}{2} \left. \frac{\partial^2 f}{\partial z^2} \right|_{z=0} + \frac{8 \, \Delta z^3}{6} \left. \frac{\partial^3 f}{\partial z^3} \right|_{z=0} \end{cases} \Rightarrow \tag{151}$$

$$8 \, Y[0] - Y[1] = 7 \, f(0) + 6 \, \Delta \left. \frac{\partial f}{\partial z} \right|_{z=0} + 2 \, \Delta z^2 \left. \frac{\partial^2 f}{\partial z^2} \right|_{z=0} \Rightarrow$$

$$\left. \frac{\partial f}{\partial z} \right|_{z=0} = \frac{8 \, Y[0] - Y[1] - 7 \, f(0)}{6 \, \Delta z} - \frac{\Delta z}{3} \left. \frac{\partial^2 f}{\partial z^2} \right|_{z=0} \Leftrightarrow$$

$$\left. \frac{\partial f}{\partial z} \right|_{z=0} = \frac{8 \, Y[0] - Y[1] - 7 \, \left[1 - \cos(\beta \, \tau) \right]}{6 \, \Delta z} - \frac{\Delta z}{3} \beta^2 \, \cos(\beta \, \tau)$$

and from the boundary condition we know that the strain at $z = 1$ is given by

$$\left. \frac{\partial f}{\partial z} \right|_{z=1} = -\mu \left. \frac{\partial^2 f}{\partial \tau^2} \right|_{z=1} = -\mu \, \frac{8 \, Y[N-2] - Y[N-3] - 7 \, Y[N-1]}{2 \, \Delta z \, (\Delta z + 3 \, \mu)} \tag{152}$$

Calling the integrand h_i at point $i = -1, 0, 1, ..., N$ (where by $i = -1$ we mean the boundary point $z = 0$) using the trapez method to approximate the integral gives

$$\xi = \frac{\mu}{2} \, Y[2 \, N - 1] + \frac{1}{2} \left[\frac{1}{2} (h_{-1} + h_N) + \sum_{n=0}^{N-1} h_n \right] \tag{153}$$

E Intermediate calculations for nonhomogeneous system

Equation 40 describes the partial differential equation with corresponding initial and boundary conditions that the displacements of the two materials must obey. To solve for the displacements the same method as for the other system can be used.

E.1 Analytical method

Again, this system was first considered in my bachelor [10] in an appendix. The solution was only found in Laplace space back then and again with the other definition of the parameter $z \to z - 1$.

E.1.1 Solution to displacements

Solution in Laplace space Laplace transforming the system, gives (where $F_1(s,z)$ is the Laplace transform of $f_1(\tau, z)$ and likewise for the other material) the same as for the other two systems where only some boundary conditions are different:

$$\begin{aligned} \frac{d^2F_1}{dz^2} + \alpha^2 F_1 &= 0 \\ \frac{d^2F_2}{dz^2} + c^2\,\alpha^2 F_2 &= 0 \\ F_1(s,0) = \frac{\beta^2}{s\,(s^2+\beta^2)} \quad &, \quad \left.\frac{dF_2}{dz}\right|_{z=1} = 0 \\ F_1(s,l) = F_2(s,l) \quad &, \quad e\ \left.\frac{dF_1}{dz}\right|_{z=l} = \left.\frac{dF_2}{dz}\right|_{z=l} \end{aligned} \tag{154}$$

where $\alpha^2 = -s^2$ to make it shorter. The general solution and the derivatives are then

$$\begin{aligned} F_1(s,z) = k_{11}\,\sin(\alpha z) + k_{12}\,\cos(\alpha z) &\Rightarrow \frac{dF_1}{dz} = \alpha\,[k_{11}\,\cos(\alpha z) - k_{12}\,\sin(\alpha z)] \\ F_2(s,z) = k_{21}\,\sin(c\alpha z) + k_{22}\,\cos(c\alpha z) &\Rightarrow \frac{dF_2}{dz} = c\alpha\,[k_{21}\,\cos(c\alpha z) - k_{22}\,\sin(c\alpha z)] \end{aligned} \tag{155}$$

Using the first and second boundary conditions give

$$\begin{aligned} F_1(s,0) = k_{12} &= \frac{\beta^2}{s\,(s^2+\beta^2)} \\ \left.\frac{dF_2}{dz}\right|_{z=1} = c\alpha\,[k_{21}\,\cos(c\alpha) - k_{22}\,\sin(c\alpha)] = 0 &\Rightarrow k_{21} = k_{22}\frac{\sin(c\alpha)}{\cos(c\alpha)} \end{aligned} \tag{156}$$

The third boundary condition gives

$$\begin{aligned} k_{11}\,\sin(\alpha l) + k_{12}\,\cos(\alpha l) = k_{21}\left[\frac{\sin(c\alpha)}{\cos(c\alpha)}\sin(c\alpha l) + \cos(c\alpha l)\right] &\Leftrightarrow \\ k_{11}\,\sin(\alpha l)\,\cos(c\alpha) + k_{12}\,\cos(\alpha l)\,\cos(c\alpha) = k_{22}\,\cos\left[c\alpha(1-l)\right] & \end{aligned} \tag{157}$$

The last boundary condition gives

$$k_{11}\,\cos(\alpha l) - k_{12}\,\sin(\alpha l) = r k_{22}\left[\frac{\sin(c\alpha)}{\cos(c\alpha)}\,\cos(c\alpha l) - k_{22}\,\sin(c\alpha z)\right] \Leftrightarrow \tag{158}$$
$$k_{11}\,\cos(\alpha l)\,\cos(c\alpha) - k_{12}\,\sin(\alpha l)\,\cos(c\alpha) = r k_{22}\sin\left[c\alpha(1-l)\right]$$

where $r \equiv c/e$. Now the last two equations give

$$r\,\tan\left[c\alpha(1-l)\right] = \frac{k_{11}\,\cos(\alpha l)\,\cos(c\alpha) - k_{12}\,\sin(\alpha l)\,\cos(c\alpha)}{k_{11}\,\sin(\alpha l)\,\cos(c\alpha) + k_{12}\,\cos(\alpha l)\,\cos(c\alpha)} \Leftrightarrow \tag{159}$$
$$k_{11}\,\left[\cos(\alpha l) - r\,\tan\left[c\alpha(1-l)\right]\,\sin(\alpha l)\right] = k_{12}\left[\sin(\alpha l) + r\,\tan\left[c\alpha(1-l)\right]\,\cos(\alpha l)\right] \Leftrightarrow$$
$$k_{11} = k_{12}\,\frac{\sin(\alpha l) + r\,\tan\left[c\alpha(1-l)\right]\,\cos(\alpha l)}{\cos(\alpha l) - r\,\tan\left[c\alpha(1-l)\right]\,\sin(\alpha l)} \Leftrightarrow$$
$$k_{11} = k_{12}\,\frac{\tan(\alpha l) + r\,\tan\left[c\alpha(1-l)\right]}{1 - r\,\tan\left[c\alpha(1-l)\right]\,\tan(\alpha l)}$$

From the equation describing continuity of displacement we can get the constant k_{22}:

$$k_{22}\,\cos\left[c\alpha(1-l)\right] = \tag{160}$$
$$k_{12}\,\cos(c\alpha)\,\frac{\left(\tan(\alpha l) + r\,\tan\left[c\alpha(1-l)\right]\right)\,\sin(\alpha l) + \cos(\alpha l) - r\,\tan\left[c\alpha(1-l)\right]\,\sin(\alpha l)}{1 - r\,\tan\left[c\alpha(1-l)\right]\,\tan(\alpha l)} \Leftrightarrow$$
$$k_{22}\,\cos\left[c\alpha(1-l)\right] = \frac{k_{12}\,\cos(c\alpha)}{\cos(\alpha l) - r\,\tan\left[c\alpha(1-l)\right]\,\sin(\alpha l)} \Leftrightarrow$$
$$k_{22} = k_{12}\,\frac{\cos(c\alpha)}{\cos(\alpha l)\,\cos\left[c\alpha(1-l)\right] - r\,\sin(\alpha l)\,\sin\left[c\alpha(1-l)\right]}$$

and so we also know k_{21} now (from the second boundary condition):

$$k_{21} = k_{12}\,\frac{\sin(c\alpha)}{\cos(\alpha l)\,\cos\left[c\alpha(1-l)\right] - r\,\sin(\alpha l)\,\sin\left[c\alpha(1-l)\right]} \tag{161}$$

Now that the constants are known, we can put them back into the general solution. For F_1 we get

$$F_1 = k_{12}\,\frac{\sin(\alpha l)\,\sin(\alpha z) + r\,\tan\left[c\alpha(1-l)\right]\,\cos(\alpha l)\,\sin(\alpha z)}{\cos(\alpha l) - r\,\tan\left[c\alpha(1-l)\right]\,\sin(\alpha l)} + \tag{162}$$
$$k_{12}\,\frac{\cos(\alpha l)\,\cos(\alpha z) - r\,\tan\left[c\alpha(1-l)\right]\,\sin(\alpha l)\,\cos(\alpha z)}{\cos(\alpha l) - r\,\tan\left[c\alpha(1-l)\right]\,\sin(\alpha l)} \Leftrightarrow$$
$$F_1 = k_{12}\,\frac{\cos\left[\alpha(z-l)\right] + r\,\tan\left[c\alpha(1-l)\right]\,\sin\left[\alpha(z-l)\right]}{\cos(\alpha l) - r\,\tan\left[c\alpha(1-l)\right]\,\sin(\alpha l)} \Leftrightarrow$$
$$F_1 = k_{12}\,\cos\left[c\alpha(1-l)\right]\,\frac{\cos\left[\alpha(z-l)\right] + r\,\tan\left[c\alpha(1-l)\right]\,\sin\left[\alpha(z-l)\right]}{\cos(\alpha l)\,\cos\left[c\alpha(1-l)\right] - r\,\sin(\alpha l)\,\sin\left[c\alpha(1-l)\right]}$$

and for F_2 we get

$$F_2 = k_{12}\,\frac{\sin(c\alpha)\,\sin(c\alpha z) + \cos(c\alpha)\,\cos(c\alpha z)}{\cos(\alpha l)\,\cos\left[c\alpha(1-l)\right] - r\,\sin(\alpha l)\,\sin\left[c\alpha(1-l)\right]} \Leftrightarrow \tag{163}$$
$$F_2 = k_{12}\,\frac{\cos\left[c\alpha(1-z)\right]}{\cos(\alpha l)\,\cos\left[c\alpha(1-l)\right] - r\,\sin(\alpha l)\,\sin\left[c\alpha(1-l)\right]}$$

Inserting the expression for k_{12} and α, we get that the solutions are

$$F_1 = \frac{\beta^2 \cos\left[c\sqrt{-s^2}(1-l)\right]}{s\,(s^2+\beta^2)} \frac{\cos\left[\sqrt{-s^2}\,(z-l)\right] + r\,\tan\left[c\sqrt{-s^2}\,(1-l)\right]\,\sin\left[\sqrt{-s^2}\,(z-l)\right]}{\cos(\sqrt{-s^2}\,l)\,\cos\left[c\sqrt{-s^2}\,(1-l)\right] - r\,\sin(\sqrt{-s^2}\,l)\,\sin\left[c\sqrt{-s^2}\,(1-l)\right]} \tag{164}$$

$$F_2 = \frac{\beta^2 \cos\left[c\sqrt{-s^2}(1-z)\right]}{s\,(s^2+\beta^2)} \frac{1}{\cos(\sqrt{-s^2}\,l)\,\cos\left[c\sqrt{-s^2}\,(1-l)\right] - r\,\sin(\sqrt{-s^2}\,l)\,\sin\left[c\sqrt{-s^2}\,(1-l)\right]}$$

Poles The inverse Laplace transform can be found the same way as for the other system. Both F_1 and F_2 have the same denominator, and the poles are

$$Q = 0 \Rightarrow \quad s_0 = 0 \quad , \quad s_\pm = \pm i\beta \tag{165}$$

and the other poles are given by

$$\begin{aligned} &\cos(\sqrt{-s^2}\,l)\,\cos\left[c\sqrt{-s^2}\,(1-l)\right] - r\,\sin(\sqrt{-s^2}\,l)\,\sin\left[c\sqrt{-s^2}\,(1-l)\right] = 0 \Rightarrow \\ &1 - r\tan(l\sqrt{-s^2})\,\tan\left[c\sqrt{-s^2}(1-l)\right] = 0 \end{aligned} \tag{166}$$

In general the poles are complex, but just call $\sqrt{-s^2} = \alpha_n$, then the equation becomes

$$1 - r\tan(l\alpha_n)\,\tan\left[c(1-l)\alpha_n\right] = 0 \Leftrightarrow r\tan\left[c(1-l)\alpha_n\right] = \cot(l\alpha_n) \tag{167}$$

Since there are two trigonometric functions with two different arguments it can be difficult to solve this equation using Newton-Rhapson because we have to give an initial guess to the solution which is hard when the two functions have different periods. It is also hard to find out whether the poles are real, imaginary or complex.

No real poles Assume that the poles are real such that $\alpha_n = \sqrt{-s^2} = iR$, then the equation giving the poles become

$$1 + r\tanh(lR)\,\tanh\left[c(1-l)R\right] = 0 \tag{168}$$

there are no solutions to this equation since the parameters are always positive and if $R > 0$ the hyperbolic tangent function is also positive so the sum above will never be zero. Also if $R < 0$ the two hyperbolic tangent functions are negative but the product is again positive and the sum will again never be zero.

Pole-equation for small c If $c \to 0$ the equation for the poles can be reduced using that the second tangent goes towards its argument so the equation becomes:

$$\begin{aligned} \text{for}\, c \to 0 : \quad & 1 - r\tan(l\alpha_n)\,c(1-l)\alpha_n = 0 \Leftrightarrow \\ & 1 - \frac{1-l}{\rho}\,\alpha_n\,\tan(l\alpha_n) = 0 \end{aligned} \tag{169}$$

but the constant can be rewritten to (where S is the object's cross section)

$$\frac{1-l}{\rho} = \frac{(L-L_1)\rho_2 S L_1}{L\rho_1 S L_1} = \frac{m_2}{m_1}\frac{L_1}{L} = \mu\, l \tag{170}$$

so the equation for the poles become

$$1 - \mu\, l\, \alpha_n \tan(l\alpha_n) = 0 \tag{171}$$

which is excactly the same equation for the poles of the system where the second material is just a point mass with $l\,\alpha_n = \Lambda_n$. This means that for small c the solution only depends on the mass ratio of the two materials.

Solution in real space Now that the poles are known we can find P and Q' at these poles. For both F_1 and F_2 the Q function is the same. This and its derivative are

$$\begin{aligned} Q =& s(s^2+\beta^2)\left(\cos(\sqrt{-s^2}\,l)\,\cos\left[c\sqrt{-s^2}\,(1-l)\right] - r\,\sin(\sqrt{-s^2}\,l)\,\sin\left[c\sqrt{-s^2}\,(1-l)\right]\right) \Rightarrow \\ Q' =& (s^2+\beta^2)\,(\cdot) + 2s^2\,(\cdot) + s(s^2+\beta^2)\frac{s}{\sqrt{-s^2}}\cdot \\ & \left(l\sin(l\sqrt{-s^2})\,\cos\left[c(1-l)\sqrt{-s^2}\right] + c(1-l)\sin\left[c(1-l)\sqrt{-s^2}\right]\,\cos(l\sqrt{-s^2})\right. \\ & \left. + rl\cos(l\sqrt{-s^2})\sin\left[c(1-l)\sqrt{-s^2}\right] + rc(1-l)\cos\left[c(1-l)\sqrt{-s^2}\right]\sin(l\sqrt{-s^2})\right) \end{aligned} \tag{172}$$

where $(\cdot)$ is the third factor in paranthesis in Q. The value of Q' at the poles are:

$$Q'(0) = \beta^2 \quad , \quad Q'(\pm i\beta) = -2\beta^2\left(\cos(\beta l)\,\cos\left[\beta c(1-l)\right] - r\sin(\beta l)\,\sin\left[\beta c(1-l)\right]\right) \tag{173}$$

and at s_n the derivative is:

$$\begin{aligned} Q'(\pm s_n) =& \lambda_n(\alpha_n^2-\beta^2)\Big(l\sin(l\alpha_n)\,\cos\left[c(1-l)\alpha_n\right] + c(1-l)\sin\left[c(1-l)\alpha_n\right]\,\cos(l\alpha_n) \\ & + rl\cos(l\alpha_n)\sin\left[c(1-l)\alpha_n\right] + rc(1-l)\cos\left[c(1-l)\alpha_n\right]\sin(l\alpha_n)\Big) \Leftrightarrow \\ Q'(\pm s_n) =& \alpha_n(\alpha_n^2-\beta^2)\Big(l\sin(l\alpha_n)\,\cos\left[c(1-l)\alpha_n\right] + l\frac{\cos^2(l\alpha_n)\,\cos\left[c(1-l)\alpha_n\right]}{\sin(l\alpha_n)\,\sin\left[c(1-l)\alpha_n\right]}\sin\left[c(1-l)\alpha_n\right] \\ & + c(1-l)\sin\left[c(1-l)\alpha_n\right]\,\cos(l\alpha_n) + c(1-l)\frac{\cos(l\alpha_n)\,\cos^2\left[c(1-l)\alpha_n\right]}{\sin(l\alpha_n)\,\sin\left[c(1-l)\alpha_n\right]}\sin(l\alpha_n)\Big) \Leftrightarrow \\ Q'(\pm s_n) =& \alpha_n(\alpha_n^2-\beta^2)\left[\frac{l\cos\left[c(1-l)\alpha_n\right]}{\sin(l\alpha_n)} + \frac{c(1-l)\cos(l\alpha_n)}{\sin\left[c(1-l)\alpha_n\right]}\right] \Leftrightarrow \\ Q'(\pm s_n) =& \alpha_n(\alpha_n^2-\beta^2)\,\frac{l\cos\left[c(1-l)\alpha_n\right]\,\sin\left[c(1-l)\alpha_n\right] + c(1-l)\cos(l\alpha_n)\,\sin(l\alpha_n)}{\sin(l\alpha_n)\,\sin\left[c(1-l)\alpha_n\right]} \Leftrightarrow \\ Q'(\pm s_n) =& \alpha_n(\alpha_n^2-\beta^2)\,\frac{l\sin\left[2c(1-l)\alpha_n\right] + c(1-l)\sin(2l\alpha_n)}{2\sin(l\alpha_n)\,\sin\left[c(1-l)\alpha_n\right]} \end{aligned} \tag{174}$$

where we know from the equation the poles satisfy that $r = \frac{\cos(l\alpha_n)\,\cos[c(1-l)\alpha_n]}{\sin(l\alpha_n)\,\sin[c(1-l)\alpha_n]}$.
For F_1 the function P_1 is

$$P_1 = \beta^2\,\cos\left[c\sqrt{-s^2}(1-l)\right]\,\left(\cos\left[\sqrt{-s^2}\,(z-l)\right] + r\,\tan\left[c\sqrt{-s^2}\,(1-l)\right]\,\sin\left[\sqrt{-s^2}\,(z-l)\right]\right) \tag{175}$$

and at the poles it has the values

$$\begin{aligned} &P_1(0) = \beta^2 \quad , \quad P_1(\pm i\beta) = \beta^2 \\ &P_1(\pm i\beta) = \beta^2 \cos\left[\beta c(1-l)\right] \left(\cos\left[\beta(z-l)\right] + r \tan\left[\beta c(1-l)\right] \sin\left[\beta(z-l)\right] \right) \\ &P_1(\pm s_n) = \beta^2 \cos\left[c(1-l)\alpha_n\right] \left(\cos\left[(z-l)\alpha_n\right] + r \tan\left[c(1-l)\alpha_n\right] \sin\left[(z-l)\alpha_n\right] \right) \end{aligned} \tag{176}$$

For F_2 the function P_2 and its value at the poles are:

$$\begin{aligned} &P_2 = \beta^2 \cos\left[c(1-z)\sqrt{-s^2}\right] \\ &P_2(0) = \beta^2 \quad , \quad P_2(\pm i\beta) = \beta^2 \cos\left[\beta c(1-z)\right] \quad , \quad P_2(\pm s_n) = \beta^2 \cos\left[c(1-z)\alpha_n\right] \end{aligned} \tag{177}$$

So the solution to the displacement of the first material in real space is given by

$$f_1 = 1 - \frac{1}{2} \frac{\cos\left[\beta c(1-l)\right] \left(\cos\left[\beta(z-l)\right] + r \tan\left[\beta c(1-l)\right] \sin\left[\beta(z-l)\right] \right)}{\cos(\beta l) \cos\left[\beta c(1-l)\right] - r \sin(\beta l) \sin\left[\beta c(1-l)\right]} 2\cos(\beta\tau) + \sum_n \frac{\beta^2}{\alpha_n(\alpha_n^2 - \beta^2)} \cdot \tag{178}$$

$$\frac{\cos\left[c(1-l)\alpha_n\right] \left(\cos\left[(z-l)\alpha_n\right] + r \tan\left[c(1-l)\alpha_n\right] \sin\left[(z-l)\alpha_n\right] \right)}{l \sin\left[2c(1-l)\alpha_n\right] + c(1-l)\sin(2l\alpha_n)} 2\sin(l\alpha_n) \sin\left[c(1-l)\alpha_n\right] 2\cos(\alpha_n\tau)$$

which then gives the following solution

$$\begin{aligned} f_1 =& 1 - \frac{\cos\left[\beta(z-l)\right] + r \tan\left[\beta c(1-l)\right] \sin\left[\beta(z-l)\right]}{\cos(\beta l) - r \tan\left[\beta c(1-l)\right] \sin(\beta l)} \cos(\beta\tau) \\ &- 2\beta^2 \sum_n \frac{\sin\left[2c(1-l)\alpha_n\right] \sin(l\alpha_n)}{\alpha_n(\beta^2 - \alpha_n^2)} \frac{\cos\left[(z-l)\alpha_n\right] + r \tan\left[c(1-l)\alpha_n\right] \sin\left[(z-l)\alpha_n\right]}{l \sin\left[2c(1-l)\alpha_n\right] + c(1-l)\sin(2l\alpha_n)} \cos(\alpha_n\tau) \end{aligned} \tag{179}$$

and the solution to the displacement of the second material in real space is

$$\begin{aligned} f_2 =& 1 - \frac{\cos\left[\beta c(1-z)\right] \cos(\beta\tau)}{\cos(\beta l) \cos\left[\beta c(1-l)\right] - r \sin(\beta l) \sin\left[\beta c(1-l)\right]} \\ &- 4\beta^2 \sum_n \frac{\sin(l\alpha_n)}{\alpha_n(\beta^2 - \alpha_n^2)} \frac{\sin\left[c(1-l)\alpha_n\right] \cos\left[c(1-z)\alpha_n\right] \cos(\alpha_n\tau)}{l \sin\left[2c(1-l)\alpha_n\right] + c(1-l)\sin(2l\alpha_n)} \end{aligned} \tag{180}$$

Solution for small c For small c (large sound velocity of the second material) this system should be reduced to the second system where we assumed a pointmass on top of an elastic material. This means that f_2 should be independent of z. This is easily seen since the ony z-dependence lies in cosines which are approximately 1 for small c:

$$\begin{aligned} f_2 =& 1 - \frac{\cos(\beta\tau)}{\cos(\beta l) - r\beta c(1-l)\sin(\beta l)} - 4\beta^2 \sum_n \frac{\sin(l\alpha_n)}{\beta^2 - \alpha_n^2} \frac{\cos(\alpha_n\tau)}{2l\alpha_n + \sin(2l\alpha_n)} \Leftrightarrow \\ f_2 =& 1 - \frac{\cos(\beta\tau)}{\cos(\beta l) - \mu\beta l \sin(\beta l)} - 4\beta^2 \sum_n \frac{\sin(l\alpha_n)}{\beta^2 - \alpha_n^2} \frac{\cos(\alpha_n\tau)}{2l\alpha_n + \sin(2l\alpha_n)} \end{aligned} \tag{181}$$

where it has been used that $rc = 1/\rho$ and $(1-l)/\rho = \mu l$. The displacement of the first material at the same limit is:

$$\begin{aligned} f_1 =& 1 - \frac{\cos\left[\beta(z-l)\right] + r\beta c(1-l)\,\sin\left[\beta(z-l)\right]}{\cos(\beta l) - r\beta c(1-l)\,\sin(\beta l)}\,\cos(\beta\tau) \\ &- 4\beta^2 \sum_n \frac{\sin(l\alpha_n)}{\beta^2-\alpha_n^2} \frac{\cos\left[(z-l)\alpha_n\right] + rc(1-l)\alpha_n\,\sin\left[(z-l)\alpha_n\right]}{2l\alpha_n + \sin(2l\alpha_n)}\cos(\alpha_n\tau) \Leftrightarrow \\ f_1 =& 1 - \frac{\cos\left[\beta(z-l)\right] + \mu\beta l\,\sin\left[\beta(z-l)\right]}{\cos(\beta l) - \mu\beta l\,\sin(\beta l)}\,\cos(\beta\tau) \\ &- 4\beta^2 \sum_n \frac{\sin(l\alpha_n)}{\beta^2-\alpha_n^2} \frac{\cos\left[(z-l)\alpha_n\right] + \mu l\alpha_n\,\sin\left[(z-l)\alpha_n\right]}{2l\alpha_n + \sin(2l\alpha_n)}\cos(\alpha_n\tau) \end{aligned} \tag{182}$$

Notice that at $z = l$ the two displacement functions are equal as they should be. This displacement f_1 can be compared to the displacement for system two by distinguishing the variables and parameters in system two from this system, for example by giving them a prime

$$z' = \frac{x}{L_1} \quad , \quad \tau' = \frac{c_1 t}{L_1} \quad , \quad \beta' = \frac{\omega L_1}{c_1} \tag{183}$$

the only difference between the two systems is that this third system has L (total length) instead of just L_1. So the relation between the two systems is:

$$z = z'l \quad , \quad \tau = \tau' l \quad , \quad \beta = \frac{\beta'}{l} \tag{184}$$

inserting these now gives the following expression for the displacement (also remembering that $l\alpha_n = \Lambda_n$, where $n = 1, 2, ...$)

$$\begin{aligned} f_1 =& 1 - \frac{\cos\left[\beta'(z'-1)\right] - \mu\beta'\,\sin\left[\beta'(z'-1)\right]}{\cos(\beta') - \mu\beta'\,\sin(\beta')}\,\cos(\beta'\tau') \\ &- 4\beta'^2 \sum_n \frac{\sin(\Lambda_n)}{\beta'^2-\Lambda_n^2} \frac{\cos\left[\Lambda_n'(z'-1)\right] - \mu\Lambda_n\,\sin\left[\Lambda_n'(z'-1)\right]}{2\Lambda_n + \sin(2\Lambda_n)}\cos(\Lambda_n\tau') \end{aligned} \tag{185}$$

also using that we know from the pole equation $\mu\Lambda_n = \cos(\Lambda_n)/\sin(\Lambda_n)$ we now get the excact same solution as for the other system where we considered an elastic object with a point mass on top:

$$f_1 = 1 - \frac{\cos\left[\beta'(z'-1)\right] - \mu\beta'\,\sin\left[\beta'(z'-1)\right]}{\cos(\beta') - \mu\beta'\,\sin(\beta')}\,\cos(\beta'\tau') + 4\beta'^2 \sum_n \frac{\sin(\Lambda_n z')}{\Lambda_n^2-\beta'^2}\frac{\cos(\Lambda_n\tau')}{2\Lambda_n + \sin(2\Lambda_n)} \tag{186}$$

E.1.2 Ejection time

The object ejects from the plate when the bottom of the object also becomes a free end $\left.\frac{\partial u_1}{\partial x}\right|_{x=0} = 0 \Rightarrow \left.\frac{\partial f_1}{\partial z}\right|_{z=0} = 0$. This then gives an equation for the ejection time τ_e. The derivative is given by

$$\begin{aligned} \frac{\partial f_1}{\partial z} =& -\frac{-\sin\left[\beta(z-l)\right] + r\tan\left[\beta c(1-l)\right]\,\cos\left[\beta(z-l)\right]}{\cos(\beta l) - r\tan\left[\beta c(1-l)\right]\,\sin(\beta l)}\,\beta\,\cos(\beta\tau) \\ &- 2\beta^2 \sum_n \frac{\sin\left[2c(1-l)\alpha_n\right]\,\sin(l\alpha_n)}{\beta^2-\alpha_n^2} \frac{-\sin\left[(z-l)\alpha_n\right] + r\tan\left[c(1-l)\alpha_n\right]\,\cos\left[(z-l)\alpha_n\right]}{l\sin\left[2c(1-l)\alpha_n\right] + c(1-l)\sin(2l\alpha_n)}\cos(\alpha_n\tau) \end{aligned} \tag{187}$$

and so the ejection time equation is given by

$$
\begin{aligned}
0 =& \frac{\sin(\beta l) + r \tan\left[\beta c (1-l)\right] \cos(\beta l)}{\cos(\beta l) - r \tan\left[\beta c (1-l)\right] \sin(\beta l)} \cos(\beta \tau_e) \\
&+ 2\beta \sum_n \frac{\sin\left[2c(1-l)\alpha_n\right] \sin(l\alpha_n)}{\beta^2 - \alpha_n^2} \frac{\sin(l\alpha_n) + r \tan\left[c(1-l)\alpha_n\right] \cos(l\alpha_n)}{l \sin\left[2c(1-l)\alpha_n\right] + c(1-l)\sin(2l\alpha_n)} \cos(\alpha_n \tau_e) \\
\Leftrightarrow\ 0 =& \frac{\tan(\beta l) + r \tan\left[\beta c (1-l)\right]}{1 - r \tan\left[\beta c (1-l)\right] \tan(\beta l)} \cos(\beta \tau_e) \\
&+ 2\beta \sum_n \frac{\sin\left[2c(1-l)\alpha_n\right] \sin(l\alpha_n)}{\beta^2 - \alpha_n^2} \frac{\sin(l\alpha_n) + r \tan\left[c(1-l)\alpha_n\right] \cos(l\alpha_n)}{l \sin\left[2c(1-l)\alpha_n\right] + c(1-l)\sin(2l\alpha_n)} \cos(\alpha_n \tau_e)
\end{aligned}
\tag{188}
$$

E.1.3 Energy transfer factor

In general the velocity of the object v at ejection time t_e is given by the total momentum divided by the total mass:

$$
\begin{aligned}
v &= \frac{1}{m_1 + m_2} \left[m_1 \frac{1}{L_1} \int_0^{L_1} \left.\frac{\partial u_1}{\partial t}\right|_{t=t_e} dx + m_2 \frac{1}{L - L_1} \int_{L_1}^{L} \left.\frac{\partial u_2}{\partial t}\right|_{t=t_e} dx \right] \Leftrightarrow \\
v &= \frac{1}{\rho_1 L_1 + \rho_2 (L - L_1)} \left[\rho_1 \int_0^{L_1} \left.\frac{\partial u_1}{\partial t}\right|_{t=t_e} dx + \rho_2 \int_{L_1}^{L} \left.\frac{\partial u_2}{\partial t}\right|_{t=t_e} dx \right]
\end{aligned}
\tag{189}
$$

where $m_1 = \rho_1 L_1 S$ and $m_2 = \rho_2 (L - L_1) S$ where S is the cross-section. Dividing by $A\,\omega$ gives the energy transfer factor ν. If the dimensionless variables are used with $\frac{\partial \tau}{\partial t} = \frac{c_1}{L}$ and $\frac{\partial z}{\partial x} = \frac{1}{L}$ we get

$$
\begin{aligned}
\nu &= \frac{1}{L\left[\rho_1 l + \rho_2 (1-l)\right]\omega} \frac{c_1}{L} L \left[\rho_1 \int_0^{l} \left.\frac{\partial f_1}{\partial \tau}\right|_{\tau=\tau_e} dz + \rho_2 \int_{l}^{1} \left.\frac{\partial f_2}{\partial \tau}\right|_{\tau=\tau_e} dz \right] \Leftrightarrow \\
\nu &= \frac{1}{\left[l(\rho - 1) + 1\right]\beta} \left[\rho \int_0^{l} \left.\frac{\partial f_1}{\partial \tau}\right|_{\tau=\tau_e} dz + \int_{l}^{1} \left.\frac{\partial f_2}{\partial \tau}\right|_{\tau=\tau_e} dz \right]
\end{aligned}
\tag{190}
$$

The two derivatives are

$$
\begin{aligned}
\frac{\partial f_1}{\partial z} =& \frac{\cos\left[\beta(z-l)\right] + r \tan\left[\beta c(1-l)\right] \sin\left[\beta(z-l)\right]}{\cos(\beta l) - r \tan\left[\beta c(1-l)\right] \sin(\beta l)} \beta \sin(\beta \tau) \\
&+ 2\beta^2 \sum_n \frac{\sin\left[2c(1-l)\alpha_n\right] \sin(l\alpha_n)}{\beta^2 - \alpha_n^2} \frac{\cos\left[(z-l)\alpha_n\right] + r \tan\left[c(1-l)\alpha_n\right] \sin\left[(z-l)\alpha_n\right]}{l \sin\left[2c(1-l)\alpha_n\right] + c(1-l)\sin(2l\alpha_n)} \sin(\alpha_n \tau) \\
\frac{\partial f_2}{\partial z} =& \frac{\beta \cos\left[\beta c(1-z)\right] \sin(\beta \tau)}{\cos(\beta l) \cos\left[\beta c(1-l)\right] - r \sin(\beta l) \sin\left[\beta c(1-l)\right]} \\
&+ 4\beta^2 \sum_n \frac{\sin(l\alpha_n)}{\beta^2 - \alpha_n^2} \frac{\sin\left[c(1-l)\alpha_n\right] \cos\left[c(1-z)\alpha_n\right] \sin(\alpha_n \tau)}{l \sin\left[2c(1-l)\alpha_n\right] + c(1-l)\sin(2l\alpha_n)}
\end{aligned}
\tag{191}
$$

and the integrals of these at ejection time are

$$\int_0^l \left.\frac{\partial f_1}{\partial z}\right|_{\tau=\tau_e} = \frac{\Big[\sin\left[\beta(z-l)\right]\Big]_0^l + r\tan\left[\beta c(1-l)\right]\Big[-\cos\left[\beta(z-l)\right]\Big]_0^l}{\cos(\beta l) - r\tan\left[\beta c(1-l)\right]\sin(\beta l)}\sin(\beta\tau_e) \tag{192}$$

$$+2\beta^2\sum_n \frac{\sin\left[2c(1-l)\alpha_n\right]\sin(l\alpha_n)}{\alpha_n(\beta^2-\alpha_n^2)}\frac{\Big[\sin\left[(z-l)\alpha_n\right]\Big]_0^l + r\tan\left[c(1-l)\alpha_n\right]\Big[-\cos\left[(z-l)\alpha_n\right]\Big]_0^l}{l\sin\left[2c(1-l)\alpha_n\right] + c(1-l)\sin(2l\alpha_n)}\sin(\alpha_n\tau_e)$$

$$\Leftrightarrow \int_0^l \left.\frac{\partial f_1}{\partial z}\right|_{\tau=\tau_e} = \frac{\sin(\beta l) + r\tan\left[\beta c(1-l)\right]\left[\cos(\beta l)-1\right]}{\cos(\beta l) - r\tan\left[\beta c(1-l)\right]\sin(\beta l)}\sin(\beta\tau_e)$$

$$+2\beta^2\sum_n \frac{\sin\left[2c(1-l)\alpha_n\right]\sin(l\alpha_n)}{\alpha_n(\beta^2-\alpha_n^2)}\frac{\sin(l\alpha_n) + r\tan\left[c(1-l)\alpha_n\right]\left[\cos(l\alpha_n)-1\right]}{l\sin\left[2c(1-l)\alpha_n\right] + c(1-l)\sin(2l\alpha_n)}\sin(\alpha_n\tau_e)$$

and

$$\int_l^1 \left.\frac{\partial f_2}{\partial z}\right|_{\tau=\tau_e} = \frac{-1}{c}\frac{\Big[\sin\left[\beta c(1-z)\right]\Big]_l^1\sin(\beta\tau_e)}{\cos(\beta l)\cos\left[\beta c(1-l)\right] - r\sin(\beta l)\sin\left[\beta c(1-l)\right]} \tag{193}$$

$$+4\beta^2\frac{-1}{c}\sum_n \frac{\sin(l\alpha_n)}{\alpha_n(\beta^2-\alpha_n^2)}\frac{\sin\left[c(1-l)\alpha_n\right]\Big[\sin\left[c(1-z)\alpha_n\right]\Big]_l^1\sin(\alpha_n\tau_e)}{l\sin\left[2c(1-l)\alpha_n\right] + c(1-l)\sin(2l\alpha_n)} \Leftrightarrow$$

$$\int_l^1 \left.\frac{\partial f_2}{\partial z}\right|_{\tau=\tau_e} = \frac{1}{c}\frac{\tan\left[\beta c(1-l)\right]\sin(\beta\tau_e)}{\cos(\beta l) - r\tan\left[\beta c(1-l)\right]\sin(\beta l)}$$

$$+4\frac{\beta^2}{c}\sum_n \frac{\sin(l\alpha_n)}{\alpha_n(\beta^2-\alpha_n^2)}\frac{\sin^2\left[c(1-l)\alpha_n\right]\sin(\alpha_n\tau_e)}{l\sin\left[2c(1-l)\alpha_n\right] + c(1-l)\sin(2l\alpha_n)}$$

Using the fact that $\rho r = c/e\cdot e/c^2 = 1/c$, the sum of the two integrals as they appear in the energy tranfer factor is

$$\rho\int_0^l \left.\frac{\partial f_1}{\partial\tau}\right|_{\tau=\tau_e} dz + \int_l^1 \left.\frac{\partial f_2}{\partial\tau}\right|_{\tau=\tau_e} dz = \frac{\rho\sin(\beta\tau_e)\Big(\sin(\beta l) + r\tan\left[\beta c(1-l)\right]\cos(\beta l)\Big)}{\cos(\beta l) - r\tan\left[\beta c(1-l)\right]\sin(\beta l)} \tag{194}$$

$$+4\rho\beta^2\sum_n \frac{\sin\left[c(1-l)\alpha_n\right]\sin(l\alpha_n)\sin(\alpha_n\tau_e)}{\alpha_n(\beta^2-\alpha_n^2)}\frac{\cos\left[c(1-l)\alpha_n\right]\sin(l\alpha_n) + r\sin\left[c(1-l)\alpha_n\right]\cos(l\alpha_n)}{l\sin\left[2c(1-l)\alpha_n\right] + c(1-l)\sin(2l\alpha_n)}$$

from the ejection time equation we know that

$$\frac{\sin(\beta l) + r\tan\left[\beta c(1-l)\right]\cos(\beta l)}{\cos(\beta l) - r\tan\left[\beta c(1-l)\right]\sin(\beta l)} = -\frac{4\beta}{\cos(\beta\tau_e)}\sum_n \cos(\alpha_n\tau_e)\cdot \tag{195}$$

$$\frac{\cos\left[c(1-l)\alpha_n\right]\sin\left[c(1-l)\alpha_n\right]\sin(l\alpha_n)}{\beta^2-\alpha_n^2}\frac{\sin(l\alpha_n) + r\tan\left[c(1-l)\alpha_n\right]\cos(l\alpha_n)}{l\sin\left[2c(1-l)\alpha_n\right] + c(1-l)\sin(2l\alpha_n)}$$

so the sum of the two integrals above can also be written as

$$\rho \int_0^l \frac{\partial f_1}{\partial \tau}\bigg|_{\tau=\tau_e} dz + \int_l^1 \frac{\partial f_2}{\partial \tau}\bigg|_{\tau=\tau_e} dz = \sum_n \frac{4\rho\beta^2 \sin\left[c(1-l)\alpha_n\right] \sin(l\alpha_n)}{(\beta^2-\alpha_n^2)\left(l\sin\left[2c(1-l)\alpha_n\right] + c(1-l)\sin(2l\alpha_n)\right)} \cdot \tag{196}$$

$$\left[\frac{\sin(\alpha_n\tau_e)}{\alpha_n}\left(\cos\left[c(1-l)\alpha_n\right] \sin(l\alpha_n) + r\sin\left[c(1-l)\alpha_n\right] \cos(l\alpha_n)\right)\right.$$

$$\left. + \frac{\tan(\beta\tau_e)}{\beta}\cos(\alpha_n\tau_e)\left(\cos\left[c(1-l)\alpha_n\right] \sin(l\alpha_n) + r\sin\left[c(1-l)\alpha_n\right] \cos(l\alpha_n)\right)\right] \Leftrightarrow$$

$$\rho \int_0^l \frac{\partial f_1}{\partial \tau}\bigg|_{\tau=\tau_e} dz + \int_l^1 \frac{\partial f_2}{\partial \tau}\bigg|_{\tau=\tau_e} dz = 4\rho\beta^2 \sum_n \frac{\sin\left[c(1-l)\alpha_n\right] \sin(l\alpha_n)\cos(\alpha_n\tau_e)}{(\beta^2-\alpha_n^2)\left(l\sin\left[2c(1-l)\alpha_n\right] + c(1-l)\sin(2l\alpha_n)\right)} \cdot$$

$$\left(\frac{\tan(\alpha_n\tau_e)}{\alpha_n} + \frac{\tan(\beta\tau_e)}{\beta}\right)\left(\cos\left[c(1-l)\alpha_n\right] \sin(l\alpha_n) + r\sin\left[c(1-l)\alpha_n\right] \cos(l\alpha_n)\right)$$

and so the energy transfer factor is then given by

$$\nu = \frac{4\rho\beta}{l(\rho-1)+1} \sum_n \frac{\sin\left[c(1-l)\alpha_n\right] \sin(l\alpha_n)\cos(\alpha_n\tau_e)}{(\beta^2-\alpha_n^2)\left(l\sin\left[2c(1-l)\alpha_n\right] + c(1-l)\sin(2l\alpha_n)\right)} \cdot \tag{197}$$

$$\left(\frac{\tan(\alpha_n\tau_e)}{\alpha_n} + \frac{\tan(\beta\tau_e)}{\beta}\right)\left(\cos\left[c(1-l)\alpha_n\right] \sin(l\alpha_n) + r\sin\left[c(1-l)\alpha_n\right] \cos(l\alpha_n)\right)$$

E.2 Numerical method

To solve the system numerically the exact same method is used as for the other system. The only difference is in the discretization of the PDE's and in the energy transfer. The expression for the ejection time is the same and the integration in τ is also the same.

E.2.1 Discretization of the PDE's

The discretization of the system in z is done the excact same way as for the other two systems. Now assume that there are N elements of the first material with spacing $\Delta z_1 = l/N$ between neigbouring points and M elements of the second material with spacing $\Delta z_2 = (l-1)/M$ between neigbouring points. All these displacements and corresponding velocities are put in a vector F that has $2N + 2M$ elements. See figure 31 below for clarity.

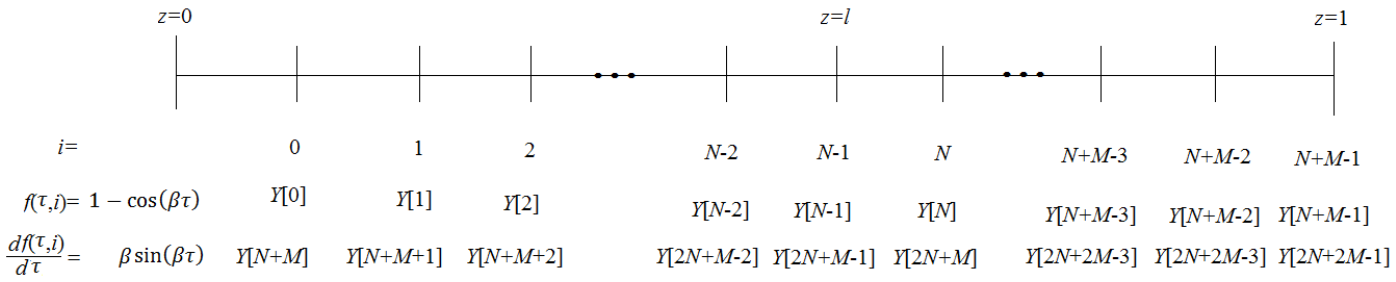

Figure 31: The figure shows how the object is discretized in space.

Just as before the velocities of each element and the accelerations are:

$$
\begin{aligned}
&F[i] = Y[N+M+i] \quad \text{for} \quad i = 1, ..., N-2 \\
&F[N+M] = \frac{Y[1] - 2\,Y[0] + 1 - \cos(\beta\,\tau)}{\Delta z_1^2} \\
&F[N+M+i] = \frac{Y[i+1] - 2\,Y[i] + Y[i-1]}{\Delta z_1^2} \quad \text{for} \quad i = 1, ..., N-2 \\
&F[2\,N+M-1+i] = \frac{Y[N+i] - 2\,Y[N-1+i] + Y[N-2+i]}{c^2\,\Delta z_2^2} \quad \text{for} \quad i = 1, ..., M-1
\end{aligned}
\tag{198}
$$

For the boundary $i = N+M-1$ ($z = 1$) we can consider the taylor expansion to third order around $z = 1$ for the points $i = N+M-2$ and $i = N+M-3$ to get

$$
\begin{cases}
Y[N+M-2] = Y[N+M-1] - \left.\frac{\partial f_2}{\partial z}\right|_{z=1} \Delta z_2 + \left.\frac{\partial^2 f_2}{\partial z^2}\right|_{z=1} \frac{\Delta z_2^2}{2} - \left.\frac{\partial^3 f_2}{\partial z^3}\right|_{z=1} \frac{\Delta z_2^3}{6} \\
Y[N+M-3] = Y[N+M-1] - \left.\frac{\partial f_2}{\partial z}\right|_{z=1} 2\,\Delta z_2 + \left.\frac{\partial^2 f_2}{\partial z^2}\right|_{z=1} \frac{(2\,\Delta_2 z)^2}{2} - \left.\frac{\partial_2^3 f}{\partial z^3}\right|_{z=1} \frac{(2\,\Delta z_2)^3}{6}
\end{cases}
\Leftrightarrow
\tag{199}
$$

$$
8\,Y[N+M-2] - Y[N+M-3] = 7\,Y[N+M-1] - 6\,\Delta z_2 \left.\frac{\partial f_2}{\partial z}\right|_{z=1} + 2\,\Delta z_2^2 \left.\frac{\partial^2 f_2}{\partial z^2}\right|_{z=1} \Rightarrow
$$

$$
\left.\frac{\partial^2 f_2}{\partial z^2}\right|_{z=1} = \frac{8\,Y[N+M-2] - Y[N+M-3] - 7\,Y[N+M-1]}{2\,\Delta z_2^2}
$$

where the boundary condition at $z = 1$ has been used to get to the last line. So this gives the following second order approximation to the derivative:

$$
F[2\,N+2\,M-1] = \frac{8\,Y[N+M-2] - Y[N+M-3] - 7\,Y[N+M-1]}{2\,c^2\,\Delta z_2^2}
\tag{200}
$$

For the boundary at the material interface $z = l$ we can find the second order approximation to the double time derivative by writing the Taylor series for the points $i = N-2$ and $i = N-3$ around $i = N-1$ ($z = l$) to get

$$
\begin{cases}
Y[N-2] = Y[N-1] - \Delta z_1 \left.\frac{\partial f_1}{\partial z}\right|_{z=l} + \frac{\Delta z_1^2}{2} \left.\frac{\partial^2 f_1}{\partial z^2}\right|_{z=l} - \frac{\Delta z_1^3}{6} \left.\frac{\partial^3 f_1}{\partial z^3}\right|_{z=l} \\
Y[N-3] = Y[N-1] - 2\,\Delta z_1 \left.\frac{\partial f_1}{\partial z}\right|_{z=l} + \frac{(2\,\Delta z_1)^2}{2} \left.\frac{\partial^2 f_1}{\partial z^2}\right|_{z=l} - \frac{(2\,\Delta z_1)^3}{6} \left.\frac{\partial^3 f_1}{\partial z^3}\right|_{z=l}
\end{cases}
\Rightarrow
\tag{201}
$$

$$
8\,Y[N-2] - Y[N-3] = 7\,Y[N-1] - 6\,\Delta z_1 \left.\frac{\partial f_1}{\partial z}\right|_{z=l} + 2\,\Delta z_1^2 \left.\frac{\partial^2 f_1}{\partial z^2}\right|_{z=l}
$$

and for the points $i = N$ and $i = N+1$ around $i = N-1$ to get

$$
\begin{cases}
Y[N] = Y[N-1] + \Delta z_2 \left.\frac{\partial f_2}{\partial z}\right|_{z=l} + \frac{\Delta z_2^2}{2} \left.\frac{\partial^2 f_2}{\partial z^2}\right|_{z=l} + \frac{\Delta z_2^3}{6} \left.\frac{\partial^3 f_2}{\partial z^3}\right|_{z=l} \\
Y[N+1] = Y[N-1] + 2\,\Delta z_2 \left.\frac{\partial f_2}{\partial z}\right|_{z=l} + \frac{(2\,\Delta z_2)^2}{2} \left.\frac{\partial^2 f_2}{\partial z^2}\right|_{z=l} + \frac{(2\,\Delta z_2)^3}{6} \left.\frac{\partial^3 f_2}{\partial z^3}\right|_{z=l}
\end{cases}
\Rightarrow
\tag{202}
$$

$$
8\,Y[N] - Y[N+1] = 7\,Y[N-1] + 6\,\Delta z_2 \left.\frac{\partial f_2}{\partial z}\right|_{z=l} + 2\,\Delta z_2^2 \left.\frac{\partial^2 f_2}{\partial z^2}\right|_{z=l}
$$

Multiplying the first equation with $e\,\Delta z_2$ and adding the second equation multiplied by Δz_1 then gives (also the boundary condition saying that the stress is continuous has been used to make the first derivatives drop out)

$$e\,\Delta z_2\,(8\,Y[N-2]-Y[N-3]) + \Delta z_1\,(8Y[N] - Y[N+1]) = \\ 7\,Y[N-1]\,(e\Delta z_2 + \Delta z_1) + 2\,\Delta z_1\,\Delta z_2\,\left(e\,\Delta z_1\;\left.\frac{\partial^2 f_1}{\partial z^2}\right|_{z=l} + \Delta z_2\;\left.\frac{\partial^2 f_2}{\partial z^2}\right|_{z=l}\right) \tag{203}$$

The displacements always obey the wave equations and at $z = l$ the accelerations must be the same since it's the same point, so we can insert $\left.\frac{\partial^2 f_2}{\partial z^2}\right|_{z=l} = c^2\;\left.\frac{\partial^2 f_1}{\partial z^2}\right|_{z=l}$. Then we get

$$e\,\Delta z_2\,(8\,Y[N-2]-Y[N-3]) + \Delta z_1\,(8Y[N] - Y[N+1]) = \\ 7\,Y[N-1]\,(e\Delta z_2 + \Delta z_1) + 2\,\Delta z_1\,\Delta z_2\,\left(e\,\Delta z_1 + c^2\,\Delta z_2\right)\;\left.\frac{\partial^2 f_1}{\partial z^2}\right|_{z=l} \tag{204}$$

Isolating the double derivative with respect to z we get the acceleration at this point (since these are the same from the wave equation):

$$F[2\,N+M-1] = \frac{e\,\Delta z_2\,(8\,Y[N-2] - Y[N-3]) + \Delta z_1\,(8Y[N] - Y[N+1]) - 7\,Y[N-1]\,(e\Delta z_2 + \Delta z_1)}{2\,\Delta z_1\,\Delta z_2\,\left(e\,\Delta z_1 + c^2\,\Delta z_2\right)} \tag{205}$$

E.2.2 Energy transfer factor

The ejection time of the object is found as described for the other system in appendix D.2. The energy transfer factor is given by

$$\nu = \frac{1}{[l(\rho-1)+1]\,\beta}\left[\rho\int_0^l \left.\frac{\partial f_1}{\partial \tau}\right|_{\tau=\tau_e} dz + \int_l^1 \left.\frac{\partial f_2}{\partial \tau}\right|_{\tau=\tau_e} dz\right] \tag{206}$$

The integrals are again approximated the same way as for the two other systems such that:

$$\int_0^l \left.\frac{\partial f_1}{\partial \tau}\right|_{\tau=\tau_e} dz \approx \\ \Delta z_1\left(\frac{1}{2}(\beta\,\sin(\beta\,\tau_e) + Y[2\,N+M-1]) + \sum_{i=0}^{N-2} Y[N+M+i]\right) \\ \int_l^1 \left.\frac{\partial f_2}{\partial \tau}\right|_{\tau=\tau_e} dz \approx \\ \Delta z_2\left(\frac{1}{2}(Y[2\,N+M-1] + Y[2\,N+2\,M-1]) + \sum_{i=0}^{M-2} Y[2\,N+M+i]\right) \tag{207}$$

E.2.3 Stability condition

In order for the numerical method to be stable for this system we must have

$$\Delta\tau \leq \min(\Delta z_1, c\,\Delta z_2) \tag{208}$$

and in all numerical calculations we have chosen $\Delta\tau$ such that the above expression is an equality.

The first argument in the above equation comes from the fact that the partial differential equation and the numerical method for the first material is the same as for the two firt systems. For the second material there is an extra factor of $1/c^2$. It still looks like the normal wave equation but the 'velocity factor' is now $1/c$ and the argument used in the paragraph about stability condition for the homogeneous object now gives that $\Delta\tau \leq c\Delta z$. This gives the second argument, and the chosen $\Delta\tau$ must then be less than or equal to the smallest of the two.

E.3 Numerical results

In the table below

e	ρ	$c = \sqrt{e/\rho}$	l	$\mu = (1-l)/(\rho\, l)$	β_{opt}	τ_e	ν^2
100	10	3.16	0.1	0.9	0.24	7.26	1.53
			0.5	0.1	1.77	1.25	2.12
			0.9	0.011	0.98	2.25	2.51
	1	10	0.1	9	0.096	22.266	2.292
			0.5	1	0.13	13.47	1.61
			0.9	0.11	0.92	2.37	2.16
	0.1	31.62	0.1	90	0.032	69.586	2.503
			0.5	10	0.055	39.347	2.336
			0.9	1.11	0.22	8.85	1.96
10	10	1	0.1	0.9	0.74	2.47	1.58
			0.5	0.1	1.66	1.31	2.21
			0.9	0.011	1.01	2.21	2.53
	1	3.16	0.1	9	0.30	7.13	2.32
			0.5	1	0.44	4.51	1.95

			0.9	0.11	0.85	2.58	2.53
	0.1	10	0.1	90	0.100	22.274	2.527
			0.5	10	0.165	13.475	2.527
			0.9	1.11	0.400	4.982	2.452
1	10	0.316	0.1	0.9	2.36	0.83	1.95
			0.5	0.1	1.56	1.40	2.54
			0.9	0.011	1.00	2.23	2.53
	1	1	0.1	9	0.91	2.45	2.53
			0.5	1	0.91	2.45	2.53
			0.9	0.11	0.91	2.45	2.53
	0.1	3.16	0.1	90	0.30	7.69	2.72
			0.5	10	0.32	7.31	2.93
			0.9	1.11	0.50	4.44	2.66
0.1	10	0.1	0.1	0.9	4.78	0.47	2.53
			0.5	0.1	1.65	1.35	2.53
			0.9	0.011	1.00	2.23	2.53
	1	0.316	0.1	9	1.70	1.37	2.93
			0.5	1	0.92	2.39	2.63
			0.9	0.11	0.91	2.45	2.53
	0.1	1	0.1	90	0.56	4.25	3.07
			0.5	10	0.37	6.37	3.01
			0.9	1.11	0.51	4.37	2.67
0.01	10	0.0316	0.1	0.9	4.71	0.46	2.59
			0.5	0.1	1.65	1.35	2.53

			0.9	0.011	1.00	2.23	2.53
	1	0.1	0.1	9	1.95	1.21	3.00
			0.5	1	0.94	2.35	2.65
			0.9	0.11	0.91	2.45	2.53
	0.1	0.316	0.1	90	0.64	3.75	3.11
			0.5	10	0.37	6.34	3.01
			0.9	1.11	0.51	4.36	2.68
0.001	10	0.01	0.1	0.9	4.82	0.46	2.62
			0.5	0.1	1.65	1.35	2.53
			0.9	0.011	1.00	2.23	2.53
	1	0.0316	0.1	9	2.00	1.19	3.01
			0.5	1	0.95	2.34	2.65
			0.9	0.11	0.91	2.45	2.53
	0.1	0.1	0.1	90	0.65	3.69	3.11
			0.5	10	0.37	6.33	3.01
			0.9	1.11	0.51	4.36	2.68
0.0001	0.1	0.0316	0.05	190	0.8947	2.6812	3.1208
			0.1	90	0.65	3.69	3.11
			0.3	23.33	0.42	5.68	3.08
			0.5	10	0.37	6.33	3.01
			0.7	4.29	0.39	5.95	2.90

Table 3: Numerical results where ν^2_{max} is found for each set of parameters ρ, l, e on the same type of $\nu^2(\beta)$ plots as shown for the other two systems. For all results the spacing between neighbouring values of β is at least 0.01, while for those columns that have three or four digits it has been chosen to $1 \cdot 10^{-3}$ or $1 \cdot 10^{-4}$.

F Intermediate calculations for homogeneous system with damping

For the analytical calculations we use the parameter $2\,\gamma = R$ instead.

F.1 Analytical method

F.1.1 Solution in Laplace space

Laplace transforming the partial differential equation and its boundary conditions gives us the following ordinary differential equation with corresponding boundary conditions in Laplace space:

$$\frac{d^2F}{dz^2} + \frac{-s^2}{1+2\,\gamma\,s}\,F = 0 \tag{209}$$
$$F(s,0) = \frac{\beta^2}{s\,(s^2+\beta^2)} \quad , \quad \left.\frac{dF}{dz}\right|_{z=1} = 0$$

where it has been used that the Laplace transform of the first order derivative is $s\,F$. The Laplace transform of the left-hand-side of the stress-free boundary condition is $\left(\frac{dF}{dz} + 2\gamma s \frac{dF}{dz}\right)\Big|_{z=1}$ and so the boundary condition reduces to that above.
Let $\alpha^2 = \frac{-s^2}{1+2\,\gamma\,s}$ for short. Then the general solution and its derivative is given by

$$F(s,z) = k_1\,\sin(\alpha\,z) + k_2\,\cos(\alpha\,z) \Rightarrow \frac{dF}{dz} = \alpha\,[k_1\,\cos(\alpha\,z) - k_2\,\sin(\alpha\,z)] \tag{210}$$

From the first boundary condition, we have that

$$k_2 = \frac{\beta^2}{s\,(s^2+\beta)^2} \tag{211}$$

and from the second boundary condition we get

$$\alpha\,[k_1\,\cos(\alpha) - k_2\,\sin(\alpha)] = 0 \Leftrightarrow k_1 = k_2\,\frac{\sin(\alpha)}{\cos(\alpha)} \tag{212}$$

such that the particular solution is

$$F(s,z) = k_2\frac{1}{\cos(\alpha)}\,[\sin(\alpha)\,\sin(\alpha\,z) + \cos(\alpha)\,\cos(\alpha\,z)] \Leftrightarrow \tag{213}$$
$$F(s,z) = \frac{\beta^2}{s\,(s^2+\beta)^2}\frac{\cos\,[\alpha\,(1-z)]}{\cos(\alpha)} \equiv \frac{P(s,z)}{Q(s,z)}$$

F.1.2 Poles

The poles are given by $Q = 0$ and as usual some of the poles are $s = 0$ and $s = \pm i\beta$. The other poles are given by:

$$\cos(\alpha) = 0 \Rightarrow \alpha_n = \frac{\pi}{2}(2n-1) \equiv \lambda_n \quad , \quad n = 1, 2, 3, ... \tag{214}$$

The actual poles themselves s_n are then

$$\alpha = \sqrt{\frac{-s_n^2}{1+2\,\gamma\,s_n}} = \lambda_n \Rightarrow -s_n^2 = \lambda_n^2\,(1+2\,\gamma\,s_n) \Leftrightarrow s_n^2 + 2\,\gamma\,\lambda_n^2\,s_n + \lambda_n^2 = 0 \Rightarrow \tag{215}$$
$$s_n = -\gamma\,\lambda_n^2 \pm \sqrt{\gamma^2\,\lambda_n^4 - \lambda_n^2} = \lambda_n\left(-\gamma\,\lambda_n \pm \sqrt{(\gamma\,\lambda_n)^2 - 1}\right)$$

It is seen that for $\gamma = 0$ the poles are the same as in equation 12 for the homogeneous object with no internal friction. Notice now that when internal friction is included some of the poles are now complex in general - without friction all the poles were only imaginary.

Let the argument of the square root be $D = (\gamma\,\lambda_n)^2 - 1$. This term determines whether the poles are real or complex. If $\gamma \geq \frac{2}{\pi} \Rightarrow D \geq 0$ and all $s_n \in \mathbb{R}$. If instead $\frac{2}{3\pi} \leq \gamma < \frac{2}{\pi} \Rightarrow s_1 \in \mathbb{C}$ and all other $s_n \in \mathbb{R}$. If $\frac{2}{5\pi} \leq \gamma < \frac{2}{3\pi} \Rightarrow s_1, s_2 \in \mathbb{C}$ and all other $s_n \in \mathbb{R}$ and so on.

This means that for $\gamma \geq \frac{2}{\pi}$ all the s_n poles are only real, but for any other $\gamma < \frac{2}{\pi}$ there will be both real and complex poles. For a given value of γ, we can find those n for which the s_n are real:

$$D > 0 \Leftrightarrow \gamma\,\lambda_n > 1 \Leftrightarrow 2\,n - 1 > \frac{2}{\pi\,\gamma} \Leftrightarrow n > \frac{2+\pi\,\gamma}{2\,\pi\,\gamma} \tag{216}$$

So for a given value of γ, the above fraction can be calculated and those integers n that are less than the fraction correspond to complex solutions s_n.

Remembering that γ is the ratio between the viscosity and the Young's modulus of the material, it looks like the s_n poles are only real when the viscosity is large and when the viscosity becomes smaller complex poles also appear. The smaller the viscosity the smaller the real parts of the complex poles become and at the same time more of the complex poles appear.

F.2 Solution in Fourier space

It would be nice to have an idea of the effect of the damping by relating the viscosity to some of the other parameters. An idea of the time scale of the damping can be found by Fourier transforming equation 50 (meaning that the infinite system is considered), i.e. guessing on the solution $u(t,x) = \exp\left[i(\omega' t + k\,x)\right]$ where k is the wave number and ω' the corresponding frequency of that wave. This then gives a relationship between ω' and k:

$$-\omega'^2 = -c^2\,k^2 - i\,\frac{\eta}{\rho}\,\omega'\,k^2 \Leftrightarrow \omega'^2 - i\,\frac{\eta\,k^2}{\rho}\,\omega' - c^2\,k^2 = 0 \Rightarrow \omega' = i\,\frac{\eta\,k^2}{2\,\rho} \pm \sqrt{c^2\,k^2 - \left(\frac{\eta\,k^2}{2\,\rho}\right)^2} \tag{217}$$

It is now seen that the first term in the equation above, which is imaginary, will give a contribution to the solution of u consisting of a factor of a decreasing exponential of the form $e^{-t/t'}$ with $t' = 2\,\rho/(\eta\,k^2)$. This is the effect of the viscosity - it will damp the wave amplitude with a characteristic time scale t'. So to get an idea of the size of the viscosity, this is the term that needs to be considered, specifically the characteristic time for the damping. Since the basic wave (the one with the largest wave length) is the

dominating wave, this is the one considered. It has wave length $2L$ corresponding to the wave number $k = 2\pi/(2\,L) = \pi/L$, so the characteristic time for the damping of this wave is

$$t' = \frac{2\,\rho\,L^2}{\pi^2\,\eta} \Rightarrow \frac{t'\,c}{L} \equiv n = \frac{2\,\rho\,c\,L}{\pi^2\,\eta} = \frac{2}{\pi^2}\,\frac{1}{R} \tag{218}$$

where $R = \frac{\eta}{\rho\,L_1\,c_1} = \frac{\eta\,c_1}{E\,L_1}$ is a new dimensionless parameter that will show up when transforming equation 50 into dimensionless form.
From the characteristic time an expression for the number of times the wave moves a distance L when it has velocity c, can be found. This is called n. Consider the elastic object on the harmonic plate again. This then means that when the object is ejected into the air and if, for example by some photo elastic effects (which F. Celestini et al [9] make use of in their experiments), it is made possible to see the waves, then the number of times the wave moves from one end to another can be counted and then an approximate scale of R can be found. For example if one counts that the number of times the wave moves from one end to another is n at which point the wave amplitude has also dropped to some percentage $p = e^{-t_n/t'} = e^{-q}$ of its original size, then R is given by

$$q\frac{t'\,c}{L} = n = \frac{2}{\pi^2}\,\frac{q}{R} \Leftrightarrow R = \frac{2}{\pi^2}\,\frac{q}{n} \tag{219}$$

where $t_n = q\,t'$.

F.3 Numerical method

Consider figure 5 again. Discretizing the PDE is done the same way as before - but now we have to keep in mind that there is an extra term in the PDE so every time we have Taylor expanded the displacement at some point and used that the double derivative in time and space is the same we need to add an extra term. This will affect the governing equations and the ejection time only. The expression for the energy transfer factor is the same.

F.3.1 Discretization of the PDE

The equation for the velocities are the same, but the double derivative in time now becomes the same as before but with an extra term containing velocities:

$$\begin{aligned}
&\frac{dY[i]}{d\tau} = F[i] = Y[N+i] \quad \text{for} \quad i = 0, 1, ..., N-1 \\
&\frac{d^2Y[i]}{d\tau^2} = F[N+i] = \frac{Y[i+1] + RY[N+1+i] - 2(Y[i] + RY[N+i]) + Y[i-1] + RY[N-1+i]}{\Delta z^2} \\
&\qquad \text{for} \quad i = 0, 1, ..., N-2
\end{aligned} \tag{220}$$

The known displacement and velocity at the boundary $z = 0$ (or $i = -1$) has to be used when defining the acceleration at the neigbouring point $i = 0$.

For the boundary $z = 1$, the double derivative in space can be found by taylor expanding the function $g = f + R\frac{\partial f}{\partial \tau}$ at the points $i = N-2$ and $i = N-3$ around $i = N-1$ (or $z = 1$) and inserting the stress-free

boundary condition and then using that the partial differential equation is $\frac{\partial^2 f}{\partial \tau^2} = \frac{\partial^2 g}{\partial z^2}$ to get the acceleration at that point:

$$\begin{cases} Y[N-2] + RY[2N-2] = Y[N-1] + RY[2N-1] - \Delta z \left.\frac{\partial g}{\partial z}\right|_{z=1} + \frac{\Delta z^2}{2} \left.\frac{\partial^2 g}{\partial z^2}\right|_{z=1} - \frac{\Delta z^3}{6} \left.\frac{\partial^3 g}{\partial z^3}\right|_{z=1} \\ Y[N-3] + RY[2N-3] = Y[N-1] + RY[2N-1] - 2\Delta z \left.\frac{\partial g}{\partial z}\right|_{z=1} + \frac{4\Delta z^2}{2} \left.\frac{\partial^2 g}{\partial z^2}\right|_{z=1} - \frac{8\Delta z^3}{6} \left.\frac{\partial^3 g}{\partial z^3}\right|_{z=1} \end{cases} \Rightarrow \tag{221}$$

$$8\left(Y[N-2] + RY[2N-2]\right) - Y[N-3] - RY[2N-3] = 7\left(Y[N-1] + RY[2N-1]\right) + 2\Delta z^2 \left.\frac{\partial^2 g}{\partial z^2}\right|_{z=1} \Rightarrow$$

$$F[2N-1] = \frac{8Y[N-2] - Y[N-3] + 7Y[N-1] + R(8Y[2N-2] - Y[2N-3] + 7Y[2N-1])}{2\Delta z^2}$$

F.3.2 Ejection time

By taylor expanding the points $i = 0$ and $i = 1$ around $z = 0$ we get an expression for the double derivative in space and inserting the differential equation we can get an expression for the double derivative in time and then find an expression for the ejection time:

$$\begin{aligned} \left.\frac{\partial^2 f}{\partial \tau^2}\right|_{(\tau,z)=(\tau_e,0)} &= \beta^2 \cos(\beta\tau_e) \\ &= \frac{8Y[0] - Y[1] + 7f_0}{2\Delta z^2} + R\frac{8Y[N] - Y[N+1] + 7f_0'}{2\Delta z^2} \end{aligned} \tag{222}$$

where $f_0 = 1 - \cos(\beta\tau_e)$ and $f_0' = \beta \sin(\beta\tau_e)$. Then we can find an expression for the ejection time:

$$E(\tau) = 2\Delta z^2 \beta^2 \left(1 - \cos(\beta\tau)\right) + 8Y[0] - Y[1] - 7\left(1 - \cos(\beta\tau)\right) + R\left(8Y[N] - Y[N+1] - 7\beta \sin(\beta\tau)\right) \tag{223}$$

and the time $\tau > 0$ where $E(\tau) = 0$ is found the same way as before.

F.4 Numerical results

Solving equation 52 numerically for some values of R and plotting the ejection times and energy transfer factors as a function of β again will give the plots shown in figure

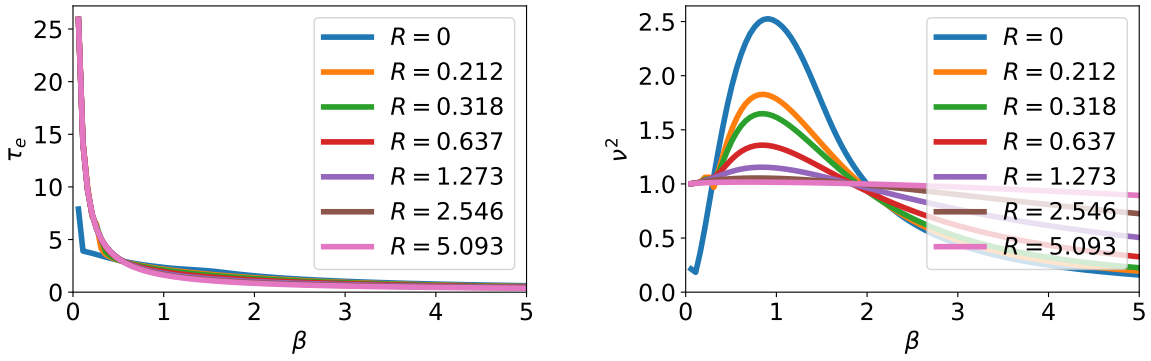

Figure 32: Ejection time (left) and energy transfer factor (right) as a function of β for three different value sof R. To obtain these plots the number of points in the mesh has been set to 100.

The value $R = 1.273$ corresponds to $\gamma = 2/\pi = \frac{1}{2}R$. For the orange graph on the figure it can be seen that for smaller values of β the value of ν^2 kind of oscillates up and down around 1. This also happens for the other graphs with smaller value of R. The larger R becomes the smaller the value of β becomes where this jumping in ν^2 happens.

When looking at the value of E (the numerically found ejection time equation) for a value of β before and after the graph of ν^2 jumps, it is seen that the found ejection time makes a big jump compared to other neighbouring values of β.

For $R = 4/(4\,\pi)$, the value of E, the ejection time equation at different times until the found ejection time is plotted for two different values of β, where the ejection time makes a large jumps. The plots are seen in figure 33 below.

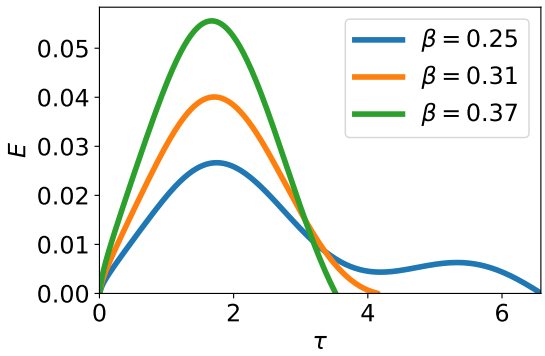

Figure 33: Graphs of E as a function of τ for three different values of β when $R = 4/(6\pi)$. To obtain these plots the number of points in the mesh is 20.

In general when looking at the value of E at β's where ν^2 jumps it is seen that where we would expect that $E = 0$, instead there is an extremum and the actual zero point comes later.

For smaller valus of R, corresponding til lower viscosities compared to Young's modulus, and relatively small values of β, corresponding til lower plate frequencies, this behaviour of the objects will begin. This jump in the ejection time, or the delay of it can be explained by realizing that for parameter values as just explained, the elastic properties of the object is stronger than the viscous properties. At first it will seem like the elastic wave can move through the object without friction, but just before it gets completely compressed so it can jump off the plate, the internal friction starts to have an effect and it damps the elastic wave so the object gets compressed slower than without friction, and so the ejection time gets delayed.

We could try to find this value of $\beta = \beta^*$ where the ejection time curve starts to jump. Values below this β^* will not give rise to a smooth curve in ν^2. Since the E curve will make an extremum at β^* (while for smaller β) while it is still a root, this value is found by the conditions:

$$E = 0 \quad , \quad \frac{\partial E}{\partial \tau} = 0 \tag{224}$$

The second condition, gives the following expression:

$$\frac{\partial E}{\partial \tau} = 2\Delta z^2 \beta^3 \sin(\beta\tau) + 8Y[N] - Y[N+1] - 7\beta \sin(\beta\tau) + R\left(8\frac{d^2 Y[0]}{d\tau^2} - \frac{d^2 Y[1]}{d\tau^2} - 7\beta^2 \cos(\beta\tau)\right) \tag{225}$$

To find the root β^* of this the bisection method can be used again.

G Intermediate calculations for point mass system with damping

The system considered is described by equation 64. Again the parameter $2\gamma = R$ is used.

G.1 Analytical method

Fourier transforming equation 64 the same ordinary differential equation is found as for the first system with damping and again the only difference is the boundary condition describing the stress at the top:

$$\begin{aligned} &\frac{d^2F}{dz^2} + \frac{-s^2}{1+2\,\gamma\,s}\,F = 0 \quad , \quad F(s,0) = \frac{\beta^2}{s\,(s^2+\beta^2)} \quad , \quad \left.\frac{dF}{dz}\right|_{z=1} = \frac{-\mu\,s^2}{1+2\,\gamma\,s}F(s,1) \Rightarrow \\ &\frac{d^2F}{dz^2} + \alpha^2\,F = 0 \quad , \quad F(s,0) = \frac{\beta^2}{s\,(s^2+\beta^2)} \quad , \quad \left.\frac{dF}{dz}\right|_{z=1} = \mu\,\alpha^2 F(s,1) \end{aligned} \tag{226}$$

with $\alpha^2 = \frac{-s^2}{1+2\,\gamma\,s}$ just as for the fist system. The general solution and its derivative are again given by

$$F(s,z) = k_1\,\sin(\alpha\,z) + k_2\,\cos(\alpha\,z) \Rightarrow \frac{dF}{dz} = \alpha\,[k_1\,\cos(\alpha\,z) - k_2\,\sin(\alpha\,z)] \tag{227}$$

From the first boundary condition, we have that

$$k_2 = \frac{\beta^2}{s\,(s^2+\beta)^2} \tag{228}$$

and from the second boundary condition we get

$$\begin{aligned} &\alpha\,[k_1\,\cos(\alpha) - k_2\,\sin(\alpha)] = \mu\,\alpha^2\,\,[k_1\,\sin(\alpha) + k_2\,\cos(\alpha))] \Leftrightarrow \\ &k_1\,\,[\cos(\alpha) - \mu\,\alpha\,\sin(\alpha)] = k_2\,\,[\sin(\alpha) + \mu\,\alpha\,\cos(\alpha)] \Leftrightarrow k_1 = k_2\,\frac{\sin(\alpha) + \mu\,\alpha\,\cos(\alpha)}{\cos(\alpha) - \mu\,\alpha\,\sin(\alpha)} \end{aligned} \tag{229}$$

such that the particular solution is

$$\begin{aligned} F(s,z) &= k_2\frac{\sin(\alpha\,z)\,\,[\sin(\alpha) + \mu\,\alpha\,\cos(\alpha)] + \cos(\alpha\,z)\,[\cos(\alpha) - \mu\,\alpha\,\sin(\alpha)]}{\cos(\alpha) - \mu\,\sin(\alpha)} \\ F(s,z) &= \frac{\beta^2}{s\,(s^2+\beta)^2}\frac{\cos\,[\alpha\,(1-z)] - \mu\,\alpha\,\sin\,[\alpha\,(1-z)]}{\cos(\alpha) - \mu\,\alpha\,\sin(\alpha)} \equiv \frac{P(s,z)}{Q(s,z)} \end{aligned} \tag{230}$$

The usual poles are found again, i.e.: $Q = 0 \Rightarrow s = 0,\ s = \pm i\beta$. And the other poles are given by

$$\cos(\alpha) - \mu\,\alpha\,\sin(\alpha) = 0 \Rightarrow \tan(\alpha) = \frac{1}{\mu\,\alpha} \tag{231}$$

This is the same equations as that for the poles of the same system without damping. So the solutions lie on the same intervals:

$$n\pi < \alpha_n < \lambda_n = \frac{\pi}{2}(2n+1) \quad , \quad n = 0, 1, 2, \ldots \tag{232}$$

where the solutions lie closer to the upper bound for smaller values of μ and closer to the lower bound for larger μ. For increasing n the solutions move closer to the lower bound. All these $\alpha \in \mathbb{R}$, and the poles s_n themselves are then given by (notice that this is the exact same equation as for the homogeneous system with damping just with α_n instead of λ_n):

$$\alpha_n^2 = \frac{-s_n^2}{1 + 2\,\gamma\,s_n} \Leftrightarrow s_n^2 + 2\,\gamma\,\alpha_n^2\,s_n + \alpha_n^2 = 0 \Leftrightarrow s_n = \alpha_n\left(-\gamma\,\alpha_n \pm \sqrt{(\gamma\,\alpha_n)^2 - 1}\right) \tag{233}$$

Now the critical value for the damping parameter $\gamma = R/2$ depends on μ because the α_n depend on this parameter - but again the first n is the important pole since this value of α_n is the smallest one and if the argument of the square root is equal to zero (or greater than zero) for the first n, then it will be greater than zero for all other n, and all the poles will be real, so the displacement will not contain any oscillation terms. Since there is a range that α_1 lies in, there is also a range that the critical value of the damping parameter lies in. This critical value thus lies in the range:

$$\gamma_c = \frac{1}{\alpha_1} \Rightarrow \frac{2}{\pi} < \gamma_c < \infty \Leftrightarrow \frac{2}{\pi} < R_c < \infty \tag{234}$$

For small values of μ the critical value is closer to the lower bound, while it is closer to the upper bound for larger μ.

The characteristic time for the damping of the different wave modes now also depends on μ and thus lies in the following range (notice again that the expression for τ_n' is the same as without the point mass, just with α_n instead of λ_n):

$$\tau_n' = \frac{1}{\gamma\,\alpha_n^2} = \frac{2}{R\,\alpha_n^2} \Rightarrow \frac{2}{\pi^2\,R}\,\frac{4}{(2n+1)^2} < \tau_n' < \frac{2}{\pi^2\,R}\,\frac{1}{n^2} \tag{235}$$

G.2 Numerical method

Taylor expanding the exact same way again as in equation 221 and inserting the new boundary condition we get:

$$\begin{cases} Y[N-2] + RY[2N-2] = Y[N-1] + RY[2N-1] - \Delta z\ \left.\frac{\partial g}{\partial z}\right|_{z=1} + \frac{\Delta z^2}{2}\ \left.\frac{\partial^2 g}{\partial z^2}\right|_{z=1} - \frac{\Delta z^3}{6}\ \left.\frac{\partial^3 g}{\partial z^3}\right|_{z=1} \\ Y[N-3] + RY[2N-3] = Y[N-1] + RY[2N-1] - 2\Delta z\ \left.\frac{\partial g}{\partial z}\right|_{z=1} + \frac{4\Delta z^2}{2}\ \left.\frac{\partial^2 g}{\partial z^2}\right|_{z=1} - \frac{8\Delta z^3}{6}\ \left.\frac{\partial^3 g}{\partial z^3}\right|_{z=1} \end{cases} \Rightarrow \tag{236}$$

$$8\,(Y[N-2] + RY[2N-2]) - Y[N-3] - RY[2N-3] = 7\,(Y[N-1] + RY[2N-1])$$
$$-\,6\Delta z \cdot (-\mu)\ \left.\frac{\partial^2 g}{\partial \tau^2}\right|_{z=1} + 2\Delta z^2\ \left.\frac{\partial^2 g}{\partial \tau^2}\right|_{z=1} \Rightarrow$$
$$F[2N-1] = \frac{8Y[N-2] - Y[N-3] + 7Y[N-1] + R(8Y[2N-2] - Y[2N-3] + 7Y[2N-1])}{2\Delta z(\Delta z + 3\mu)}$$